UNIVERSITÀ DEGLI STUDI FIRENZE

DOTTORATO DI RICERCA IN SCIENZE CHIMICHE

CICLO XXVIII

COORDINATORE Prof. ANDREA GOTI

DECORATED CARBON NANOTUBES AS VECTORS TO BOOST THE EFFECT OF AN ANTICANCER DRUG - FROM SYNTHESIS TO IN VIVO RESULTS

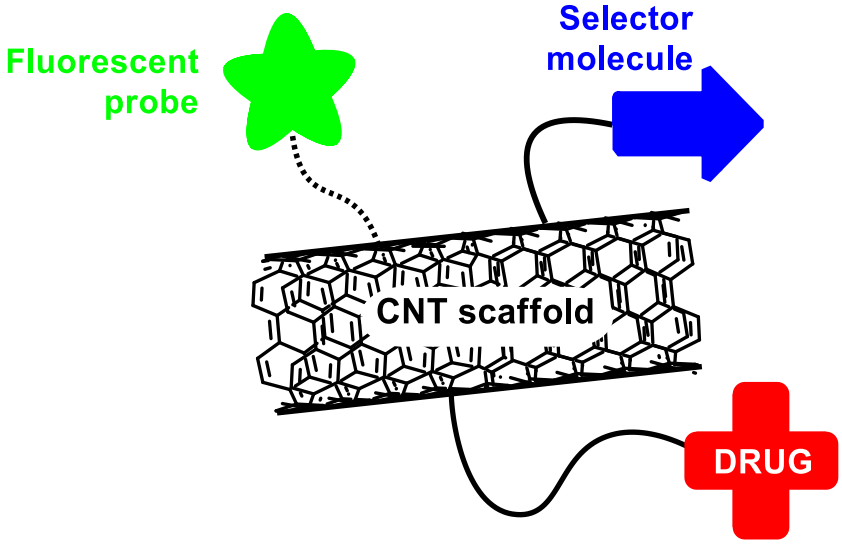

Dottorando
Dott. Stefano Fedeli

Tutore
Prof. Stefano Cicchi

UNIVERSITÀ
DEGLI STUDI
FIRENZE

DOTTORATO DI RICERCA IN SCIENZE CHIMICHE

CICLO XXVIII

COORDINATORE Prof. Andrea Goti

DECORATED CARBON NANOTUBES AS VECTORS TO BOOST THE EFFECT OF AN ANTICANCER DRUG - FROM SYNTHESIS TO *IN VIVO* RESULTS

Settore Scientifico Disciplinare CHIM/06

Dottorando
Dott. Fedeli Stefano

Tutore
Prof. Cicchi Stefano

Coordinatore
Prof. Goti Andrea

Anni 2012/2015

... «Signore, fui un giorno dal Re Pescatore e vidi la lancia il cui ferro sanguina senza posa e nulla ho cercato di sapere di quella goccia di sangue che cola dalla bianca punta d'acciaio. Meglio non ho fatto in seguito, e del Santo Vaso ch'io vidi non so a chi fosse servito. Da quel momento ne ho avuto tal duolo che ho desiderato morirne, dimenticando Dio. Non ho chiesto perdono e nulla ho fatto, ch'io sappia, per esser perdonato.»

«Ebbene, caro amico» disse l'eremita «dimmi il tuo nome.»

«Parsifal, signore.»

- Perceval o il racconto del Graal -
Chrétien de Troyes, XII sec.

Index

Abstract

This doctoral project concern the preparation, the characterization, and the biological testing of a drug delivery system based on decorated carbon nanotubes aimed to the transport an anticancer drug inside cancer cells. Multi-walled carbon nanotubes have been modified to deliver doxorubicin inside cancer cells, resulting in an enhanced chemotherapic effect respect to the free drug. Decoration of the carbon nanotubes was accomplished through both covalent and non-covalent approaches: versatile click reactions and π-π interactions were exploited.

To assess the internalization of the carbon nanotubes inside cells, a decoration with a fluorescent molecule, namely BODIPY, was performed. Next, the nanotubes were decorated with a selector molecule, biotin, to increase the uptake of the system by cancer cells. A representation of the system is depicted below (Figure 1).

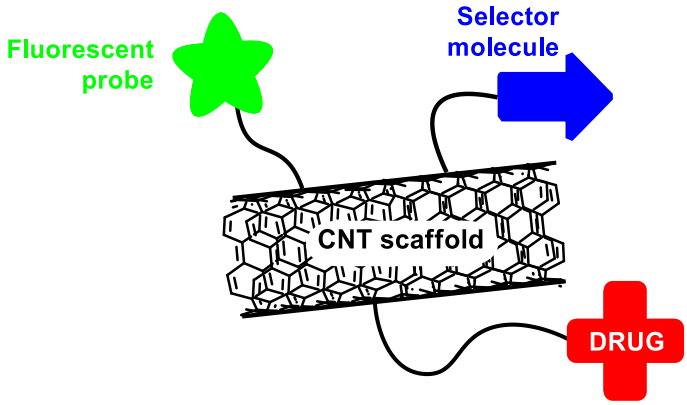

Figure 1. Schematic representation of the nanotube completely decorated.

The non-toxicity of the simple delivery system alone (without drug) as well as the role of the selector have been investigated by parallel biological tests. Finally, the decorated system was loaded with the drug: doxorubicin. Comparative studies were performed on the loaded drug delivery system to highlight its effect respect to the free drug and to mark the role of the selector in the internalization efficiency.

The overall project is composed by two parts: a) a comprehensive study of synthesis and characterization on the fluorescent probes suitable for the decoration of carbon nanotubes, with preliminary biological tests, and b) modification of carbon

nanotubes and their decoration with a selector and the drug. The second part was complemented by extensive biological tests.

In the first part boron dipyrromethene complexes (BODIPY) were synthesized and fully characterized, giving a series of novel fluorescent probes able to cover a large part of the absorption and emission visible spectra. Fluorescent molecules were also equipped with functional groups for the decoration of the nanotubes. The biological tests performed confirmed that the fluorescent nanotubes were easily located inside different model cancer cells. The biological data on internalization were obtained through confocal microscopy analysis and cytofluorimetric tests.

In the second part, the drug delivery system has been completed with biotin as selector molecule and with doxorubicin. Finally, the system was tested again *in vitro* on breast cancer cells MCF-7 and *in vivo* on nude mice xenograft model. In both cases comparative assays have been carried out with free doxorubicin, providing remarkable results. The adoption of biotin-decorated carbon nanotubes as vector to boost the drug internalization process, has resulted into increasing the chemotherapic efficiency of doxorubicin, both in cellular models and animal models.

Appendix

During the work, there has been the opportunity to further exploit the acquired knowledge on florescent molecules and on carbon nanotubes. This has resulted positively in two studies: the synthesis of a BODIPY-type molecule as component of a Molecular Dyad (appendix A), and a study on a different way to decorate carbon nanotubes for the engineering of carbon-based nanostructures (appendix B).

Part one - Azido substituted BODIPY dyes for the production of fluorescent carbon nanotubes

As first step of the development of a carbon nanotubes (CNTs) based drug delivery system, we have synthesized carbon nanotubes decorated with fluorescent molecules (Figure 2). In a drug delivery system is necessary the presence of a fluorescent probe to study, by cytofluorimetric and imaging analysis, its internalization inside the cells.

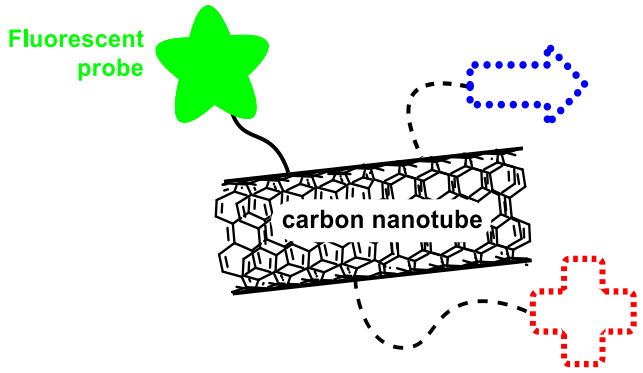

Figure 2. General scheme; the fluorescent decoration on nanotubes is the first step of the project.

Concerning the fluorescent molecule, we have synthesized and characterized new derivatives of a class of fluorescent molecules known as BODIPY. The stability and the high fluorescence of these molecules are proven, as well as the tunability of their absorption and fluorescence wavelengths. Various BODIPY probes have been tested, and as carbon nanotubes we have adopted oxidized multiwalled carbon nanotubes. The functionalization of the nanotubes surface was performed through a covalent approach summarised in 3 steps: (i) the CNTs were preliminary functionalized with an azido function, (ii) the proper BODIPY and the biotin derivatives, bearing an alkyne function, were synthesized, (iii) the coupling between the CNT and the alkyne molecules was obtained through a simple "click" reaction. The CNTs have been characterized by spectrofluorimetric analysis, and their internalization inside cells was

evaluated by confocal microscopies and cytofluorimetric studies. Initial data of their cytotoxicity were also collected.

In this first part of the work a series of azido-dyes have been synthesized through Knoevenagel reactions of an azido-BODIPY with aromatic aldehydes. The nature of the substituents allowed a fine tuning of their spectroscopic properties. The dyes were used to decorate oxidized multiwalled carbon nanotubes (ox-MWCNTs), bearing terminal triple bond groups, via CuAAC reactions affording fluorescent materials. This decoration allowed the efficient determination of the internalization of the ox-MWCNTs derivatives by different model cancer cells.

1.1 Introduction on BODIPY fluorophores

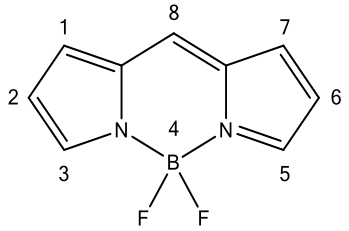

Figure 3. The core structure of BODIPY with the position.

BODIPY type molecules (Figure 3) have found a widespread application as fluorescent probes.[1] The chemical stability of the BODIPY core goes along with its synthetic versatility.[2] The various reviews on the subject propose a large number of different structures.[3,4,5] Such structural variety allows the coverage of a great part of the UV-visible spectrum, both in absorption and emission. However, despite their wide applications, BODIPY probes have been used sparingly with nanostructured carbonaceous materials.[6,7,8] In our ongoing study for the production of drug delivery systems based on CNTs[9,10] it was chosen to decorate oxidized multiwalled carbon nanotubes, bearing terminal alkyne groups, with a fluorescent probe through a simple CuAAC reaction.[11] The choice for the use of MWCNTs is related, among other more practical reasons (cost, easy control of oxidation) to their higher dispersibility

and suitability in biological applications. For this goal, it was necessary to synthesize simple dyes, bearing an azido group, whose absorption and emission properties could be finely modulated to fulfill the requirements for the detection during biological tests. In this part of the work it is described the synthesis of azido-substituted BODIPY dyes in which the reactivity of the methyl groups present on the pyrrole rings is exploited in a series of Knoevenagel reactions to extend the conjugation of the core and to obtain derivatives whose spectroscopic properties were modulated by the nature of the substituents. This synthetic approach is a straightforward way of extending the molecular conjugation of the BODIPY dye,[12,13,14,15,16,17] and is applied on azido-substituted BODIPY dyes for the first time. The availability of a library of BODIPY dyes bearing an azido group adds a useful alternative for their application in medicinal[18,19] and material chemistry[20] and, in our case, revealed to be a practical tool for the easy decoration of ox-MWCNTs. The coupling of properly modified ox-MWCNTs with BODIPY dyes afforded fluorescent material whose internalization inside cells has been monitored through cytofluorimetry and confocal microscopy analyses.

1.2 Results and Discussion

The starting material is represented by the BODIPY dye **5**, whose synthesis is already described.[21] Compound **5** is easily obtained from 2,4-dimethylpyrrole (**2**) and 4-nitrobenzaldehyde (**3**). Among the several different procedure reported in the literature we found more convenient to use the mechanochemical approach[22] up to the intermediate **3** while the treatment with $BF_3{\cdot}Et_2O$ was performed in dry CH_2Cl_2.[21] The reduction of the nitro group with Fe powder/HCl afforded the corresponding amino group[23] and the final conversion into the azido derivative **5** was performed with TMS-N_3 and isoamyl nitrite (Figure 4).[24]

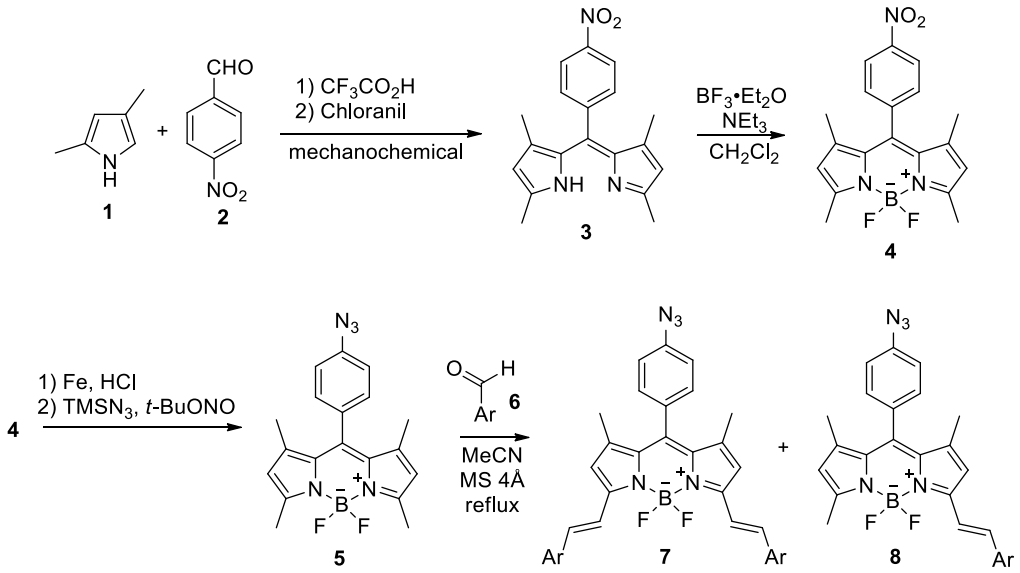

	Ar	7	8
a	Ph	97	-
b	4-HO-C_6H_4	34	22
c	2-Py	37	18
d	4-$CO_2HC_6H_4$	29	-

Figure 4. Synthesis of the various BODIPY derivatives. Compound **5** and its transformation into azido-substituted dyes **7a**-**d** and **8b**-**c**.

The reactivity of the two methyl groups in position 3 and 5 of the BODIPY core allowed to perform the Knoevenagel reaction with four different aromatic aldehydes,

6a-**d**, to afford the corresponding mono- and disubstituted derivatives (Figure 4). Previous examples of Knoevenagel reaction on BODIPY derivatives were performed treating the dye with an excess of aromatic aldehyde in the presence of acetic acid and pyrrolidine in refluxing toluene[25] or in absolute ethanol.[26]

However, the presence of the azido group on compound **5** made it sensitive to prolonged heating and required a compromise between conversion of the starting material and the final yields of the adducts. Even after a short reflux in toluene, the crude reaction material showed the presence of compounds in which the azido group had been lost. The best reaction conditions revealed to be reflux in MeCN for very short time, checking the reaction mixture by TLC. The results are reported in Figure 4. The reaction conditions were not optimized for the synthesis of the double or mono substituted derivatives but for the obtainment, when possible, of both compounds. This choice was due to the need to explore the potentiality of these compounds to cover a large part of the visible spectrum, in absorption as well as in emission. The reaction with benzaldehyde (**6a**) and 4-HO_2C-benzoic acid (**6d**) afforded exclusively the doubly substituted compound 7a[24] and **7d**, respectively, while 4-hydroxybenzaldehyde (**6b**) and pyridine-2-carbaldehyde (**6c**) afforded a mixture of mono- and disubstituted compounds (Figure 4). The structure of the final compounds were easily determined by 1H NMR spectroscopy showing the signals of the AX system related to the newly formed *E* double bonds.

In line with our expectation, the absorption spectra (Figure 5) covered a wide part of the visible spectrum ranging from 500 to 650 nm. For the sake of clarity, the UV spectra of the dyes were normalized. The molar attenuation coefficients of the compounds are reported.

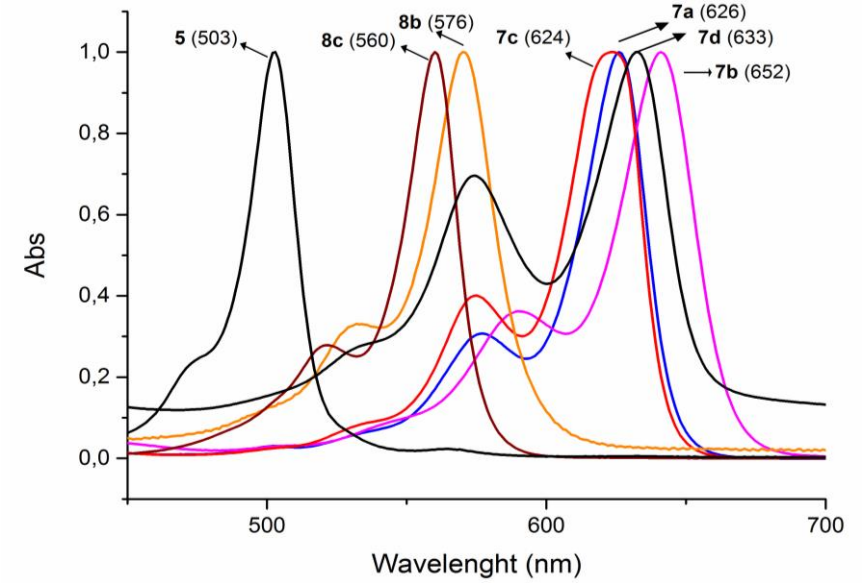

Figure 5. Absorption spectra (normalized) of compounds, **5**, **7b**, **8b**, **8c** (DMF), **7d** (H_2O/DMF) and **7a**, **7c** (CH_2Cl_2).

Compound	UV_{max} (nm)	solvent	ε (M^{-1} cm^{-1})
5	503	DMF	$7.5\ 10^3$
7a	626	CH_2Cl_2	$1.4\ 10^5$
7b	641	CH_2Cl_2	$6.8\ 10^4$
	652	DMF	$6.5\ 10^4$
	673	H_2O	$8.7\ 10^3$
8b	570	CH_2Cl_2	$9.9\ 10^3$
	576	DMF	$8.7\ 10^3$
7c	624	CH_2Cl_2	$3.2\ 10^5$
8c	560	CH_2Cl_2	$2.0\ 10^5$
	560	DMF	$1.1\ 10^5$
7d	633	H_2O/DMF	$3.7\ 10^3$

Table 1. UV_{max} and molar attenuation coefficient (ε) of compound **5**, **7** and **8**.

Table 1 shows also a remarkable solvatochromic effect. Compound **7b**, sufficiently soluble in water, showed a 32 nm red shift moving from CH_2Cl_2 to H_2O.

Also the maxima (see Figure 6) in the emission spectra were scattered, covering a range of 150 nm. The Stokes shift values are very low as usually happens with this kind of fluorescent dyes, ranging from 8 nm (compound **8c**) to 18 nm (compound **7c**).[5]

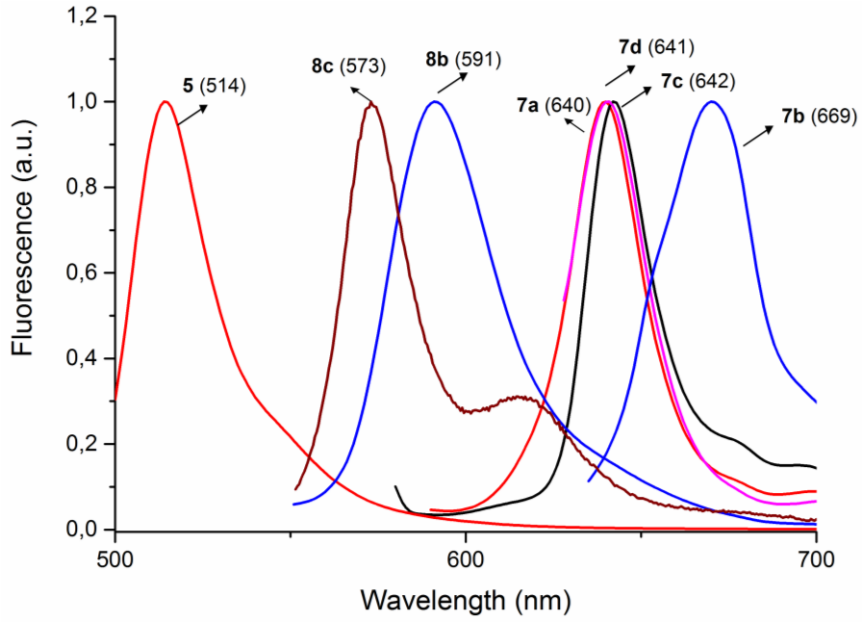

Figure 6. Emission spectra (normalized) of compounds **5**, **7b**, **8b**, **8c** (DMF), **7d** (H_2O/DMF) and **7a**, **7c** (CH_2Cl_2).

The presence of the azido group on all the substituents allows their use in CuAAC reactions with compounds bearing a terminal triple bond. This reactivity was used for the decoration of ox-MWCNTs **9** bearing terminal triple bonds (for the synthesis and characterization see experimental section, and from Figure 33 to Figure 39).[27,28,29] The CuAAC reaction with dyes **5**, **7b** and **8c** was performed in DMF and afforded the fluorescent ox-MWCNTs derivatives **10**-**12** (Figure 7). The decoration of the MWCNTs afforded fluorescent materials whose absorption and emission properties can be easily tuned using differently substituted BODIPY dyes. This material revealed stable since, after several months, no apparent degradation of the fluorescence was observed.

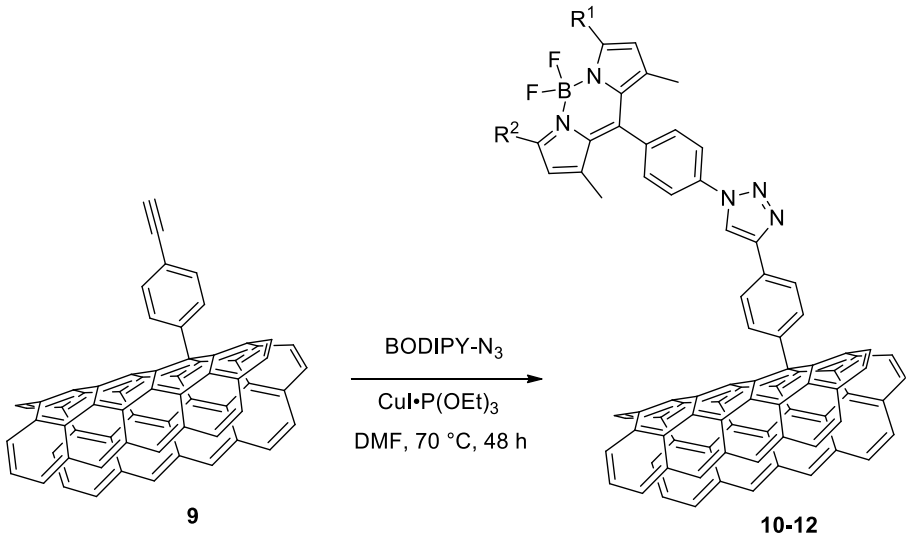

BODIPY-N_3	R^1	R^2	product
5	Me	Me H	**10**
8c	vinyl Py	vinylC_6H_4OH	**11**
7b	vinylC_6H_4OH		**12**

Figure 7. The CuAAc reaction between CNTs **9** and BODIPY dyes **5**, **7b** and **8c**.

Figure 8 and Figure 9 show the absorption and emission spectra of compound **10**-**12**. The decoration of the CNTs walls did not alter significantly the absorption and the emission maxima of the BODIPY derivatives. This appears evident comparing the UV and fluorescence maxima of compounds **5** and **7b** with those of **10** and **12**, respectively: the wavelengths of absorption and emission (measured in DMF) are the same for each sample. This might be rationalized considering that the fluorescent probe is efficiently solvated by DMF reducing to a minimum the interaction with the CNTs. On the contrary, compound **8c** shifted its UV and fluorescence maxima by 11 and 22 nm, respectively, when anchored to ox-MWCNTs to give compound **11**. This might be due to the presence of a pyridine ring on the dye and its interaction with the carboxylic groups present on the ox-MWCNTs

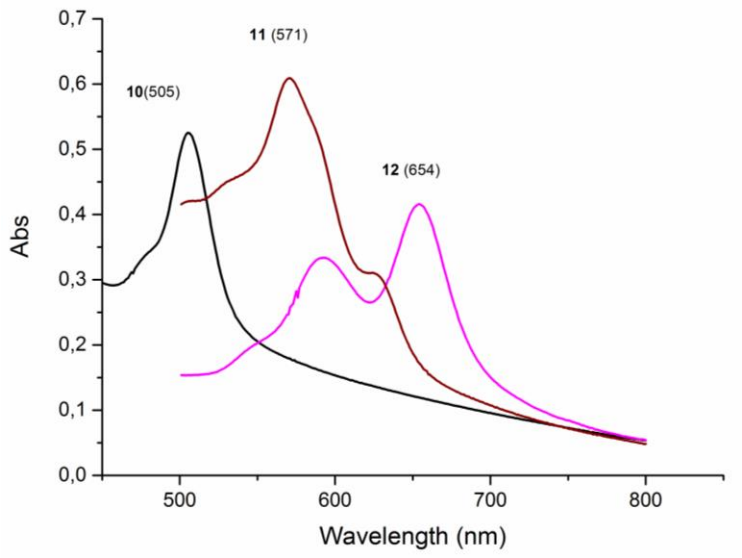

Figure 8. Absorption spectra of compounds **10**-**12**. All spectra are registered in DMF (0.05 mg/mL).

A main issue, working with CNTs, is the determination of their functionalization degree obtained after a reaction. Very often this information is obtained through elemental or thermogravimetric analysis.

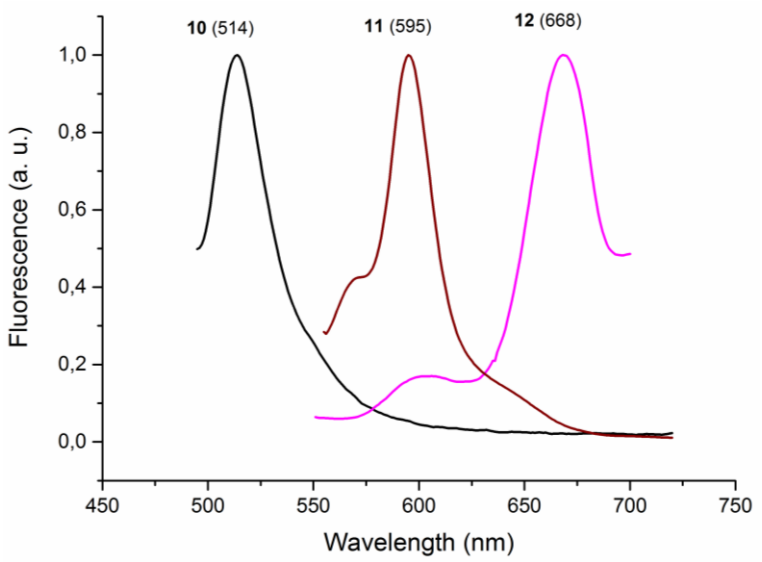

Figure 9. Emission spectra (normalized) of compounds **10**-**12**. All spectra are registered in DMF (0.05 mg/mL).

The presence of the BODIPY dyes, bearing a boron atom, allowed the use of inductively coupled plasma atomic emission spectroscopy (ICP-AES) for a quantitative determination of the functionalization degree of decorated ox-MWCNTs. In the case of compound **10** the analysis revealed a presence of 12.4 mg of Boron per gram of material (1.14 mmol/g of material) while for compound **11** the analysis revealed the presence of 6.2 mg per gram of material (0.57 mmol/g of material). The certification of the capacity of the fluorescent probes to show the internalization of CNTs inside cancer cells was granted by a series of cytofluorimetric analyses performed on three different cancer cell lines: MCF-7 (human breast adenocarcinoma), PC3 (prostatic small cell carcinoma) and HT29 (human colon cancer) after incubation ,with compound **10**, **11** and **12** (Figure 10 and Table 2).

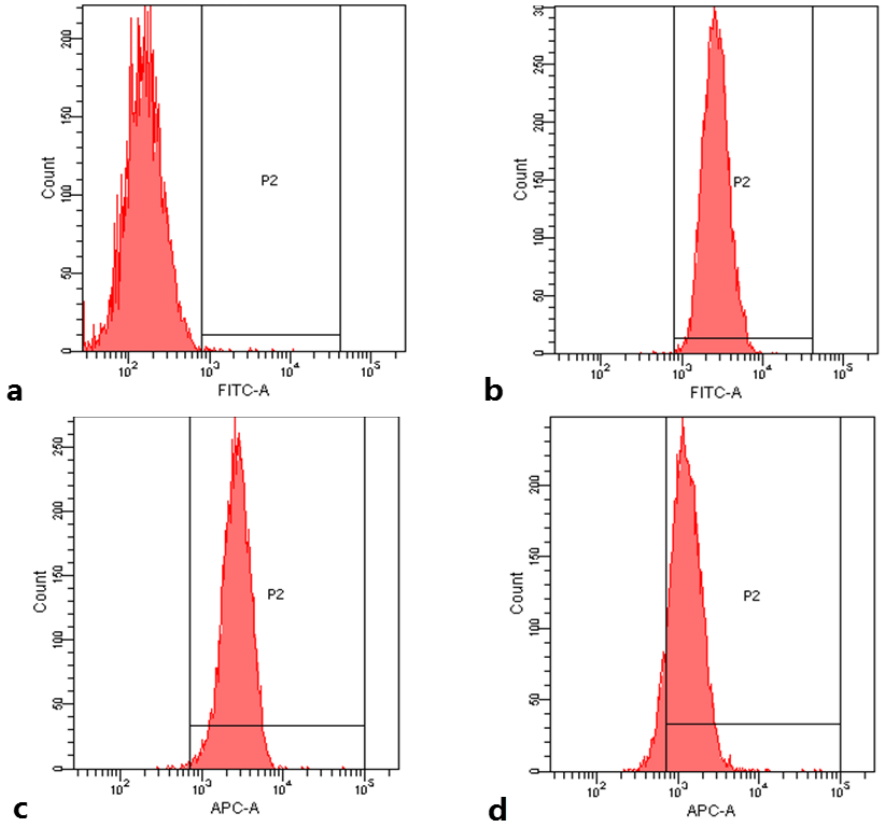

Figure 10. Cytofluorimetric analysis of MCF-7 cell lines after incubation with fluorescent CNTs: a) control experiment, b) incubation with **10**, c) incubation with **11**, d) incubation with **12**

Figure 10 shows the results of three cytofluorimetric analyses performed with compounds **10**-**12** on MCF-7 cancer cell lines. The figure show the remarkable increase of fluorescence of the cells, directly related to the internalization of the CNTs. Table 2 resumes all the cytofluorimetric data collected for the three different cancer cell lines. In all cases there is a net increase of the cellular fluorescence demonstrating that the decorated carbon nanotubes are efficiently internalized by different cell lines.[30] While it is not possible to compare the internalization degree of the different compounds inside one kind of cell cultures, since any enhancement or quenching effect might be different, it is possible to compare the difference between the internalization degrees of the same compound inside different kind of cells. For example MCF-7 cells showed a much higher fluorescence when incubated with **10** respect to HT29 and PC3 (5-fold the final fluorescence value). The opposite holds for **12** for which HT29 and PC3 cells showed a 3-fold value of the final fluorescence. Since the functionalization degree of the compound used is the same, it is possible to correlate, at least qualitatively, the degree of internalization with the enhancement of fluorescence.

Table 2. Fluorescence data from cytofluorimetry analysis after incubation of three different cell lines with compounds **10**-**12**.[a]

Cell line	**10**		**11**		**12**	
	Control	Treated	Control	Treated	Control	Treated
HT29	136	597	344	4190	69	1350
PC3	93	531	247	4879	158	1260
MCF-7	180	2650	275	1380	275	2900

[a] Each cell culture was incubated for 90 min with a water dispersion of the decorated nanotubes **10**-**11** (10 μg/mL). Data reported in the table, represent the mean values of the fluorescence of the cells.

Finally, compound **11** was used in a confocal microscopy analysis performed on MCF-7 cells after incubation (Figure 11).

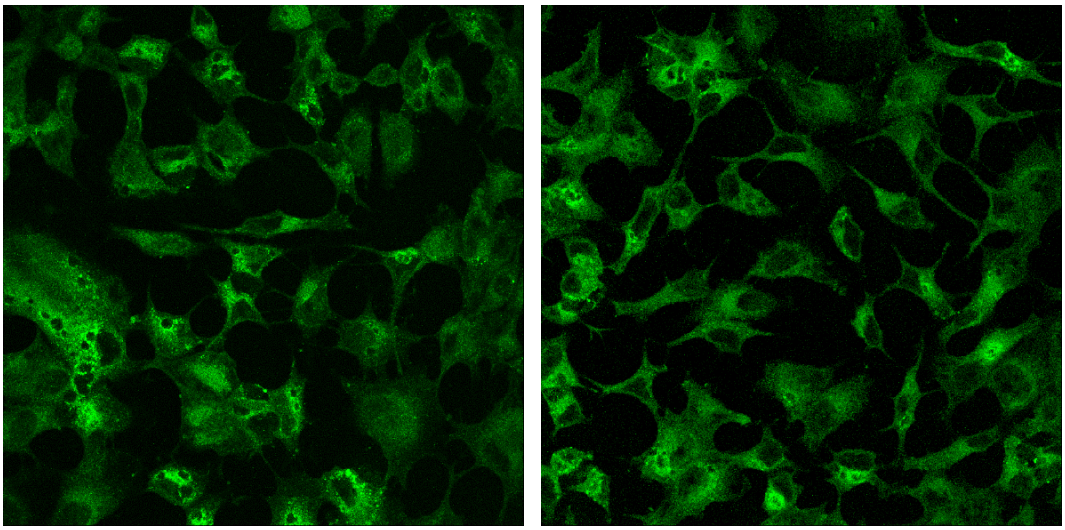

Figure 11 images of a MCF-7 cell culture after incubation with MWCNTs **11**.

Compound **11** has been chosen since it best fitted the excitation frequency (571 nm) of the laser used in the confocal microscopy analysis. Despite MCF-7 cells were those that evidenced the smaller increase in fluorescence upon incubation with compound **11**, the confocal analysis afforded clear pictures (Figure 11): the fluorescence of compound **11** is well distributed in the cytoplasm of the cells while the nuclei remain unaffected. Concerning the amount of material internalized, during the biological tests it was not possible to determine any difference between the cell cultures incubated with simple ox-MWCNTs and those incubated with compound **11**.

1.3 Toxicity tests

To verify any possible toxic effect of the nanostructured materials, MTT vitality assays have been performed and the results are reported in Figure 12 (for details on MTT assay see experimental section). MCF-7 breast cancer cells were incubated for 24 hours in the presence of 10 µg/mL of compound **11** or 10 µg/mL of ox-MWCNTs, after this time, viability of cells was evaluated using MMT assay.

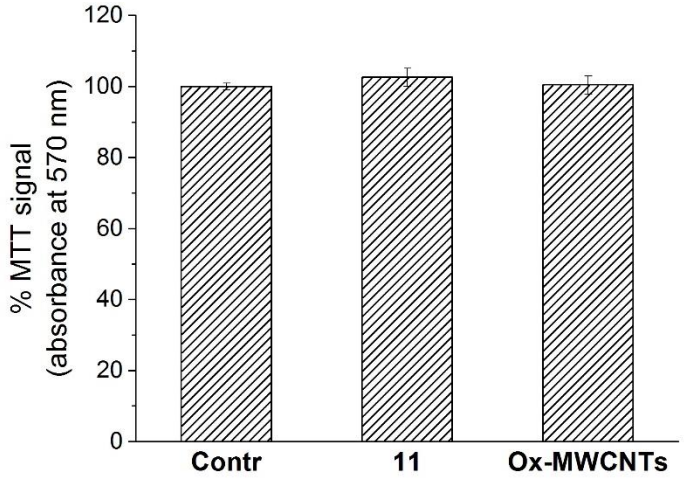

Figure 12. MTT test. The data report the cell survival rate (%) normalized with respect to control experiments. Data reported represent the mean value ± S.E.M. (n = 3).

As it is clear, neither simple ox-MWCNTs nor compound **11** show any sign of cytotoxicity towards MCF-7 cell lines using a concentration of 10 mg/mL of the material.

Conclusions of Part One

A series of Knoevenagel reactions of an azido-BODIPY derivative allowed the production of a small library of azido-substituted fluorescent dyes whose spectroscopic properties are tuned by the nature of their substituents. The presence of an azido group on the fluorescent dyes allowed their easy anchoring onto properly substituted ox-MWCNTs. This affords fluorescently labeled nanostructured carbon materials that are internalized efficiently inside cells after a brief incubation time. This material can thus be easily exploited as platform for the selective delivery of drugs into cancer cells.

Part two - Decorated carbon nanotubes for the delivery of doxorubicin into cancer cells

In the first part of the project, a series of azido-substituted BODIPY dyes have been developed and used for the decoration of ox-MWCNTs bearing terminal triple bonds on their surface. The material showed very good ability to penetrate the cellular membranes and has been proven to be not toxic towards cells. On the base of these results, the work has progressed with the further decoration of nanotubes to assembly the complete drug delivery system (Figure 13). To avoid the manipulation of small organic azides, we have reversed the functional groups involved in the "click" reaction, but without any observed change, nor in the reactivity, neither of biological activity of the compounds. As selector, to increase the uptake of the system by cells, biotin have been already tested as simple and general targeting molecule for cancer cells.[31,32,33,34] Finally, the decoration with doxorubicin (DOX). This drug has become a common benchmark for the comparison of efficiency of drug delivery with CNTs. The system has been therefore subject to several tests *in vitro* to assess the biological activity.

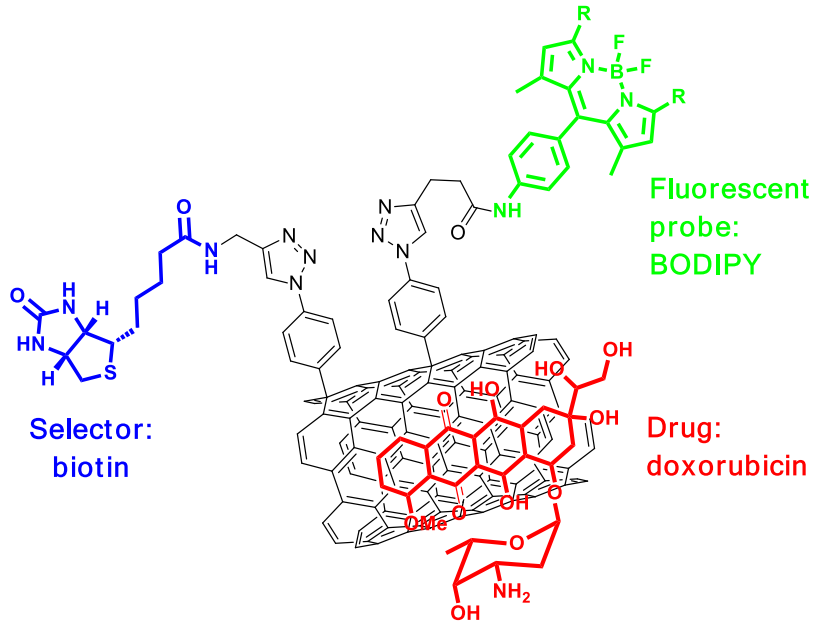

Figure 13. The complete drug delivery system into its components

The project has been thus completed with the realization of multiple-decorated ox-MWCNT as vectors able to carry doxorubicin inside breast MCF-7 cancer cells. The ox-MWCNT conjugated doxorubicin resulted in an enhanced cytotoxic effect with respect to the free drug.

2.1 Overview on CNTs for the drug delivery

The use of carbon nanotubes as carriers for antitumoral drugs has emerged, both *in vitro* and *in vivo*, as a valuable method for the treatment of tumors.[35,36,37] The efficient, and non-selective, mechanism of internalization of functionalized CNTs by cells paved the way to the use of CNTs as drug carriers, but also rose severe concerns about their toxicity and lack of selectivity.[38,30] Recent studies revealed that the toxicity of CNTs can be controlled by the functionalization of the walls, making them more hydrophilic and short, avoiding the formation of bundles.[39] Meantime, the decoration of functionalized CNTs with efficient selectors for receptors, expressed on the surface of target cells, afforded selectivity required to propose a modern and effective drug.[40] While the fluorescent probe and the selector were anchored through the "click on tubes" approach (covalent conjugation through the formation of triazole rings obtained with CuAAC reactions between azido substituted ox-MWCNTs and HC≡C-bearing molecules), the doxorubicin molecules were anchored via the formation of supramolecular complexes with the CNTs wall.[41] Such synthetic approach is designed to be modular, allowing an easy variation of the fluorescent probe, selector and drug without redesigning the whole procedure.

2.2 Result and discussion

2.2.1 Preparation of the carbon nanotube support

The starting materials for this second part of the work were the functionalized CNTs carrying the azido groups. In a reported study, a demonstrative feasibility of the synthesis of functionalized CNTs carrying the azido groups was carried out on single-walled CNTs.[9] However, the use of ox-MWCNTs was kept for sake of continuity

as well as for the initially described reasons. Commercially available MWCNTs were oxidized by treatment with the sulphonitric mixture,[29] and the resulting material results easily dispersible in water and polar solvents as DMF and DMSO. The ox-MWCNTs were, eventually, functionalized following the Tour[42] protocol using 4-azido-phenylamine (**13**), Figure 14.

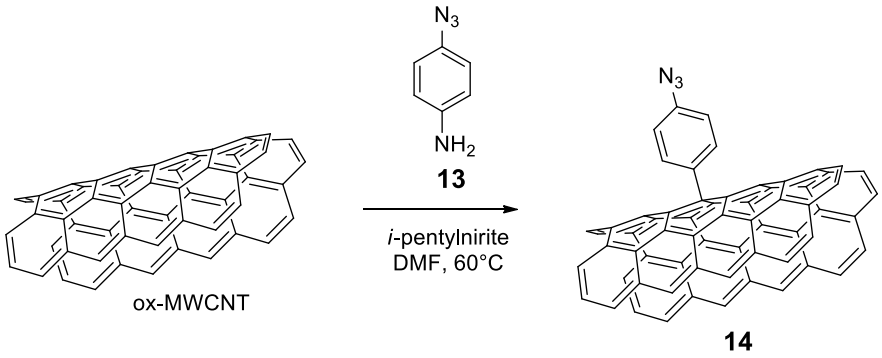

Figure 14: Functionalization of ox-MWCNTs through the Tour reaction.

Compound **14** exhibited in a net and sharp absorption at 2100 cm^{-1} IR spectrum (Figure 40, experimental section) suggesting a high level of functionalization that was quantitatively determined through both Elemental Analysis and Thermo Gravimetric Analysis (TGA), (see Table 3 and experimental section). Furthermore, a CuAAC reaction of compound **14** with *N*-Boc propargylamine (**15**) to confirm the level of functionalization was performed (Figure 15)**.** A TGA-Mass Spectrometer analysis of cycloaddition product **16** (TGA-MS, see experimental section, Figure 41), by measuring the amount of isobutene generated at high temperature from nanotubes **16**, made possible to evaluate also the yield of the click reaction. Collected data are summarized in Table 3.

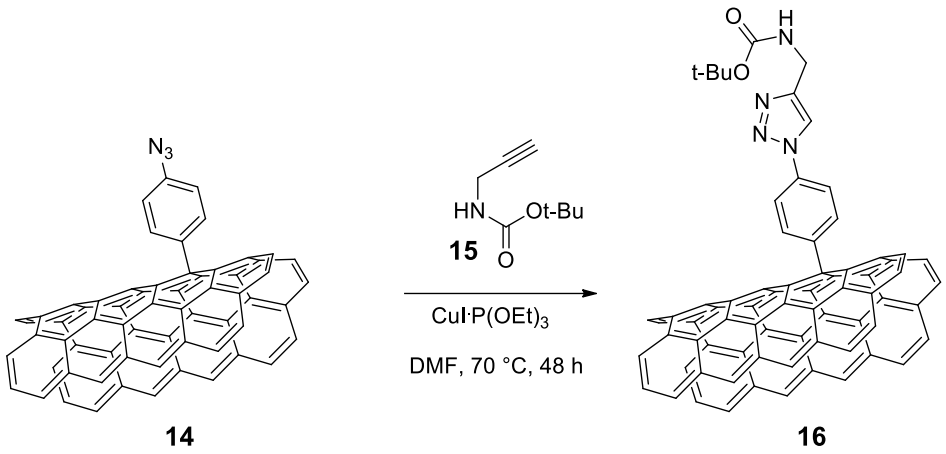

Figure 15: CuAAC reaction of CNTs **14** with N-Boc protected propargylic amine.

Compound	N_3 content (Elem. An.) mmol/g	N_3 content (TGA) mmol/g	isobutene content (TGA) mmol/g
14	2.06	2.13	-
16	-	-	2.13

Table 3: Functionalization degree evaluated through Elemental Analysis and TGA of compounds **14** and **16**.

Both elemental and TGA analyses of compound **14** gave very close values of functionalization while the TGA analysis performed on **16** suggests that the conversion of the CuAAC reaction is quantitative.

*2.2.2 Decoration of carbon nanotubes **14** through CuAAC reactions*

Once obtained the functionalized platform the work focused on its decoration with the different building blocks needed for the production of the drug delivery system. The first step was the decoration of **14** with fluorescent probes **17** and **18**, bearing a terminal triple bond, by cycloaddition onto the azido-CNT **14**. The CuAAC reaction proceeded smoothly using CuI·P(OEt)$_3$ as catalyst and afforded, the corresponding

fluorescent CNTs **19** and **20** (Figure 16). The same synthetic approach, using the propargyl biotin derivative **21**, afforded biotinylated-CNT **22** (Figure 17).

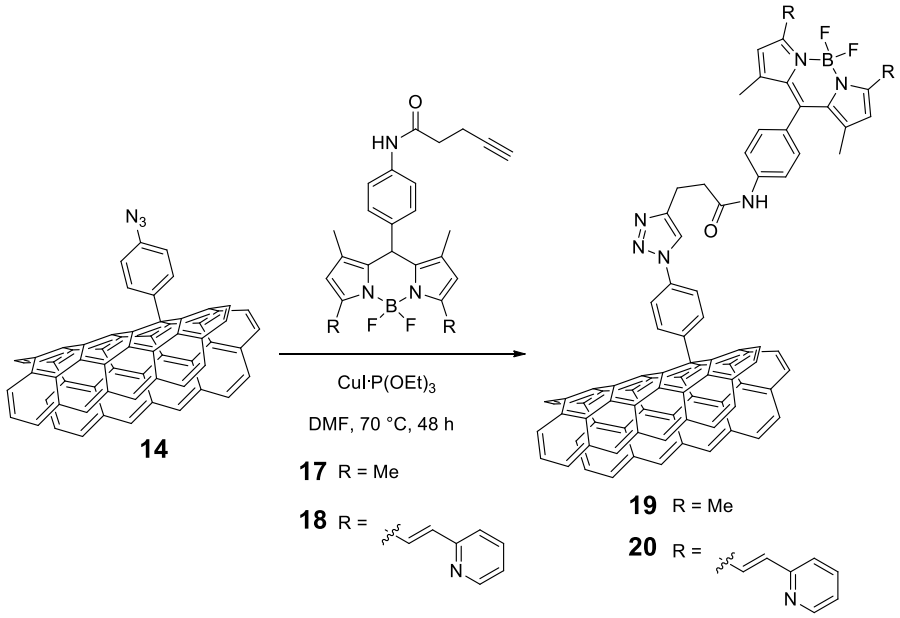

Figure 16. CuAAC reaction of CNTs **14** with BODIPY dyes **17** and **18**.

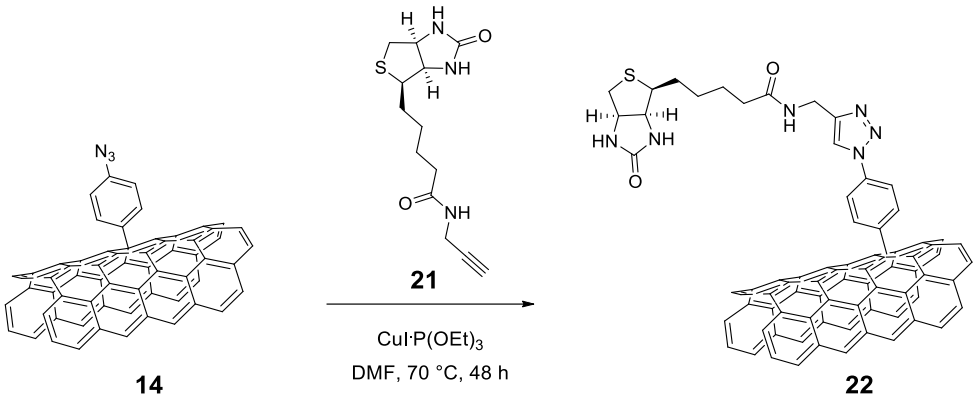

Figure 17. CuAAC reaction of ox-MWCNT **14** with biotin derivative **21**.

A doubly functionalized CNT, with a fluorescent probe and a selector, was synthesized using a 1:1 mixture of the biotin derivative **21** and either one of the BODIPY derivatives **17** and **18** (Figure 18).

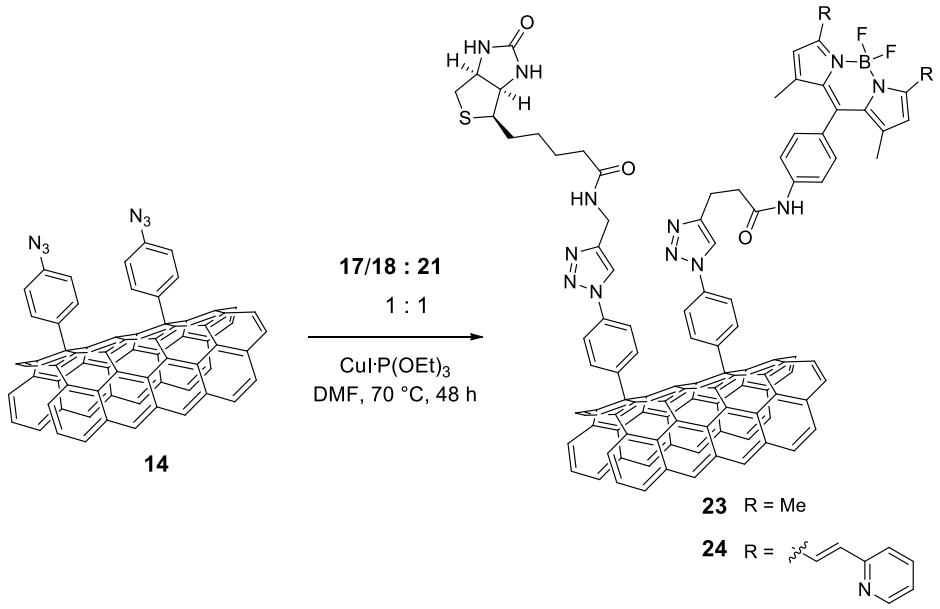

Figure 18. CuAAC reaction of ox-MWCNT **14** with a 1:1 mixture of compounds **17**/**21** or **18**/**21** to afford compounds **23** and **24**, respectively.

The presence of boron in the BODIPY derivatives, as well as sulphur in biotin, allowed the use of ICP-AES analyses to evaluate their content and the functionalization degree of MWCNTs (see Table 4).

entry	CNT	Boron (mg/g)	Boron (mmol/g)	Sulphur (mg/g)	Sulphur (mmol/g)
1	**19**	9.76	0.90	-	-
2	**20**	3.05	0.28	-	-
3	**22**	-	-	4.26	0.13
4	**23**	7.37	0.68	5.12	0.16
5	**24**	0.99	0.09	1.55	0.05

Table 4. Content of Boron and Sulphur of MWCNT **19**, **20**, **22**, **23** and **24** by ICP-AES analysis.

The nanotubes **19**, containing the BODIPY dye **17**, showed a good level of loading, although lower that that obtained with nanotubes **16** (see Table 3). Likely the bulkiness of the BODIPY derivative hampers an efficient cycloaddition process. The trend of a decrease of loading is confirmed with the bulkier dye **18** and biotin **21** (entries 2 and 3, Table 4). Regarding the doubly decorated compounds **23** and **24**, whereas the functionalization degree is still relatively high for **23** (entry 4, Table 4), it becomes roughly ten times lower in the CNT **24** (entry 5, Table 4). Albeit a detailed study to maximize the loading of the material was not performed, simple variations of the reaction conditions did not afford a higher loading. Nevertheless, both compounds **23** and **24** revealed a sufficient loading useful for the biological tests (see below).

The UV and fluorescence spectra, performed in DMF solution, confirmed the presence of the fluorescent dye on the CNTs walls of **19**-**24** (Figure 19).

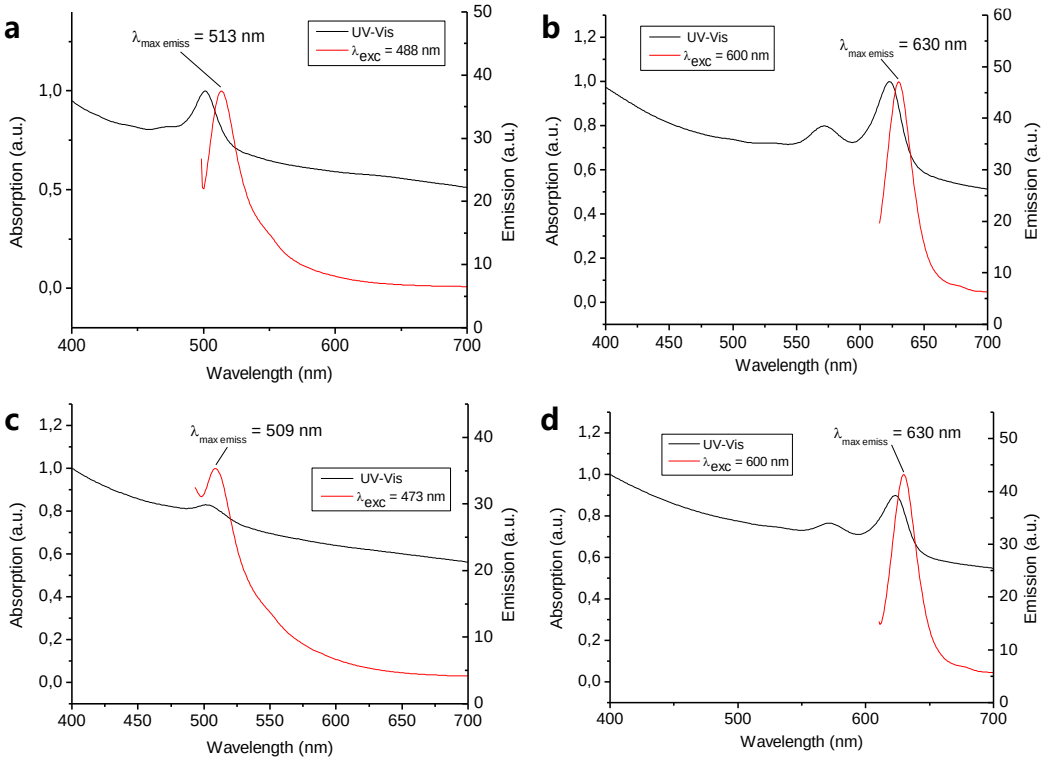

Figure 19. UV-Vis absorption (black) and fluorescence emission (red) spectra of compounds **19**, **20**, **23**, **24**, (respectively a, b, c, d) performed in DMF.

2.3 Biological tests

A series of biological tests were performed to establish the internalization of the prepared nanotubes **19** and **20** by MCF-7 cells and, eventually, to measure the toxicity of the compounds. Cell cultures have been incubated with ox-MWCNT **19** and **20** for 24h, and two cytofluorimetric analyses showed a net increase in the fluorescence (see experimental section). Furthermore, the uptake of ox-MWCNTs **20** was then evaluated through confocal microscopy, and a good incorporation of fluorescent material inside the cytoplasm of cells was observed (see Figure 20). It still appreciable a sharp prevalence of the fluorescent material in the cytoplasm respect to the nucleus.

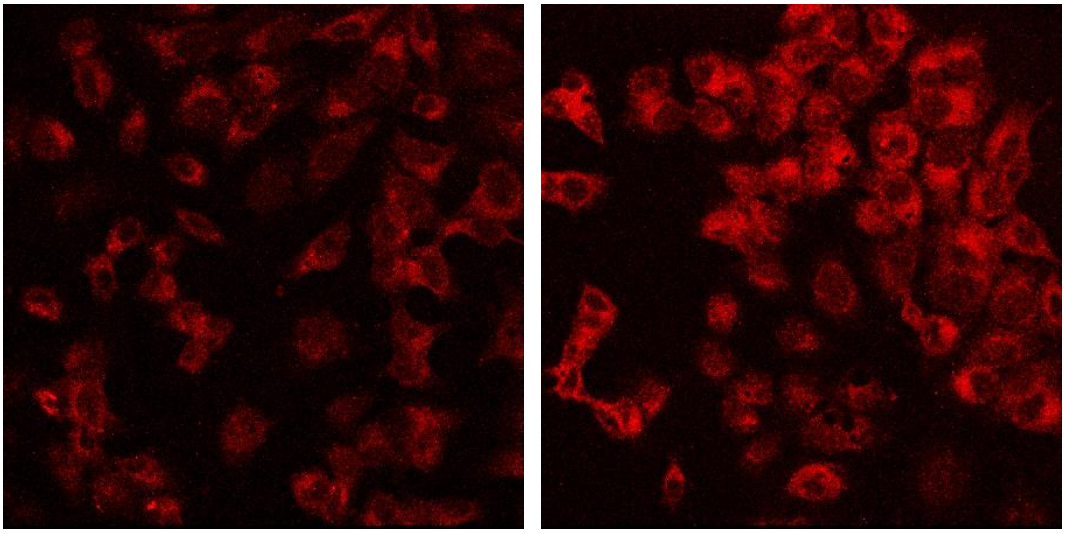

Figure 20. Confocal images of a MCF-7 cell culture after incubation with CNTs **20**. Two experiments have been conducted: with 5 μg/ml (left), and with 10 μg/ml of material (right).

The synthetic approach used for the decoration of CNTs afforded highly fluorescent materials able to permeate efficiently the cellular membrane of the model tumor cells. To evaluate the influence of the biotin residues introduced on nanotubes towards the internalization process, the CNTs **19** and **23** were tested in two parallel experiments under the same conditions. After incubation, the cellular samples were washed repeatedly, counted, and lysed. Then, the respective amounts of boron of the

samples were evaluated through ICP-AES analysis (Table 5). As blank, an ICP analysis was also performed on a culture grown in absence of nanotubes. To obtain the average quantity of CNTs per cell has been taken in account the number of cells (around 10^6 cells) in the sample and the boron content per milligram of CNT.

Data from ICP	Compound **19**	Compound **23**	Internalization ratio **23** : **19**
mg Boron/Cell	$3.5 \cdot 10^{-11}$	$4.3 \cdot 10^{-10}$	16.9
mg CNT/cell	$4.03 \cdot 10^{-9}$	$6.8 \cdot 10^{-8}$	

Table 5. ICP data show the boron content of lysed cells, the respective quantity of internalized CNTs **23** and **19**.

The data in Table 5 show the clear role of biotin in favoring the internalization process. Biotin and BODIPY decorated CNTs are internalized one order of magnitude better than simply BODIPY decorated CNTs.

Once the internalization and the role of the selector was assessed, a series of toxicity tests were performed on nanotubes with BODIPY (**19**) and with both biotin and BODIPY (**23**) to evaluate the toxicity of the carrier system alone. MCF-7 cells were incubated in the presence of growing doses of nanotubes and analyzed through MMT assay to evaluate the cell viability. The results are reported in Figure 21 and show no appreciable decrease in the cellular viability.

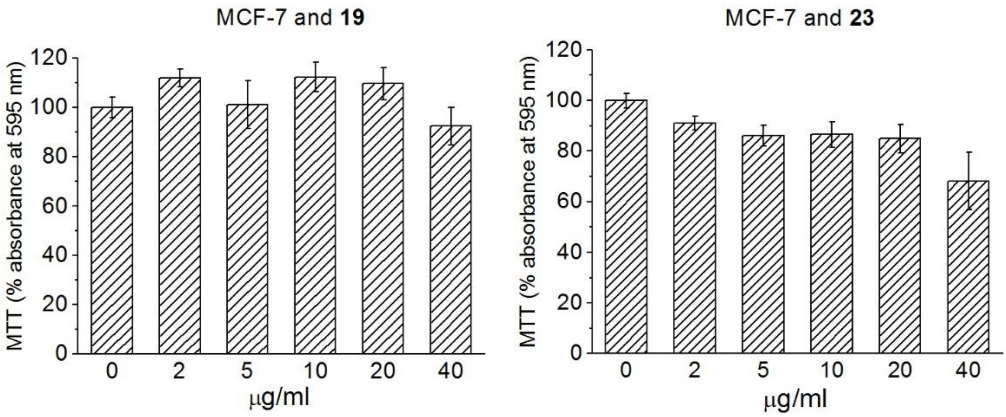

Figure 21. MMT vitality assays of MCF-7 incubated with different concentration of nanotubes **19** and **23**, no appreciable decrease in the cellular viability is observed.

2.3.1 Loading of doxorubicin on the carrier.

Once assessed that the decorated CNTs are non-toxic towards MCF-7 cells, biotin and BODIPY decorated CNTs were loaded with doxorubicin (DOX). The loading of DOX on carbon nanotubes was performed exploiting the π-stacking interaction between the aromatic surface of CNTs and the aromatic rings of doxorubicin. Stirring an aqueous dispersion of CNTs **24** and doxorubicin afforded the desired complex **25** (see Figure 22).

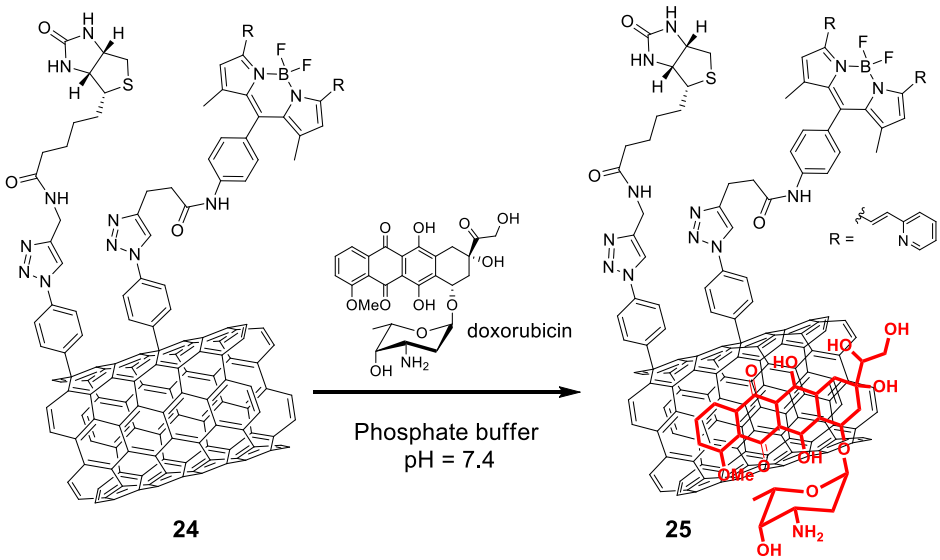

Figure 22. Loading of doxorubicin on biotin- BODIPY-decorated CNTs **24**.

The grafting of doxorubicin on CNTs **24** is reversible and the equilibrium is strictly dependent from pH, since the protonation of the glycosidic amino group renders doxorubicin more hydrophilic. To ensure a good loading of drug on CNT and reduce the risk of decomposition of doxorubicin, likely in alkaline conditions,[43] a phosphate buffered solution with a pH = 7.4 was used. To evaluate the efficiency of the loading reaction, after stirring overnight the doxorubicin and the CNTs dispersion, the phosphate buffer solution was filtered off and the solid material was washed repeatedly with new phosphate solution to remove the free drug. A sample of the solid filtrate was dispersed in a buffer solution and an UV-visible spectrum registered. From Figure 23 is clearly observable the presence of doxorubicin in the CNTs **25**.

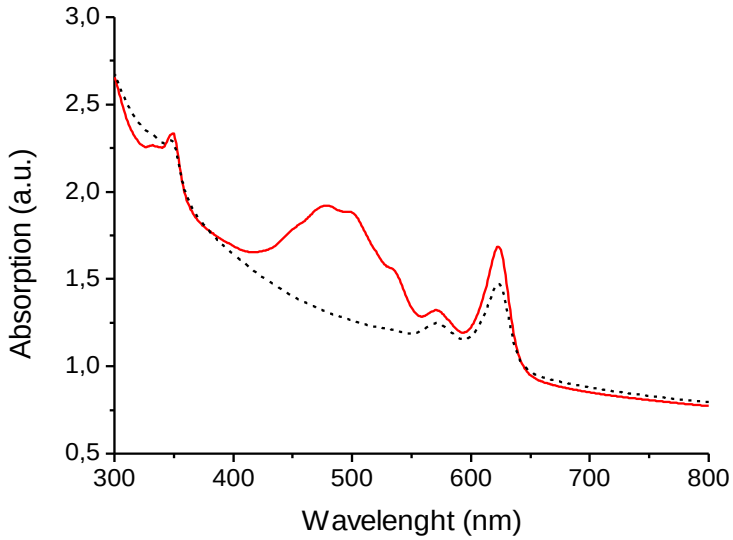

Figure 23. UV-visible spectra of compound **25** (solid line), and **24** (dashed line).

The quantitative data were then obtained through a calibration curve of doxorubicin in buffer solution. The DOX loading on nanotubes **25** is reported in Table 6, showing the large amount of drug attached on ox-MWCNTs compared to the quantity used for the loading reaction.

Load of DOX on nanotubes	
DOX/CNT (g/g)	DOX attached
0,60	90,6 %

Table 6. Loading and percentage of DOX attached on MWCNT **25**. The DOX attached is referred to the total amount of DOX added in the loading reaction.

To monitor the release over time of doxorubicin from CNT, nanotubes were stirred for 120 h in a buffer solution, centrifuging and renewing periodically the solvent. The amount of drug released at each wash was measured, as before, by UV-visible analysis of the supernatant solution. The drug release profile was observed at two different pH: 7.4 and 5.3 (Figure 24), and the collected data are summarized in Table 7.

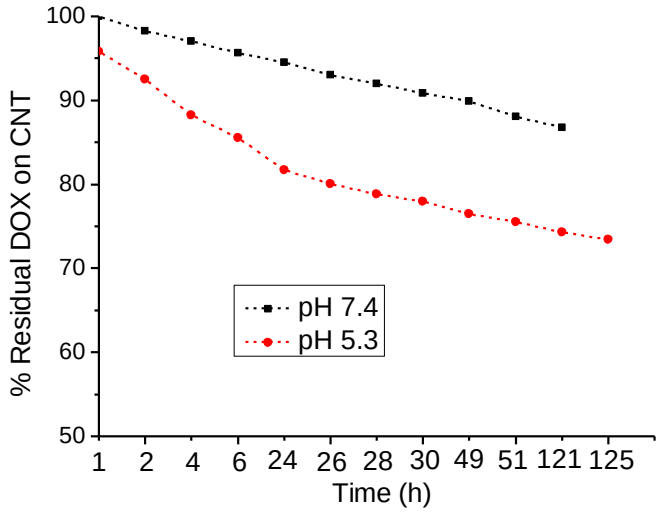

Figure 24. Release profiles of doxorubicin from CNTs **25** in buffer phosphate solution at different pH.

	Release of DOX	
	g DOX released / g CNT	DOX released / DOX loaded
pH 7.4	0,16	13,2%
pH 5.3	0,32	26,5%

Table 7. Total value of doxorubicin released from CNTs **25**.

The two different profiles show the strict dependence of the complexation equilibrium on pH. Because it is known that cancer tissues show a higher level of acidity compared to normal tissues,[44] very high acidity conditions were chosen to underline the pH-dependent detaching mechanism of doxorubicin from carbon nanotubes.

The cytotoxicity of the DOX/BODIPY/biotin decorated carbon nanotubes, was then tested to measure the efficiency of the whole drug delivery system. Cells viability was assessed using the same protocol adopted for the carrier alone (see paragraph 3.2) and compared with that of carrier without drug (Figure 25).

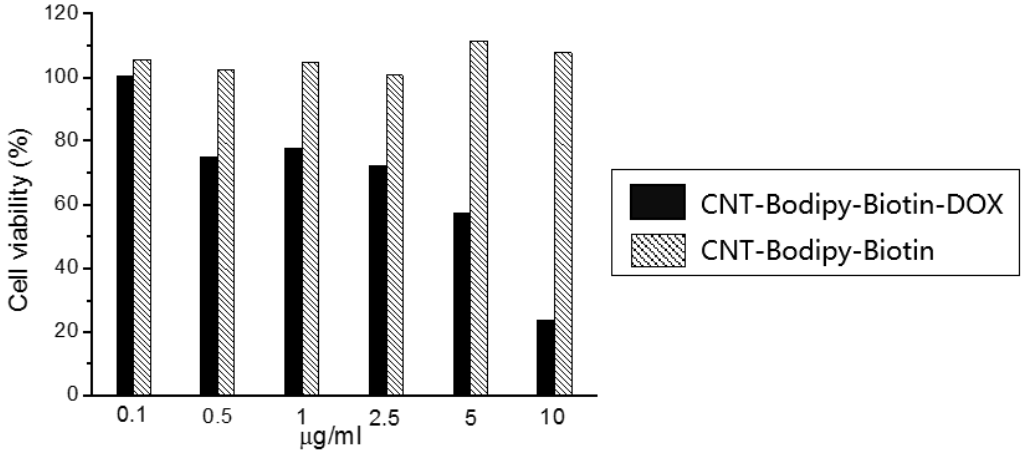

Figure 25. The cytotoxic effect of the complete system (**25**) compared with the carrier without drug (**24**).

2.3.2 Final tests in vitro *on the ultimate drug delivery system*

In the last step the fluorescent probe is no longer required and the system was evaluated directly in terms of cytotoxic efficiency. The final drug delivery system was compared with free doxorubicin and with an analogous without biotin to complete the investigations about the role of the selector. Biological experiments have been performed on CNTs functionalized only with biotin (CNT-biotin, compound **22**, Figure 17), on CNTs functionalized with biotin and doxorubicin (CNT-biotin-DOX, compound **26**), and on CNTs loaded only with doxorubicin (CNT-DOX, compound **27**). The biological tests were carried out in the same conditions of the previous (incubation time 24h). The preparation of these compounds as well as the details on the biological experiments are described in the experimental section. To homogenize the results, the quantity of sample incubated is weighted by the relative load of doxorubicin. The structures of **26** and **27** with the relative loads of DOX are depicted in Figure 26. The overall results are explicated in Figure 27.

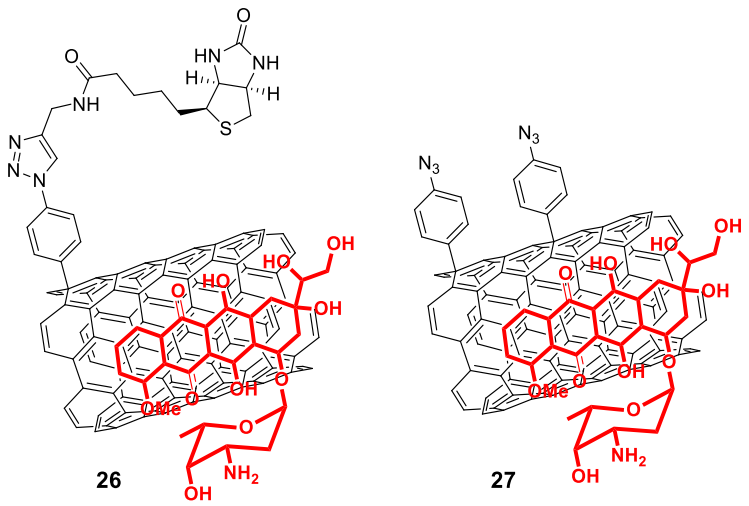

DOX load = 0.57 g/g DOX load = 0.50 g/g

Figure 26. Structures of DOX decorated CNT with the relative load of doxorubicin. Data on cytotoxic efficiency are reported below.

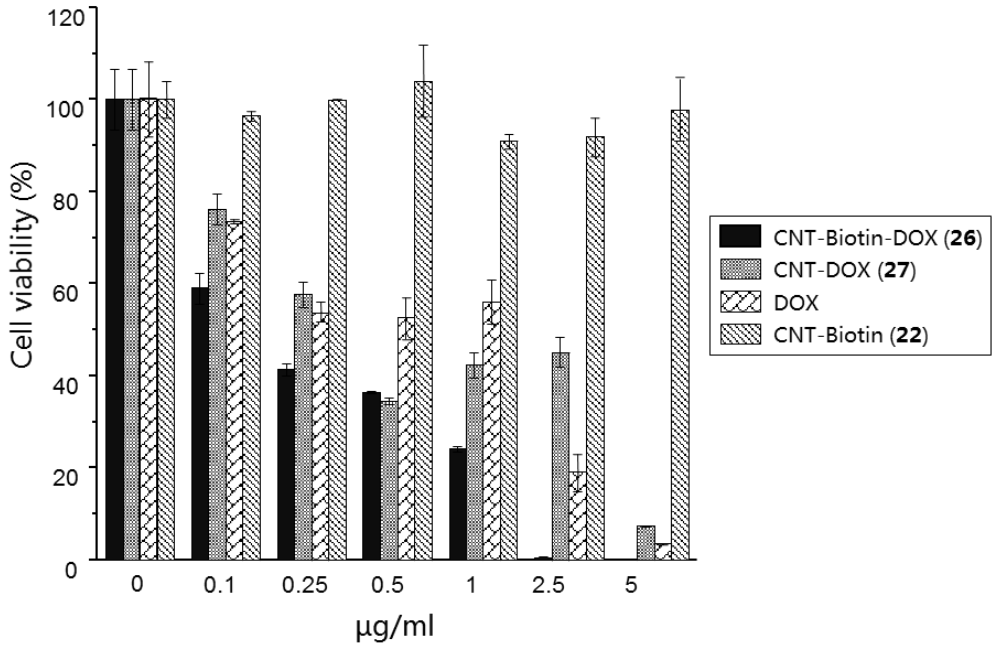

Figure 27. The differences of cytotoxicity between CNT biotin-decorated and DOX loaded respect to simply MWCNT DOX loaded or free DOX.

The data show clearly the increased cytotoxic effect of biotin-decorated nanotubes respect to the simple drug-loaded nanotubes, but also respect to free doxorubicin. In both comparisons, the major cytotoxic effect can be ascribed to the role of biotin-decorated carbon nanotubes as vector in the drug internalization process. As blank, to ensure again the absence of toxicity of the system in absence of the drug, biotin-MWCNT **22** was tested again. It is worth to be noted that delivery of doxorubicin through the CNT-biotin drug-delivery system reduces sensibly the amount of doxorubicin required for the same cytotoxic effect. Therefore, for the complete system **26**, on the base of the data showed in Figure 27, a preliminary value of IC_{50} can be estimated around 0.2 µg/ml. The cytotoxicity of this drug delivery system is higher than the drug alone, currently adopted for the tumor treatments; this is a positive result about the possibility to boost the cytotoxicity of doxorubicin by the use of carbon nanotubes as vectors.

A last series of cytotoxicity test was performed on MCF-7 cancer cells to observe the effect of exposure to high concentration of product for a short time

(Figure 28). In this case, MCF-7 cells have been incubated with 50 µg/ml of substance for 1 hour, then washed, and let to grow in a normal culture medium. After 48 and 72 hours, MTT vitality assays were performed as usually.

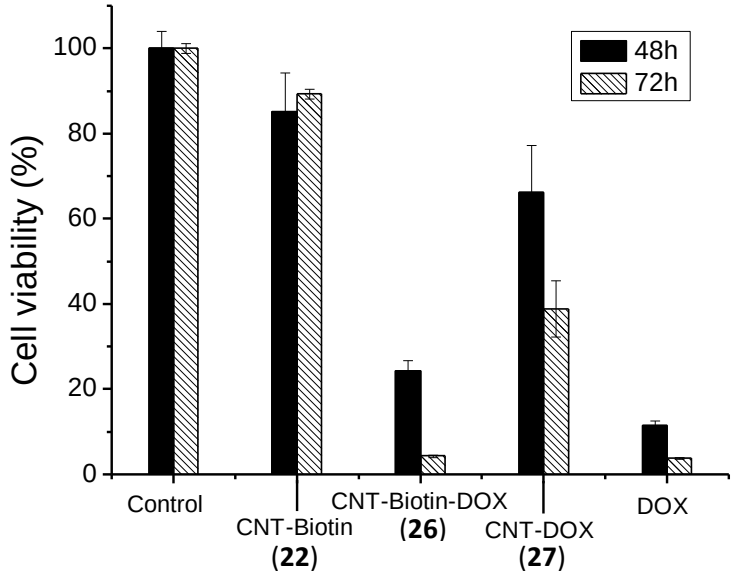

Figure 28. Test of toxicity at high concentration of sample for short time, the conditions are the same for all samples: 50 µg/ml of substance for 1 hour of exposition.

The results of this further series of tests show a behavior analogous to the previous test, confirming the trend of the toxicity previously observed.

2.3.3 In vivo *study*

On the base of the encouraging results so far obtained *in vitro*, the work has progressed with the biological tests *in vivo*. Tests have been performed on nude mice subcutaneously injected with MCF-7 cancer cells. 30 days after the injection, the tumor mass reached the dimension of 5 mm and the treatments have been started. The animals were divided in three groups and subjected, once a week, for 21 days, to a tail injection (200 µL/mouse) of the compounds. The first group was treated with CNT-biotin-DOX (compound **26**), the second with pure DOX, and the third with CNT-biotin (compound **22**). The quantity of sample administrated to the mice is weighted

by the relative load of doxorubicin, and amount to 5 mg of DOX per Kg of animal weight. The tumors sizes were measured with caliber every week and are reported in mm^3 in Figure 29.

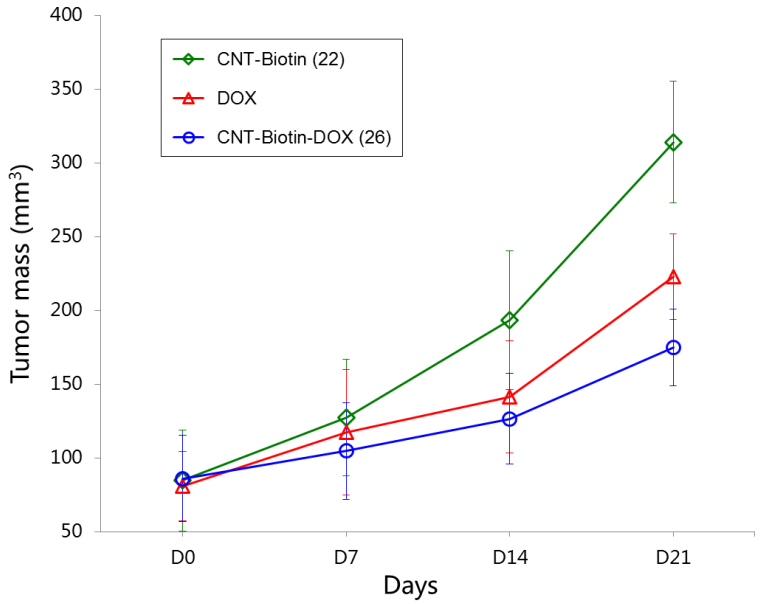

Figure 29. Evolution of the tumor size according to the different treatments.

At day 22 euthanasia have been performed and the tumors masses were excised and weighted. The results of the different treatments are reported in Figure 30 (photography of the excised tumors) and Figure 31 (weight of the tumors).

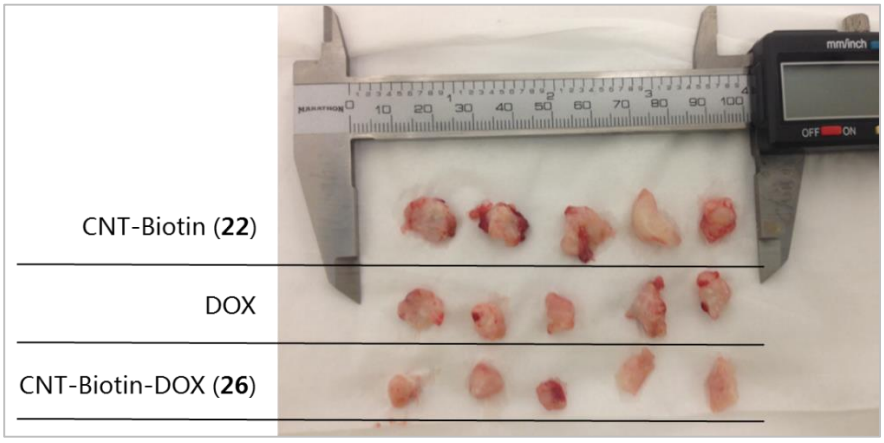

Figure 30. Photography of the tumors excised at day 22 of the treatment. The differences between the various treatments are appreciable.

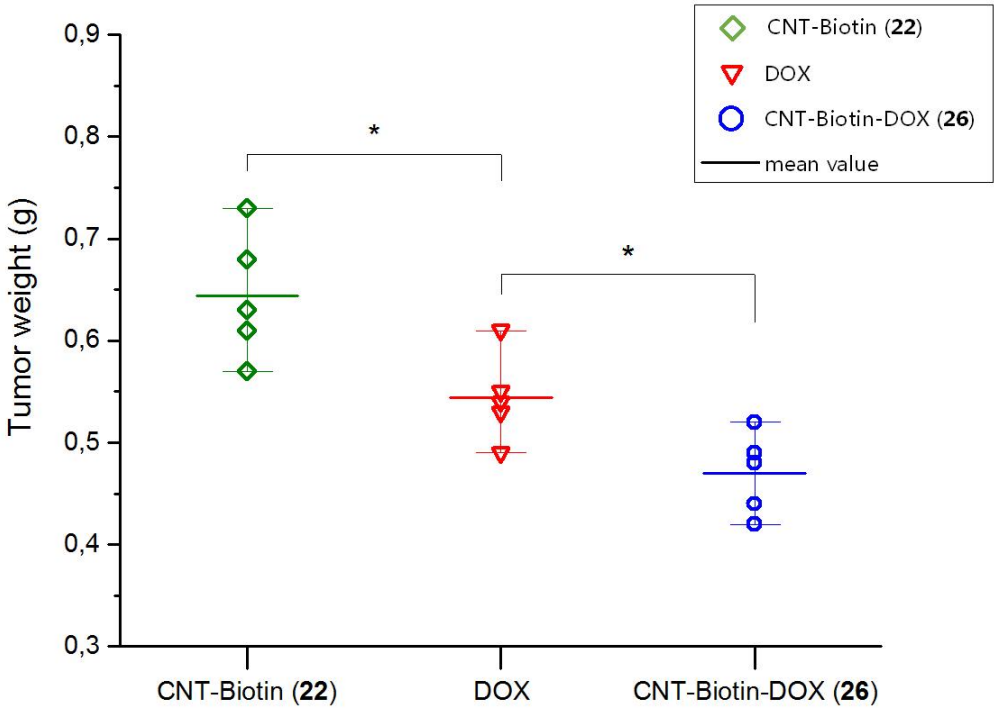

Figure 31. Weight of the tumor masses according to the different treatments, (*) *t*-tests indicate significant differences between the experiments at $p<0.05$

As can be observed from these pictures, the difference between tumors treated with DOX and tumors treated with the DOX on nanotubes **26** is easily appreciable. Immunohistochemistry assays were also performed on paraffin embedded tumors. The samples were stained with marker of proliferation Ki67 and with H&E (Figure 32); the microscopy images show the strong reduction in the proliferation of tumor treated with doxorubicin on nanotubes respect to the one treated with free doxorubicin.

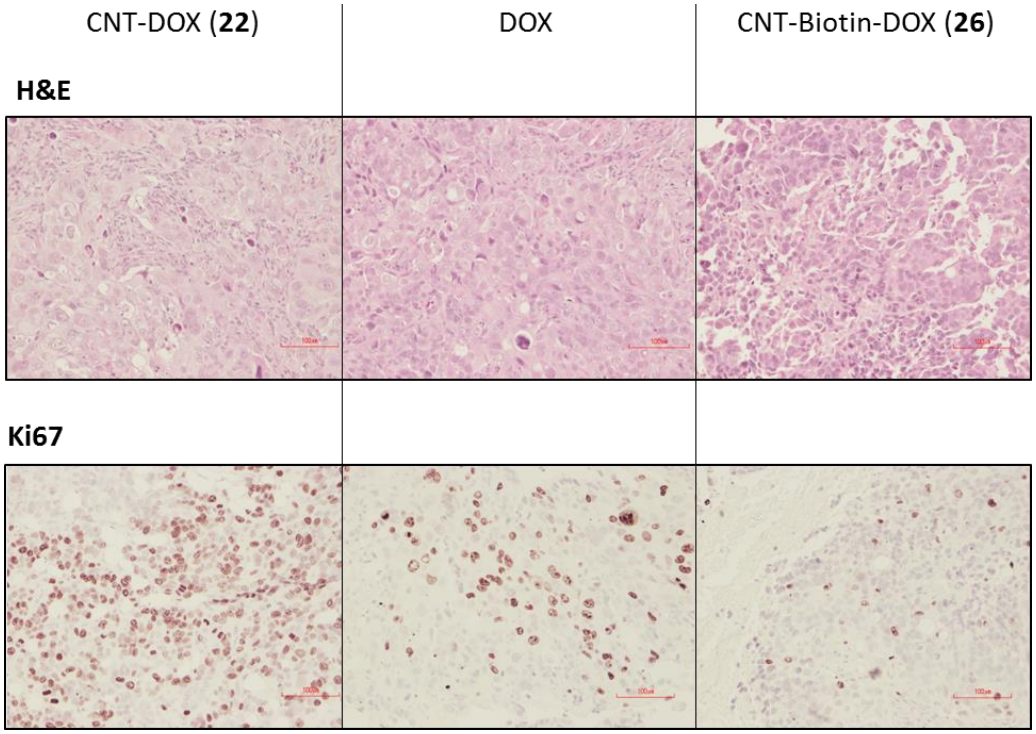

Figure 32. Paraffin embedded tumor tissue stained with H&E and Ki67 (bright field microscopy images). The lowest proliferation of cancer cells is clearly observable in the treatments with nanotubes-delivered doxorubicin (compound **26**).

Summarizing the data obtained *in vivo*, a net increase of the drug effect was founded, confirming the positive results of the *in vitro* experiments.

The mayor anticancer activity of the doxorubicin administrated through this drug delivery system respect to free drug was founded. This consolidate the way to improve the existing anticancer therapies by the use of modified carbon nanotubes as drug delivery systems.

Concluding remarks

A new level of cytotoxic efficiency was found for doxorubicin, respect to the free drug, adopting decorated multiwalled carbon nanotubes as drug delivery system. Although the literature flourishes with new examples of drug delivery system based on carbon nanotubes, a direct comparison of our data, related to the use of CNT, doxorubicin and MCF-7 cell lines, restrict the choice to few articles. In particular, a good comparison is offered by the extensive work by Jain[45] and co-workers in which the authors reports the IC_{50} of several functionalized CNT loaded with doxorubicin towards MCF-7 cell lines. The IC_{50} values reported ranged from 5.6 to 0.6 μg/mL.

In the present PhD work, Figure 27, shows that the plausible value of IC_{50} for this DOX drug delivery system, stands between 0.1 and 0.25 μg/mL. The *in vivo* study, although preliminary, confirms the good performances obtained and support the prosecution of the work.

Finally, it should be stressed the simplicity of the approach: the oxidation of the MWCNTs and their derivatization with azido aniline afforded an easy tunable platform for further decorations. The materials obtained are easily dispersible in water and, when higher concentration are needed, in DMSO/Water. This kind of approach allows the covalent grafting of polar drugs (through simple modifications and CuAAC reaction) as well as the supramolecular complexation of hydrophobic drugs likes doxorubicin. Such activity is actually ongoing in our laboratories

Summarizing the overall results of this PhD project, all the starting goals have been fulfilled: a new carbon nanotube-based drug delivery system was designed, developed, characterized and extensively tested. The biological tests showed positive results: a sharp increment of the chemotherapic effect of the drug was achieved. On the base of these solid data, the work has progressed with tests on animal models. The *in vivo* results have been conclusive too, confirming the data obtained *in vitro*; a significant reduction of the tumoral mass respect to the administration of the free drug was observed. These outcomes have evidenced the clear role of the drug delivery system developed, consolidating the comprehensive results.

Perspectives

Although a wide work of biological testing and chemical characterizations have been performed on the prepared drug delivery system, in the aim to obtain chances to develop such a pharmaceutical product, more stringent, and more extensive characterizations are required. For instance, concerning the biological aspect, an exhaustive study of the pharmacodynamics and pharmacokinetics must to be performed. On the other hand, a strict definition of all the chemical species involved - in terms of molecules, nanostructures, and supramolecular aggregates - is mandatory.

The fulfillment of these aims means also to establish and consolidate a *proof of concept* about the working of the system. Once established the proof of concept, the developed system gains a high added value, since is proven its ability to work in a real biological environment. This allows to continue with more chances the drug development process and also to try, with more awareness, a proper tuning of the properties of the delivering platform developed, as well as to test other drugs to be carried on, or new selectors, in order to address different type of cancer.

3. Experimental

3.1 Materials and methods

All reagents, whose synthesis is not described, have been purchased and used, if not specified, without further purification. Compounds, **13**,[46] **15**,[47] **21**,[48] and BODIPY **A**[22,23] were synthesized according to respective literature procedures. The catalyst CuI•P(OEt)$_3$ was synthesized according to ref.[49] but using toluene as solvent instead of benzene. Multi walled carbon nanotubes were purchased from Sigma-Aldrich (Lot. n. MKBH7743V). Yields refer to chromatographically and spectroscopically pure compounds. R_f values, refer to silica gel plates (0.25 mm, Merck Silica gel 60 F_{254}) or aluminum oxide gel plates (0.25 mm, Merck Aluminum oxide 150 F_{254}) as specified, and obtained using the same eluent as in the separation of the compound by flash column chromatography. NMR spectra were recorded on a Varian Gemini 200 and on Varian Mercury 400 at room temperature. Chemical shifts (δ) were reported in parts per million (ppm) relative to residual solvent peaks rounded to the nearest 0.01 for proton and 0.1 for carbon (reference: $CHCl_3$ [^{1}H: 7.26, ^{13}C: 77.2], DMSO [^{1}H: 2.50, ^{13}C: 39.5], CH_3OH [^{1}H: 3.35, ^{13}C: 49.3]. Coupling constants (*J*) were reported in Hz to the nearest 0.1 Hz. Peak multiplicity was indicated as follows: s (singlet), d (doublet), t (triplet), q (quartet), m (multiplet) and br (broad). Thermogravimetric analyses (TGA) were performed under N_2 atmosphere (50 mL min^{-1}) on an EXSTAR thermogravimetric analyzer (TG/DTA) Seiko 6200 coupled with a ThermoStar GSD 301T (TGA-MS) for MS analysis of volatiles. The ICP multielemental analysis were made using an Optima 2000 Perkin Elmer Inductively Coupled Plasma (ICP) Optical Emission Spectrophotometry Dual Vision after acid mineralization. MS Spectra were recorded using LCQ-Fleet Thermo Scientific Electron Spray Ionization (ESI); spectra were recorded on 10^{-4}-10^{-5} M samples in HPLC grade MeOH. Infrared spectra were recorded on a Perkin-Elmer FT-IR 881 spectrometer. IR data are reported as frequencies in wavenumbers (cm^{-1}). Elemental analyses were performed with a Perkin-Elmer 240 analyzer and a CHN-S Flash E1112 Thermofinnigan analyzer. UV-

visible spectra were registered using a Varian Cary 4000 Uv-vis spectrophotometer using a 1 cm cuvette. Fluorescence spectra were registered using a FP750 spectrofluorimeter using a 1 cm cuvette. UV and fluorescence spectra of the dyes were registered using a 10^{-5} M solution of the compound in the reported solvent. Centrifugations were performed on a Hettich Universal 320 centrifuge at 1400 *g* and on a Labnet 24D Spectrafuge at 15000*g*, for the time stated.

3.2 Preparation and characterization of the compounds

8-(4-Azidophenyl)-1,3,5,7-tetramethyl-4,4-difluoro-4-bora-3a,4a-diaza-s-indacene (5).

Compound **5** was obtained with a multistep synthesis. Compound **3** was obtained following the mechanochemical procedure reported in reference 22. Compound **4** was obtained following the procedure reported in reference 21. Transformation of compound **4** into **5** was performed following procedure reported in reference 23 and 24.

8-(4-Azidophenyl)-1,7-dimethyl-3,5-distyryl-4,4-difluoro-4-bora-3a,4a-diaza-s-indacene (7a). See reference 24.

8-(4-Azidophenyl)-1,7-dimethyl-3,5-bis-[2-(4-phenolyl)ethenyl]-4,4-difluoro-4-bora-3a, 4a-diaza-s-indacene (7b)

And

8-(4-Azidophenyl)-1,5,7-trimethyl-3-[2-(4-phenolyl)ethenyl]-4,4-difluoro-4-bora-3a,4a-diaza-s-indacene (8b).

4-Azidophenyl-Bodipy (**5**) (80 mg, 0.22 mmol) and 4-hydroxybenzaldehyde (108 mg, 0.88 mmol, 4 eq.) were dissolved in anhydrous CH_3CN (10 mL), with pyrrolidine (109 µL, 1.31 mmol, 6 eq.) and acetic acid (75 µL, 1.31 mmol, 6 eq.). Activated molecular sieves (4 Å, 200 mg) were added. The mixture was stirred at 80 °C under N_2 atmosphere. After few minutes a quick change in the color of the mixture is observed, from red to dark blue and TLC on silica (CH_2Cl_2/AcOEt 5:1), revealed the presence of a red spot (R_f = 0.83) and a blue one (R_f = 0.33). The reaction was monitored by TLC

and after 1 h was cooled to room temperature, filtered and the resulting solution diluted with AcOEt (50 mL). The organic phase was washed with aqueous HCl (3x50 mL, 0.05 M), brine (100 mL), dried over anhydrous Na_2SO_4, filtered and concentrated. The crude reaction mixture was purified by flash chromatography on silica, eluting first with CH_2Cl_2/AcOEt 11:1 until the first fraction was collected and then changing to CH_2Cl_2/AcOEt 9:2 to collect the second fraction. The two fractions were concentrated and dried to give compound **7b** (43 mg, 34%) and compound **8b** (23 mg, 22%).

Compound 7b: ^{1}H NMR (CD_3OD) δ = 7.50 (d, *J* = 8.8 Hz, 4H), 7.49 (d, *J* = 16.0 Hz, 2H), 7.38 (d, *J* = 8.4 Hz, 2H),7.31 (d, *J* = 16.0, 2H), 7.26 (d, *J* = 8.4 Hz, 2H),6.84 (d, *J* = 8.8 Hz, 4H), 6.74 (s, 2H), 1.51 (s, 6H) ppm. $^{13}C\{^1H\}$ NMR (CD_3OD) δ = 158.7, 152.9, 141.5, 141.2, 136.3, 132.8, 131.7, 130.3, 128.7, 128.3, 119.4, 117.2, 115.7, 115.5, 53.4, 13.6 ppm. UV-Vis (nm, CH_2Cl_2): 360, 595, 641; (nm, DMF): 378, 601, 652; (nm, H_2O): 379, 612, 673. Fluorescence (nm, DMF): 671; (nm, H_2O): no emission peaks are observed. IR ($CDCl_3$): 3608, 2971, 2927, 2854, 2127, 2099, 1603, 1512, 1256, 1199, 1162 cm^{-1}. MS calc. for $C_{33}H_{26}BF_2N_5O_2$: 573.21. Found (ESI): m/z (%) = 572.29 (27) $[M-H]^+$. El. Anal. calc. for $C_{33}H_{26}BF_2N_5O_2$: C, 69.12; H, 4.57; N, 12.21. Found C, 69.43; H, 4.26; N, 12.10.

Compound 8b: ^{1}H NMR ($CDCl_3$): δ = 7.52 (d, *J* = 16.4 Hz, 1H), 7.45 (d, *J* = 8.4 Hz, 2H), 7.30 (d, *J* = 8.8 Hz 2H), 7.19 (d, *J* = 16.4 Hz, 1H), 7.17 (d, *J* = 8.8 Hz, 2H), 6.83 (d, *J* = 8.4 Hz , 2H), 6.59 (s, 1H), 6.02 (s, 1H), 2.59 (s, 3H), 1.47 (s, 3H), 1.43 (s, 3H) ppm. $^{13}C\{^1H\}$ NMR ($CDCl_3$) δ = 157.1, 155.0, 153.9, 142.7, 142.2, 141.2, 139.0, 138.3, 136.8, 133.1, 131.8, 130.1, 129.5, 121.4, 119.8, 119.1, 117.9, 116.9, 116.0, 29.9, 15.1, 14.8. UV-Vis (nm, DMF): 346, 538, 576. Fluorescence (nm, DMF): 592. IR ($CDCl_3$): 3584, 2966, 2928, 2853, 2125, 2100. 1731, 1603, 1543, 1500, 1301, 1269, 1195, 1160 cm^{-1}. MS calc. for $C_{26}H_{22}BF_2N_5O$: 469.19. Found (ESI): m/z (%) = 468.19 (100) $[M-H]^+$. Anal. calc. for $C_{26}H_{22}BF_2N_5O$: C, 66.54; H, 4.73; N, 14.92. Found C, 66.23; H, 4.96; N, 14.70.

8-(4-Azidophenyl)-1,7-dimethyl-3,5-bis-[2-(pyridin-2-yl)ethenyl]-4,4-difluoro-4-bora-3a,4a-diaza-s-indacene (7c)

And

8-(4-Azidophenyl)-1,5,7-trimethyl-3-[2-(pyridin-2-yl)ethenyl]-4,4-difluoro-4-bora-3a,4a-diaza-s-indacene (8c).

4-Azidophenyl-Bodipy (**5**) (100 mg, 0.27 mmol) and picolinaldehyde (104 µL, 1.09 mmol, 4 eq.) were dissolved in anhydrous CH_3CN (14 mL), with pyrrolidine (137 µL, 1.64 mmol, 6 eq.) and acetic acid (94 µL, 1.64 mmol, 6 eq.). Activated molecular sieves (4 Å, 200 mg) were added. The mixture was stirred at 80 °C under N_2 atmosphere. After few minutes a quick change in the color of the mixture is observed, from red to deep purple and TLC on alumina (eluent CH_2Cl_2), revealed the presence of a red spot (R_f = 0.88) and a blue one (R_f = 0.49). After 1 h the mixture was cooled to room temperature, filtered and diluted with CH_2Cl_2. The organic layer was washed with saturated $NaHCO_3$ solution (3x25 mL), brine (35 mL), dried over anhydrous Na_2SO_4, filtered, and evaporated. The crude reaction mixture was purified by flash chromatography on alumina, eluting first with CH_2Cl_2/pet. et. 1:1 until the first fraction was collected and then changing to pure CH_2Cl_2 to collect the second fraction. The two fractions were concentrated and dried to give compound **7c** (54 mg, 37% yield) and compound **8c** (22 mg, 18% yield).

Compound 7c: ^{1}H NMR ($CDCl_3$) δ = 8.75 (d, J = 1.6 Hz, 2H), 8.55 (d, J dd, 4.7, 1.6 Hz, 2H), 8.03 (d, *J* = 8.0 Hz, 2H), 7.77 (d, J = 16.4 Hz, 2H), 7.36-7.18 (m, 8H), 6.68 (s, 2H), 1.52 (s, 6H) ppm. $^{13}C\{^1H\}$ NMR ($CDCl_3$) δ = 167.8, 152.2, 150.2, 149.7, 149.6, 148.6, 142.6, 141.3, 139.0, 134.9, 133.7, 133.1, 132.4, 132.2, 131.2, 129.0, 123.7, 123.5, 123.1, 121.0, 119.8, 118.2, 14.9. UV-Vis (nm, CH_2Cl_2): 347, 575, 624. Fluorescence (nm, CH_2Cl_2): 643. IR ($CDCl_3$): 3037, 2977, 2128, 2106, 1538, 1492, 1265, 1250 cm^{-1}. MS calc. for $C_{31}H_{24}BF_2N_7$: 543.38. Found (ESI): m/z (%) = 544.30 (100) $[M+H]^+$. El. Anal. calc. for $C_{31}H_{24}BF_2N_7$: C, 68.52; H, 4.45; N, 18.04. Found C, 68.74; H, 4.28; N, 18.10.

Compound 8c: ^{1}H NMR ($CDCl_3$) δ = 8.62 (d, *J* = 5.1 Hz, 1H), 7.98 (d, *J* = 16.5, 1H), 7.69 (m, 2H), 7.36-7.27 (m, 3H), 7.20-7.16 (m, 3H), 6.65 (s, 1H), 6.05 (s, 1H), 2.61 (s, 3H), 1.48 (s, 3H), 1.45 (s, 3H). $^{13}C\{^1H\}$ NMR ($CDCl_3$) δ = 154.2, 148.8, 142.8, 140.8, 140.2, 135.4, 134.2, 130.4, 128.8, 121.8, 121.7, 121.1, 120.7, 118.8, 117.1, 28.7, 13.8. UV-Vis (nm, CH_2Cl_2): 322, 522, 560. Fluorescence (nm, CH_2Cl_2): 568. IR ($CDCl_3$): 2927, 2856, 2129, 2102, 1543, 1500, 1195, 1160. MS calc. for $C_{25}H_{21}BF_2N_6$: 454.19. Found (ESI): m/z (%) = 455.17 (100) $[M+H]^+$. Anal. calc. for $C_{25}H_{21}BF_2N_6$: C, 66.10; H, 4.66; N, 18.50. Found C, 66.34; H, 4.38; N, 18.73.

8-(4-Azidophenyl)-1,7-dimethyl-3,5-bis-[2-(4-carboxyphenyl)ethenyl]-4,4-difluoro-4-bora-3a,4a-diaza-s-indacene (7d)

4-Azidophenyl-Bodipy (**5**) (60 mg, 0.16 mmol) and 4-formyl-benzoic acid (96 mg, 0.64 mmol, 4 eq.) were dissolved in anhydrous CH_3CN (10 mL), with pyrrolidine (133 µL, 1.6 mmol, 10 eq.) and acetic acid (55 µL, 0.96 mmol, 6 eq.). Activated molecular sieves (4 Å, 200 mg) were added. The mixture was stirred at 80 °C under N_2 atmosphere. After few minutes a quick change in the color of the mixture is observed, from red to dark purple and TLC on silica (CH_2Cl_2/MeOH 6:1), revealed the presence of a blue spot (R_f = 0.50). The reaction was monitored by TLC and after 1 h was cooled to room temperature, filtered and the resulting solution diluted with a methanolic solution of HCl (0.5 M, 10 mL). The solution was concentrated and the crude reaction mixture was purified by flash chromatography (CH_2Cl_2/MeOH 10:1 + 1% CH_3COOH, to afford compound **7d** (30 mg, 29%).

Compound 7d: ^{1}H NMR (DMSO, 400 MHz) δ = 8.02 (d, *J* = 8 Hz, 4H), 7.71 (d, *J* = 8 Hz, 4H), 7.66-7.60 (m, 4H), 7.51 (d, *J* = 8 Hz, 2H), 7.34 (d, *J* = 8 Hz, 2H), 7.06 (s, 2H) ppm; ^{13}C{^{1}H} NMR (DMSO, 100 MHz) δ = 172.27, 152.0, 144.8, 142.2, 138.8, 136.5, 130.6, 130.2, 130.0, 129.6, 129.1, 128.9, 128.3, 127.0, 119.36, 118.9, 21.2 ppm; Anal. calc. for $C_{35}H_{26}BF_2N_5O_4$: C, 66.79; H, 4.16; N, 11.13. Found C, 66.54; H, 4.38; N, 11.27.

Preparation of modified carbon nanotubes 9.

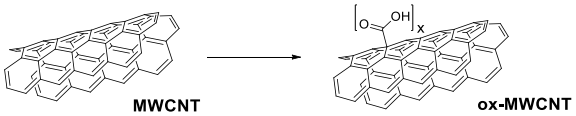

Oxidized carbon nanotubes (ox-MWCNT):[29] A mixture of commercially available MWCNTs (Sigma-Aldrich, O.D. x L. = 6-9 nm x 5 µm, carbon > 95%, CoMoCat©) (507 mg), H_2SO_4 96% (15 mL) and HNO_3 65% (5 mL) was stirred at 100°C for 30'. The suspension was then diluted with cold water and filtered on Teflon filter (Wathmann, pore size 0.2 µm). The residue was washed with water to neutral pH. The solid was dried at 80 °C under vacuum for 12 h affording a black powder (237 mg). IR (KBr, Figure 33): 3434, 2913, 2845, 1706, 1627, 1577, 1381, 1102 cm^{-1}. Elem. Anal. C, 78.8; N, 0.0; H, 0.37.

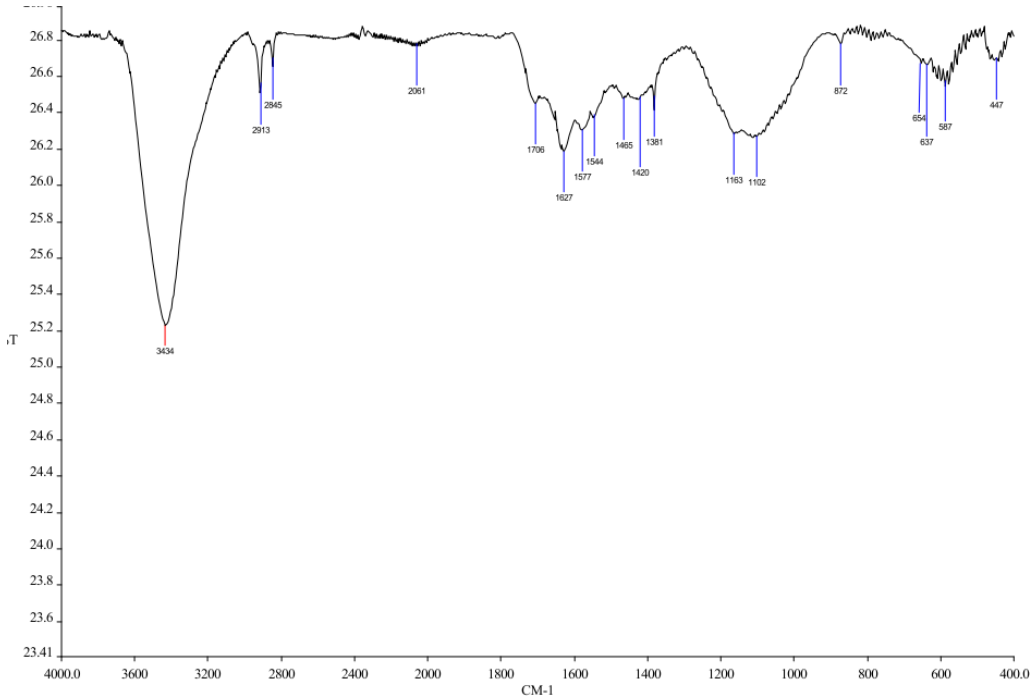

Figure 33. IR spectrum (KBr) of ox-MWCNTs

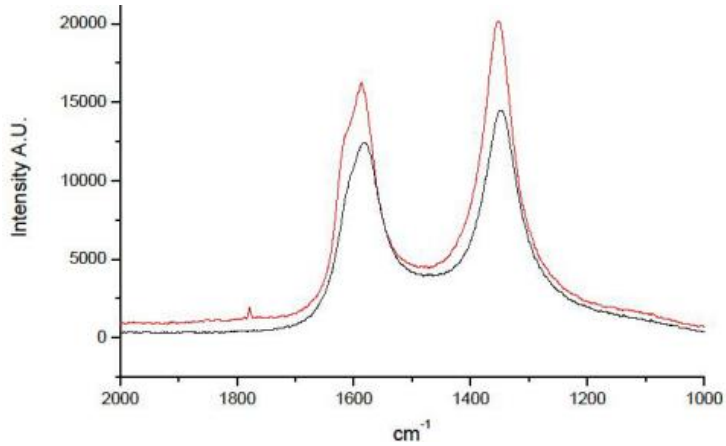

Figure 34. Raman spectra (μ-Raman, 514.5 nm) on pristine MWCNTs (black line) and ox-MWCNTs (red line)

The Raman spectra (Figure 34) show two main bands: the G band (1590 cm^{-1}) and the D band (1350 cm^{-1}). For pristine MWCNTs I_G/I_D = 0.85 while ox-MWCNTs I_G/I_D = 0.80. Furthermore, G band shows a shoulder due to the presence of defects on the π-system.

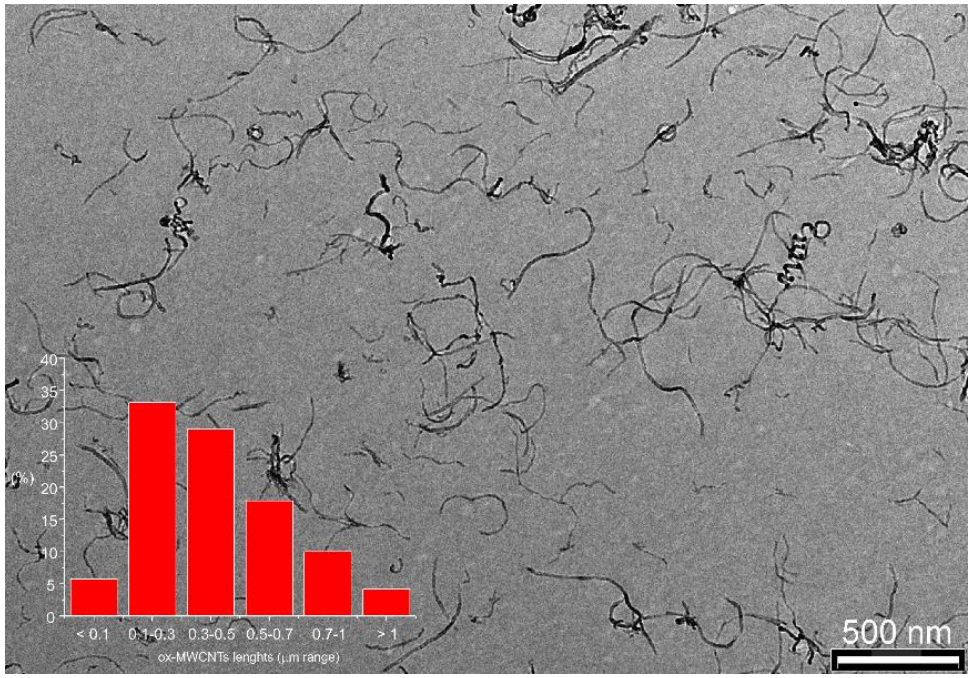

Figure 35.TEM image of ox-MWCNTs and statistical distribution of their lengths

The TEM analysis of the Ox-MWCNTs shows the integrity of the CNTs scaffold and their reduced lengths (from 5 µm of the pristine MWCNT).

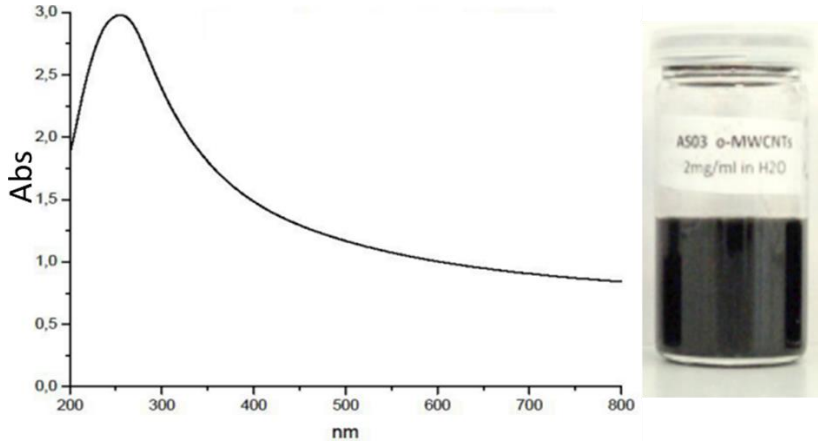

Figure 36. Uv absorption spectrum of ox-MWCNTs (H_2O, 0.02 mg mL^{-1}) and an image of a solution in water (2 mg mL^{-1})

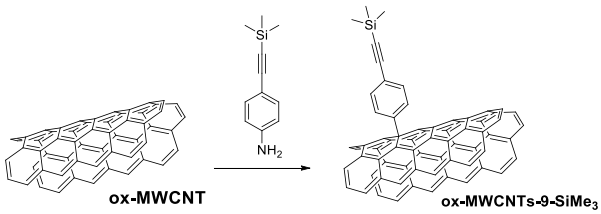

Tour reaction (synthesis of ox-MWCNTs-9-SiMe$_3$): The oxidized carbon nanotubes (20 mg) was dispersed in water (5 mL), the pH was adjusted to 11 with ammonia, 4-(2-(trimethylsilyl)ethynyl)aniline (76 mg, 0.40 mmol) and isopentylnitrite (66 µL, 0.49 mmol) were added and the dispersion was sonicated for 10'. The mixture was stirred at 80 °C under N_2 atmosphere for 48 h. The reaction mixture was then filtered on teflon filter (Whatmann, pore size 0.2 µm) washing with water, MeOH, and acetone until a colorless filtrate was observed for each solvent. The solid residue was dried under vacuum affording a black powder (27 mg). The IR spectrum shows a net peak at 2155 cm^{-1} related to the presence of the -C≡C-SiMe$_3$ group. IR (KBr, Figure 37): 3396, 2913, 2155, 1724, 1582, 1389, 1247, 1174 cm^{-1}.

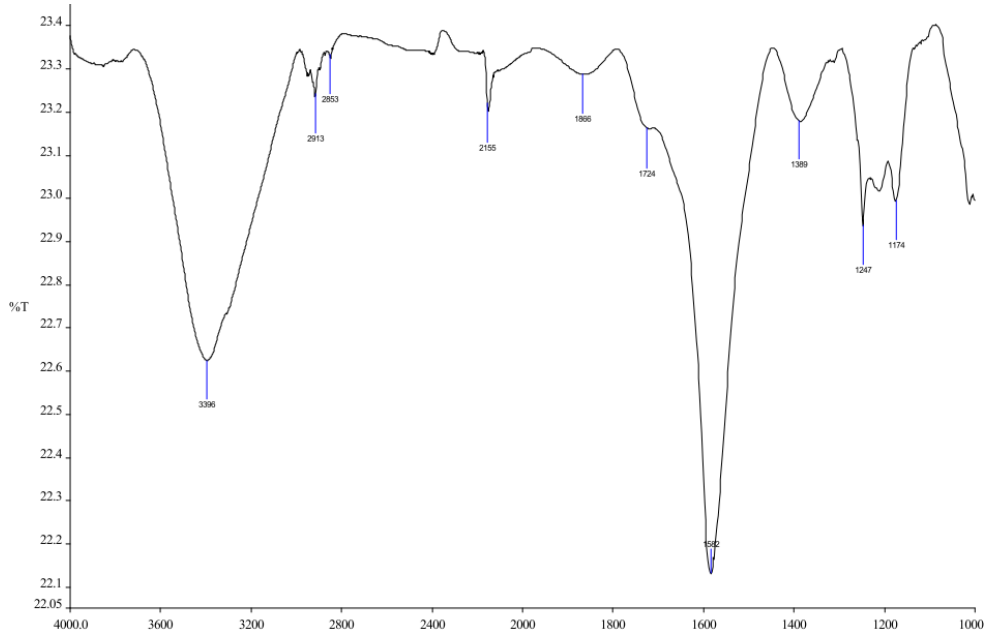

Figure 37. IR spectrum (KBr) of ox-MWCNTs-9-SiMe$_3$

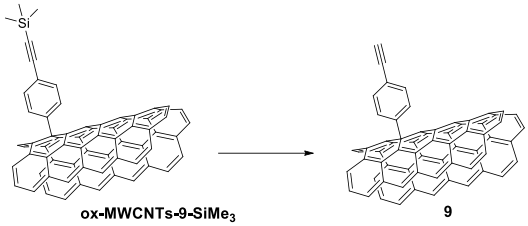

Compound 9 (desilylation procedure)**:** ox-MWCNTs-**9**-$SiMe_3$ (25 mg) was dissolved in DMF (20 mL), the mixture was sonicated for 10', and tetrabutylammonium fluoride 1.0 M in THF (1 mL) was slowly added to the dispersion at 0 °C. The reaction mixture was stirred for 2h and filtered on teflon filter (Whatmann, pore size 0.2 μm) washing with DMF, CH_2Cl_2, and acetone until a colorless filtrate was observed for each solvent. The solid residue was dried under vacuum affording a black powder (24 mg). IR (KBr, Figure 38): 3422, 2956, 2922, 2870, 1729, 1574, 1384, 1169 cm^{-1}.

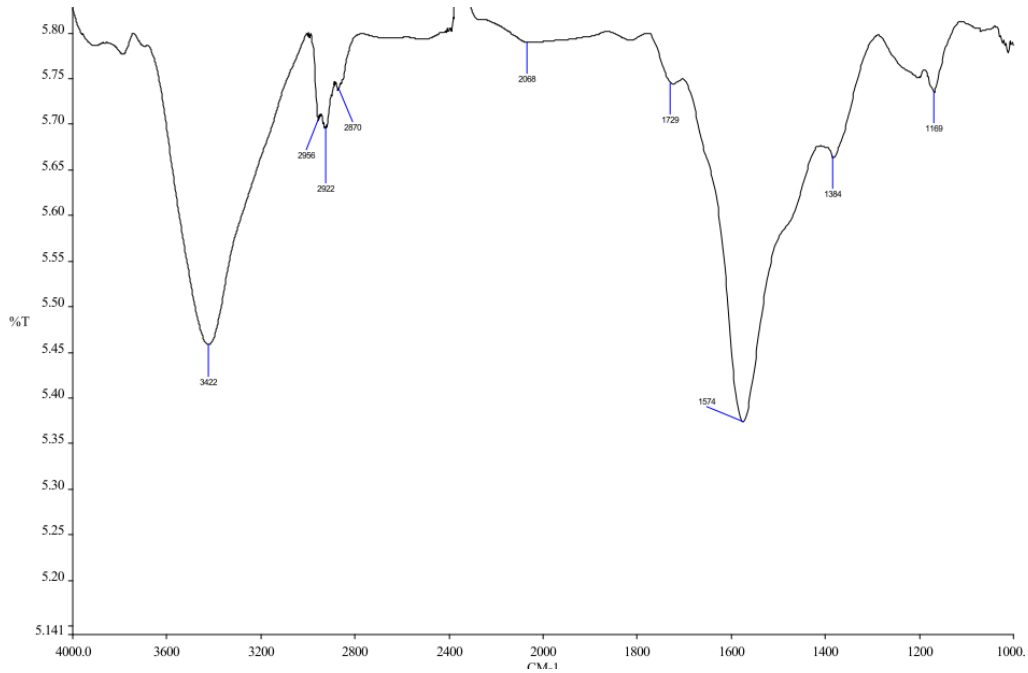

Figure 38. IR spectrum (KBr) of ox-MWCNTs-9

A TGA-MS analysis was performed on the decorated ox-MWCNTs after the Tour reaction (ox-MWCNTs-**9**-$SiMe_3$) and after the desilylation procedure (ox-MWCNTs-**9**) to evaluate the amount of chemically accessible C≡C-$SiMe_3$ groups present on the ox-MWCNTs (Figure 39).

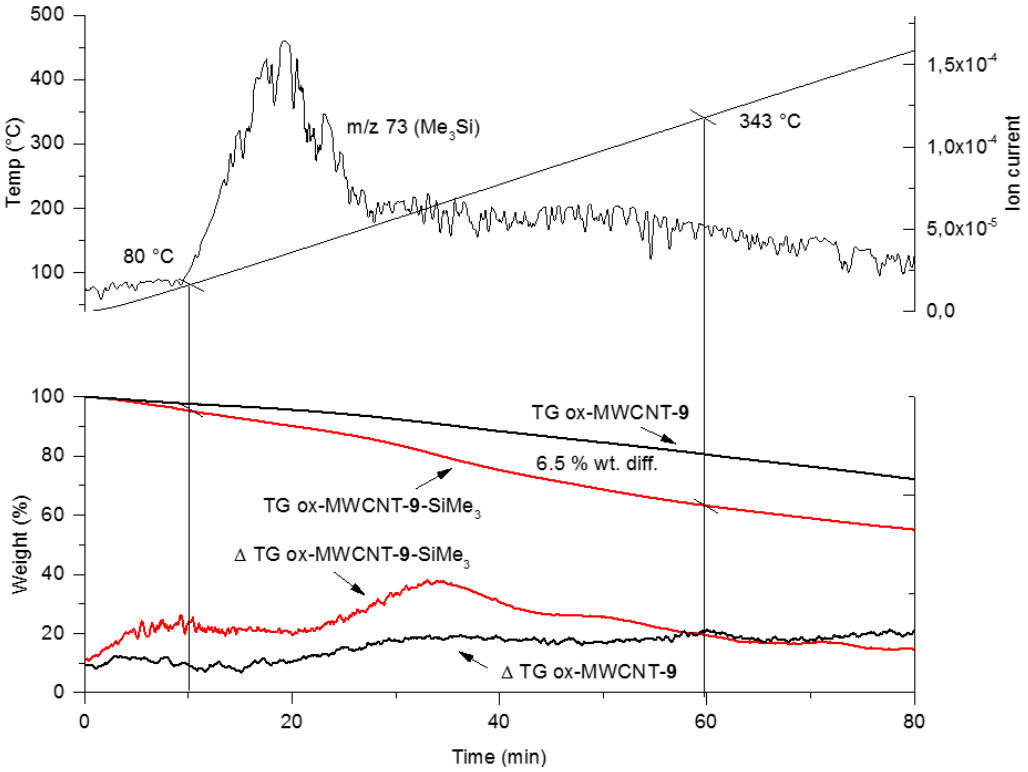

Figure 39. TGA-MS analysis of MWCNTs-9-SiMe3 and ox-MWCNTs-9. Upper graph: temperature range and Ion current of ion m/z 73. Lower graph: TG and ΔTG lines

The TGA analysis showed a 6.5 % weight loss of ox-MWCNTs-**9**-$SiMe_3$ with respect to the desilylated sample in the temperature range 80-343 °C. The temperature range was chosen according to the presence of the ion m/z 73 (Me_3Si group) in the mass spectrum (see upper graph in Figure 39). The abundance of the ion m/z 73 is higher from 80 to 174 °C but it is persistent (even if lower than before) up 350 °C. The limit of the temperature range (343 °C) was chosen when the ΔTG lines of the two sample crossed, suggesting the same thermal behavior. A weight loss of 6.5 % corresponds to the presence of 0.9 mmol of $SiMe_3$ per gram of material, a value in accord with the functionalization degree found with the ICP data obtained for compound **10** and **11**.

Compound 10 (coupling between 4-Azidophenyl-Bodipy (**5**) and modified carbon nanotubes **9**). Modified carbon nanotubes **9** (23 mg) were dissolved in anhydrous DMF (3 mL) and sonicated for 10', 4-Azidophenyl-Bodipy (27 mg, 0.074 mmol) and CuI·$P(OEt)_3$ (3 mg, 0.008 mmol) were added to the suspension. The mixture was

stirred at 70 °C under N_2 atmosphere for 48 h. Every 16 h an additional amount of catalyst (3 mg, 0.008 mmol) was added and the mixture was sonicated for 5 min. The reaction mixture was then filtered on teflon filter (Anodisc, pore size 0.2 μm) washing with DMF and AcOEt until a colorless filtrate was observed for each solvent. The solid residue was dried under vacuum affording the compound **10** as a black powder (15 mg). UV-Vis (nm, DMF): 506. Fluorescence (nm, DMF): 514. IR (KBr): 3398, 2914, 1723, 1581, 1543, 1510, 1401, 1306, 1192, 1155, 1027, 979 cm^{-1}. ICP analysis: B, 12.4 mg/g.

Compound 11 (coupling between Bodipy **8c** and modified carbon nanotubes **9**). Modified carbon nanotubes **9** (7 mg) together with Bodipy **8c** (5 mg, 0.011 mmol) and $CuI{\cdot}P(OEt)_3$ (1 mg, 0.003 mmol) as catalyst were dispersed in anhydrous DMF (4 mL), the suspension was sonicated for 5' and N,N-diisopropylethylamine (5 μL, 0.02 mmol) was added. The mixture was stirred vigorously at 60 °C under N_2 atmosphere for 48 h. Every 16 h the mixture was sonicated for 5 min. The reaction was then cooled to room temperature, diluted with $(i\text{-}Pr)_2O$ (50 mL), and centrifuged for 5' at 1400 g. Then the centrifugation and dispersion passages were repeated for additional three times, with fresh $(i\text{-}Pr)_2O$ and sonication each time, to completely remove unreacted materials. The last supernatant appear clear and colorless. The precipitate was dried under vacuum to obtain carbon nanotubes **11** as a dark powder (15.3 mg). UV-Vis (nm, DMF): 571. Fluorescence (nm, DMF): 595. IR (KBr): 3445, 2963, 2918, 1591, 1514, 1434, 1157, 1110, 987, 830 cm^{-1}. ICP analysis: B, 6.2 mg/g

Compound 12 (coupling between Bodipy **7b** and modified carbon nanotubes **9**). Modified carbon nanotubes **9** (18 mg) together with Bodipy **7b** (26 mg, 0.045 mmol) and $CuI{\cdot}P(OEt)_3$ (2 mg, 0.006 mmol) as catalyst were dispersed in anhydrous DMF (3 mL), the mixture was sonicated for 10' and stirred at 70°C under N_2 atmosphere for 48h. Every 16 h an additional amount of catalyst (2 mg, 0.006 mmol) was added and the mixture was sonicated for 5'. The reaction mixture was then filtered on teflon filter (Whatmann, pore size 0.2 μm) and washed with DMF, *i*-PrOH, and acetone until a colorless filtrate was observed for each solvent. The residue was sonicated 10' and the filtration with acetone was repeated to ensure the absence of unreacted Bodipy.

The solid residue was dried under vacuum affording the compound **12** as a blue-black powder (15 mg). UV-Vis (nm, DMF): 653. Fluorescence (nm, DMF): 668.

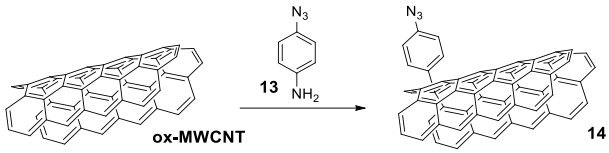

Synthesis of ox-MWCNT modified carbon nanotubes 14: Oxidized carbon nanotubes, (40 mg) and 4-azidoaniline (**13**) (93 mg, 0.69 mmol) were dispersed in anhydrous DMF (5 mL), isopentylnitrite (93 μL, 0.69 mmol) was added and the dispersion was sonicated for 10'. The mixture was stirred vigorously at 60°C under N_2 atmosphere for 24 h. The reaction was then cooled to room temperature and diluted with (*i*-Pr)$_2$O (100 mL). The black mixture was centrifuged for 5 minutes at 1400*g*, the supernatant was removed and the precipitate was redisperded in (*i*-Pr)$_2$O and sonicated for 5 minutes. The centrifugation and dispersion process was repeated for f our times, with fresh (*i*-Pr)$_2$O to completely remove unreacted products. Finally, the precipitate was dried under vacuum to obtain carbon nanotubes **14** as a black powder (48 mg). IR (KBr): 3411, 2918, 2112, 1720, 1580, 1502, 1379, 1261, 1015. Elem. Anal. C, 72,6; N, 8,15; H, 1,74.

The TGA analysis, performed in comparison with a sample of ox-MWCNT showed a significant loss of weight in the 130-200 °C range assigned to the loss of N_2 (Figure 40).

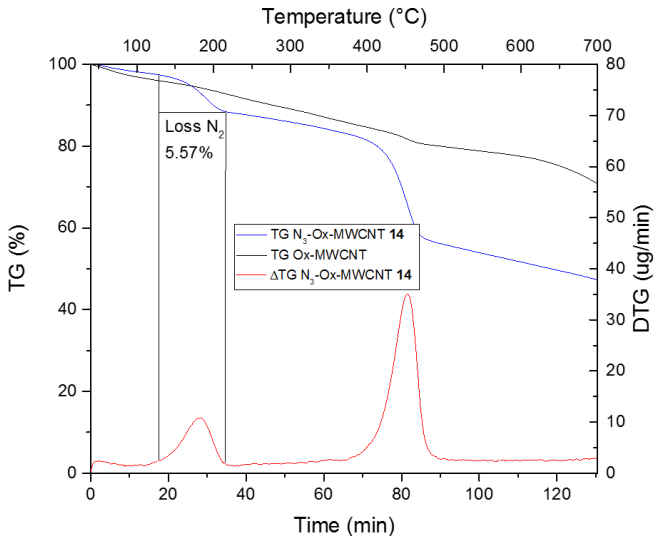

Figure 40. TGA analysis of ox-MWCNT and compound **14**

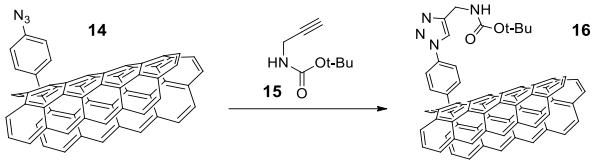

Compound 16: Modified carbon nanotubes **14** (7 mg) were dispersed in anhydrous DMF (4 mL) with BOC-propargilamine (**15**) (15 mg, 0.096 mmol) and CuI·P(OEt)$_3$ (5 mg, 0.014 mmol). The suspension was sonicated for 10' and N,N-diisopropylethylamine (10 μL, 0.06 mmol) was added. The suspension was stirred vigorously at 60°C under N_2 atmosphere for 48 h. Every 16 h the mixture was sonicated for 5'. The reaction was then cooled to room temperature, diluted with (*i*-Pr)$_2$O (50 mL), and centrifuged for 5 minutes at 1400 *g*. Then, the centrifugation and dispersion process was repeated for additional three times, with fresh (*i*-Pr)$_2$O to remove completely unreacted materials. The last supernatant liquid appeared clear and colorless. Finally, the solid was dried under vacuum to obtain carbon nanotubes **16** as a dark-brown powder (8.5 mg). IR (KBr): 3385, 2913, 1689, 1578, 1505, 1364, 1248, 1162, 1043, 836.

A TGA-MS analysis, performed in comparison with ox-MWCNT, showed a loss of isobutene as revealed by the correspond ions present in the MS spectrum of the effluent gas.

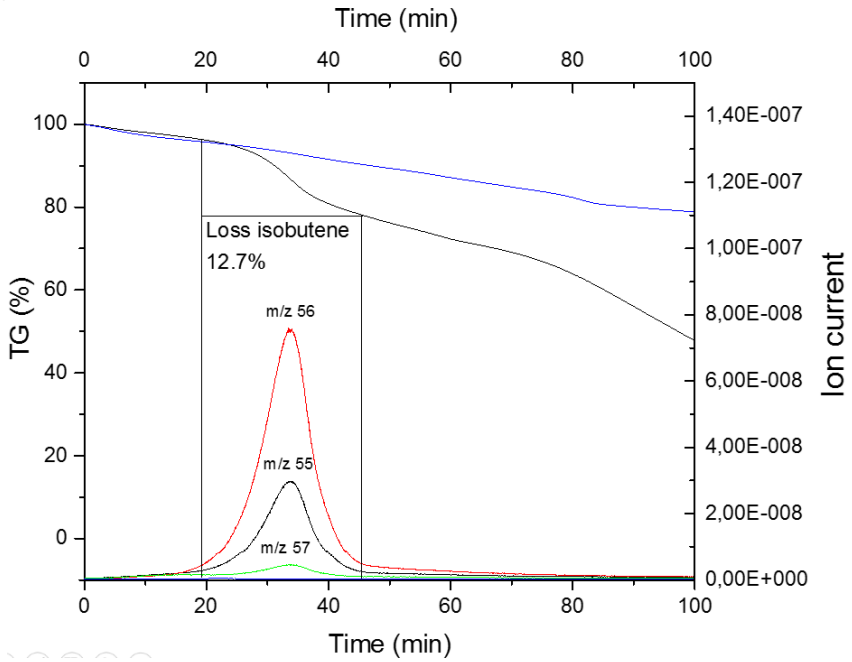

Figure 41. TGA-MS analysis of ox-MWCNT and compound **16**

Compound 17: A solution of *N,N*-dicyclohexylcarbodiimide (87 mg, 0.43 mmol) in anhydrous dichloromethane (1 mL), was added with 4-pentynoic acid (27 mg, 0.28 mmol) followed by the addition of a solution of BODIPY **A**[22,23] (94 mg, 0.2 mmol) in anhydrous dichloromethane (2 mL). Dimethylaminopyridine (4 mg, 0.03 mmol) was added and the reaction was stirred at room temperature under nitrogen. After 24 h the mixture was diluted with AcOEt (20 mL) and washed with water (2x10 mL), HCl 0.5 M (2x20 mL), saturated $NaHCO_3$ solution (2x30 mL), brine (2x30 mL). After drying over anhydrous Na_2SO_4 the solution was filtered and the solvent was evaporated. The crude reaction product was purified by flash chromatography on silica (R_f = 0.30) eluting with AcOEt/Hexane 1:2 to give compound **17** as an orange solid (100 mg, 87% yield). UV-Vis (CH_2Cl_2): 501 nm. Fluorescence (CH_2Cl_2): 511 nm. ^1H NMR ($CDCl_3$) δ =7.67 (d, *J* = 8.6 Hz, 2H), 7.53 (s, 1H), 7.21 (d, *J* = 8.6 Hz, 2H), 5.97 (s, 2H), 2.63 (m, 4H), 2.54 (s, 6H), 2.08 (m, 1H), 1.41 (s, 6H). $^{13}C\{^1H\}$ NMR ($CDCl_3$) δ = 169.4, 155.4, 143.1, 138.7, 131.6, 130.6, 128.7, 121.7, 120.0, 82.8, 69.8, 36.3, 33.9, 25.5, 24.9, 14.6.

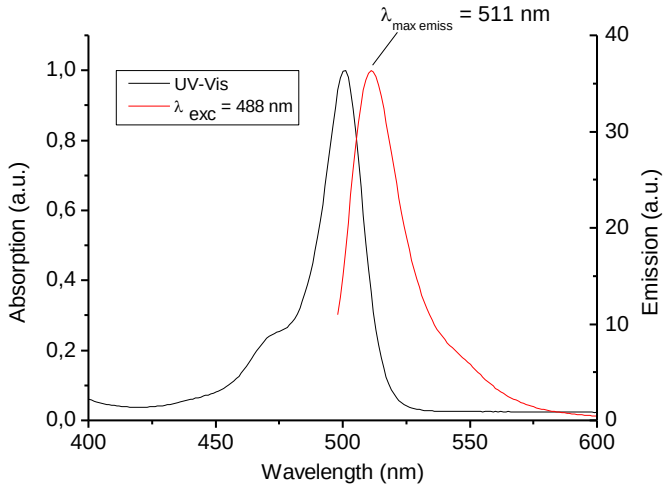

Figure 42. UV-Vis (black) and Fluorescence (red) spectrum of compound 17

Compound 18: Compound **17** (120 mg, 0.29 mmol) and 2-pyridinecarboxaldehyde (108 μL, 1.14 mmol) were dissolved in anhydrous CH_3CN (10 mL), with pyrrolidine (142 μL, 1.70 mmol) and acetic acid (97 μL, 1.7 mmol). The condensation reaction was performed under molecular sieves. The mixture was stirred at 80°C under N_2 atmosphere. After few minutes a change in the color of the mixture is observed, from

red to dark blue. After 20 minutes the mixture was cooled to room temperature and diluted with AcOEt (30 mL). The organic layer was washed with saturated $NaHCO_3$ solution (3x30 mL), water (2x40 mL), brine (2x40 mL), dried over anhydrous Na_2SO_4 and filtered, then the solvent was evaporated. The crude reaction product was purified by flash chromatography on silica (R_f = 0.34), eluting with CH_2Cl_2/EtOAc 10:3 to give compound **18** (79 mg, 53% yield).

Compound **18:** ^{1}H NMR (D_6-DMSO) δ = 10.22 (s, 1H), 8.71 (d, *J* = 3.8 Hz, 2H), 8.12 (d, *J* = 16.4 Hz, 2H), 7.86-7.79 (m, 4H), 7.59 (d, *J* = 16.4 Hz, 2H), 7.51 (d, *J* = 7.6, 2H), 7.38-7.32 (m, 4H), 7.03 (s, 2H), 2.81 (t, *J* = 2.5 Hz, 1H) 2.58 (t, J = 7.1 Hz, 2H), 2.50 (m, 2H), 1.50 (s, 6H). ^{13}C{^{1}H} NMR (D_6-DMSO) δ = 170.2, 154.1, 152.1, 142.7, 140.7, 140.6, 137.7, 136.2, 133.9, 129.2, 128.8, 125.0, 124.1, 122.1, 119.7, 119.4, 84.1, 72.0, 35.8, 14.9, 14.4. UV-Vis (DMF): 349, 574, 623 nm. Fluorescence (DMF): 629. IR ($CDCl_3$): 3685, 2926, 2866, 2245, 1685, 1503, 1434, 1408, 1094. MS calc. for $C_{36}H_{30}BF_2N_5O$: 597.25. Found (ESI): *m/z* (%) = 596.33 (100) M^-.

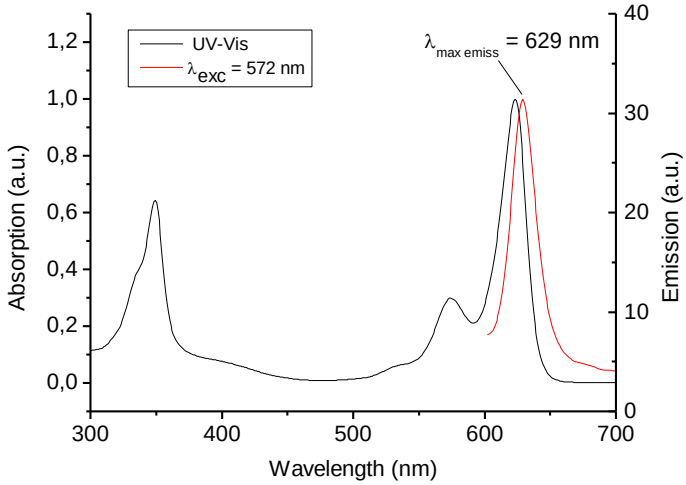

Figure 43. UV-Vis (black) and Fluorescence (red) spectrum of compound **18**

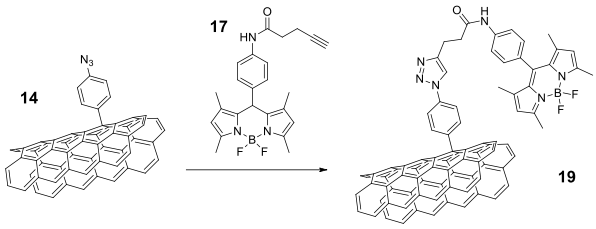

Compound 19

Modified carbon nanotubes **14** (10 mg) together with BODIPY **17** (7 mg, 0.017 mmol) and CuI·P(OEt)$_3$ (1.4 mg, 0.004 mmol) were dispersed in anhydrous DMF (5 mL). The suspension was sonicated for 5' and N,N-diisopropylethylamine (5.8 μL, 0.03 mmol) was added. The suspension was stirred at 60°C under N_2 atmosphere for 48 h. Every 16 h the mixture was sonicated for 5'. The reaction was then cooled to room temperature, diluted with (*i*-Pr)$_2$O (50 mL), and centrifuged for 5 minutes at 1400 *g*. The centrifugation and dispersion steps were repeated for additional four times, with fresh (*i*-Pr)$_2$O and sonication each time, to remove the unreacted materials completely. The last supernatant solution appeared clear and colorless. Finally, the solid was dried under vacuum to obtain carbon nanotubes **19** as a dark-brown powder (15 mg). UV-Vis (nm, DMF): 501. Fluorescence (nm, DMF): 513. IR (KBr): 3428, 2913, 2845, 2095, 1588, 1510, 1381, 1303, 1186, 1135, 1046. ICP analysis: B, 9.76 mg/g.

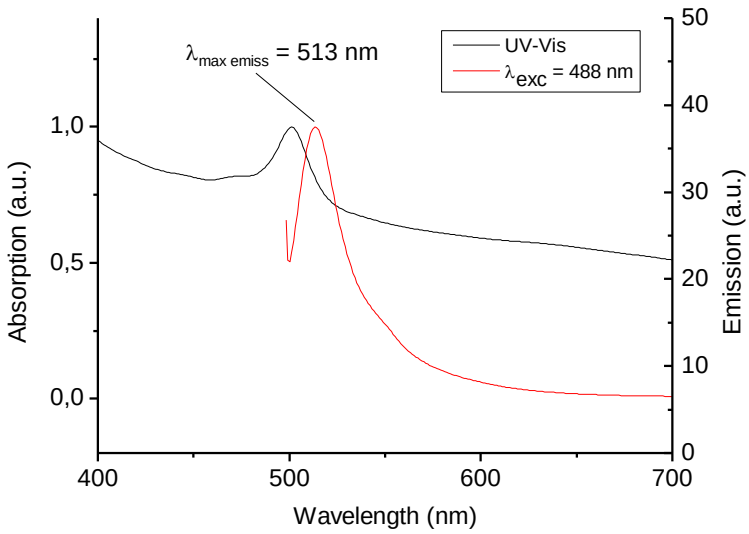

Figure 44. UV-Vis (black) and Fluorescence (red) spectrum of compound **19**

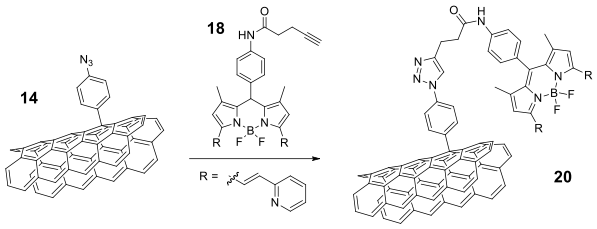

Compound 20: Modified carbon nanotubes **14** (5 mg) together with Bodipy **18** (5 mg, 0.010 mmol) and CuI·P(OEt)$_3$ (1 mg, 0.003 mmol) as catalyst were dispersed in anhydrous DMF (3.5 mL), the suspension was sonicated for 5' and N,N-diisopropylethylamine (5.8 μL, 0.03 mmol) was added. The suspension was stirred at 60°C under N_2 atmosphere for 48h. Every 16h the mixture was sonicated for 5'. The reaction was then cooled to room temperature, diluted with (*i*-Pr)$_2$O (50 mL), and centrifuged for 5' at 1400*g*. Then the centrifugation and dispersion passages were repeated for additional four times, with fresh (*i*-Pr)$_2$O and sonication each time, to completely remove unreacted materials. The last supernatant appear clear and colorless. Finally the precipitate was dried under vacuum to obtain carbon nanotubes **20** as a blue-black powder (5.8 mg). UV-Vis (nm, DMF): 350, 573, 627. Fluorescence (nm, DMF): 630. ICP analysis: B, 3.1 mg/g.

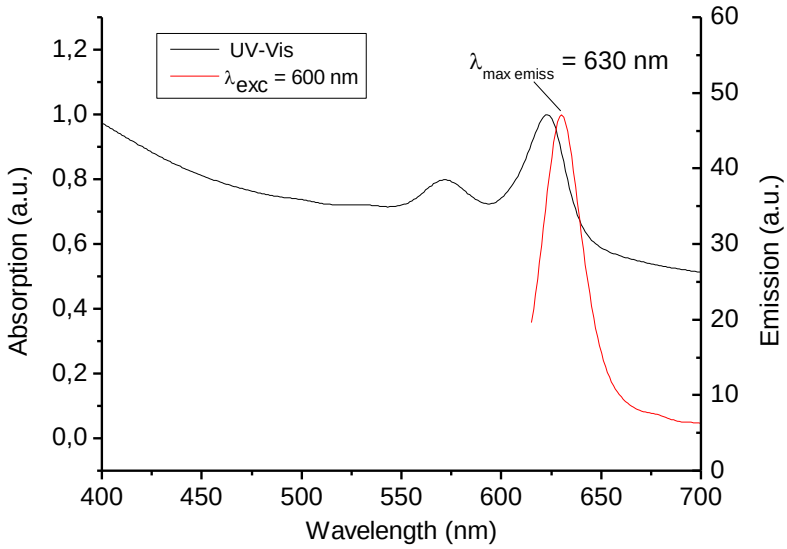

Figure 45. UV-Vis (black) and Fluorescence (red) spectrum of compound 20.

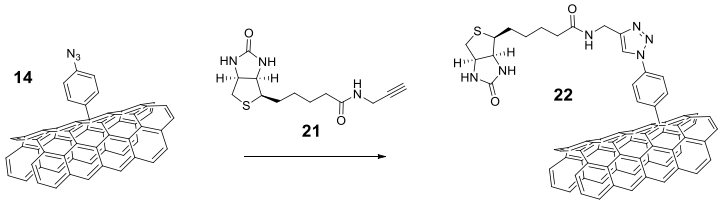

Compound 22: Modified carbon nanotubes **14** (20 mg) together with alkyno-biotin **21** (9.3 mg, 0.033 mmol) and CuI·P(OEt)$_3$ (3 mg, 0.008 mmol) as catalyst were dispersed in anhydrous DMF (7 mL), the suspension was sonicated for 5' and N,N-diisopropylethylamine (17 μL, 0.09 mmol) was added. The suspension was stirred at 60°C under N_2 atmosphere for 48h. Every 16h the mixture was sonicated for 5'. The reaction was then cooled to room temperature, diluted with (*i*-Pr)$_2$O (50 mL), and centrifuged for 5' at 1400*g*. Then the centrifugation and dispersion passages were repeated for additional two times, with fresh (*i*-Pr)$_2$O and sonication each time, to completely remove unreacted materials. The last supernatant appear clear and colorless. The residue was then redispersed in water and washed by centrifugation for 20' at 15.000*g* four times to completely remove the biotin unbound to carbon nanotubes. Finally the precipitate was dried under vacuum to obtain carbon nanotubes **22** as a dark powder (14.4 mg). ICP analysis: S, 5.9 mg/g.

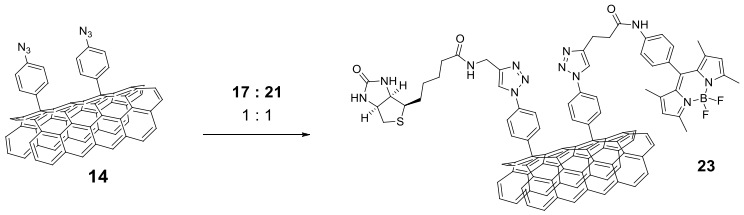

Compound 23: Modified carbon nanotubes **14** (15 mg) together with alkyno-biotin **21** (3.4 mg, 0.012 mmol), Bodipy **17** (5 mg, 0.012 mmol) and CuI·P(OEt)$_3$ (2 mg, 0.006 mmol) as catalyst were dispersed in anhydrous DMF (5 mL), the suspension was sonicated for 5' and N,N-diisopropylethylamine (8.6 μL, 0.05 mmol) was added. The suspension was stirred at 60°C under N_2 atmosphere for 48h. Every 16h the mixture was sonicated for 5'. The reaction was then cooled to room temperature, diluted with (*i*-Pr)$_2$O (50 mL), and centrifuged for 5' at 1400*g*. Then the centrifugation and dispersion passages were repeated for additional three times, with fresh (*i*-Pr)$_2$O and sonication each time, to completely remove unreacted materials. The last supernatant appear clear and colorless. The residue was then redispersed in water and washed by

centrifugation for 20' at 15.000*g* four times to completely remove the biotin unbound to carbon nanotubes. The precipitate was dried under vacuum to obtain carbon nanotubes **23** as a dark powder (16.2 mg). UV-Vis (nm, DMF): 500. Fluorescence (nm, DMF): 511. IR (KBr): 3422, 2918, 1580, 1099, 1255, 1630, 2846, 1382, 1537, 1510, 806. ICP analysis: B, 6.3 mg/g; S, 6.8 mg/g.

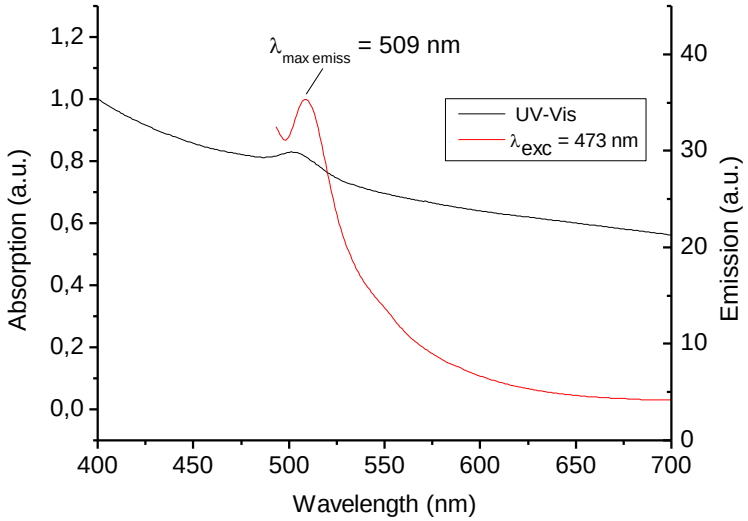

Figure 46. UV-Vis (black) and Fluorescence (red) spectrum of compound 23.

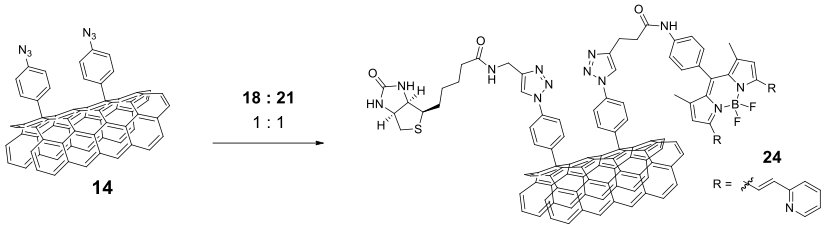

Compound 24. Modified carbon nanotubes **14** (30 mg) together with alkyno-biotin **21** (10 mg, 0.035 mmol), Bodipy **18** (13 mg, 0.025 mmol) and CuI·P(OEt)$_3$ (4 mg, 0.011 mmol) as catalyst were dispersed in anhydrous DMF (7 mL), the suspension was sonicated for 5' and N,N-diisopropylethylamine (25 μL, 0.14 mmol) was added. The suspension was stirred at 60°C under N_2 atmosphere for 48h. Every 16h the mixture was sonicated for 5'. The reaction was then cooled to room temperature, diluted with (*i*-Pr)$_2$O (50 mL), and centrifuged for 5' at 1400*g*. Then the centrifugation and dispersion passages were repeated for additional five times, with fresh (*i*-Pr)$_2$O and sonication each time, to completely remove unreacted materials. The last supernatant

appear clear and colorless. The residue was then redispersed in water and washed by centrifugation 20' at 15.000*g* four times to completely remove the biotin unbound to carbon nanotubes. Finally the precipitate was dried under vacuum to obtain carbon nanotubes **24** as a dark powder (26.3 mg). UV-Vis (nm, DMF): 571, 623; (phosphate buffer pH 7.4): 572, 635. Fluorescence (nm, DMF): 630. ICP analysis: B, 1.0 mg/g; S, 1.6 mg/g.

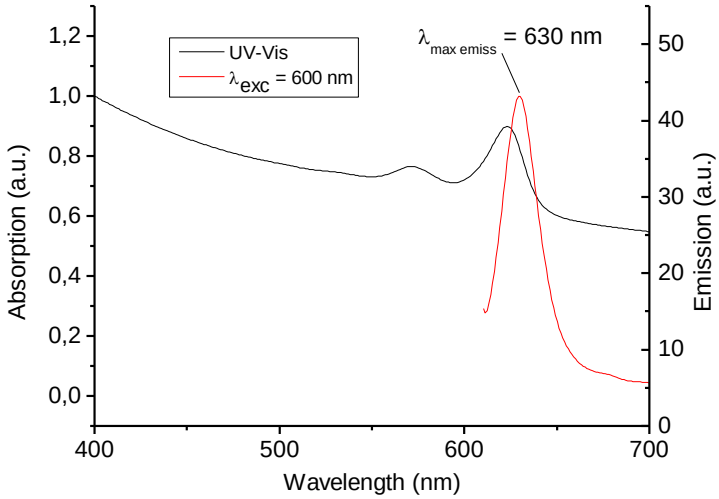

Figure 47. UV-Vis (black) and Fluorescence (red) spectrum of compound 24.

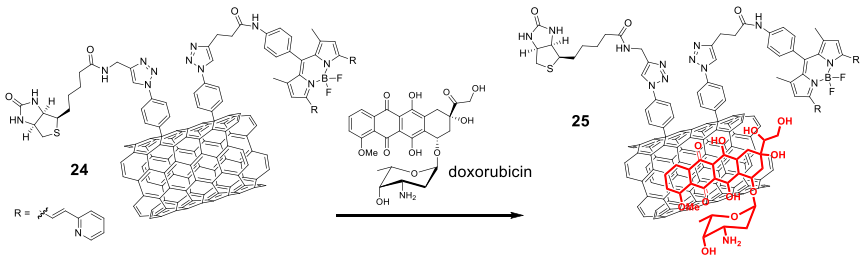

Compound 25 (DOX-loaded CNT): Nanotubes **24** (6 mg) were dissolved in a phosphate buffer solution 0.2 M at pH 7.4 (6 mL), the dispersion was sonicated for 5' and doxorubicin hydrochloride (4 mg, 0.007 mmol) was added. The mixture was stirred vigorously overnight at room temperature and in the dark. The reaction mixture was filtered on a Teflon filter (Whatmann, pore size 0.2 μm) washing five times with phosphate buffer to completely remove the unbound doxorubicin (constant content of doxorubicin in the washing water, measured by UV-visible analysis). The solid residue was dried under vacuum to obtain DOX-loaded CNT **25**

as a black-brown powder 8.1 mg. DOX loading (evaluated by difference from filtration waters): 0.60 g DOX/g CNT. UV-Vis (nm, phosphate buffer pH 7.4): 234, 254, 481, 637; (nm, DMF): 349, 478, 496, 571, 623.

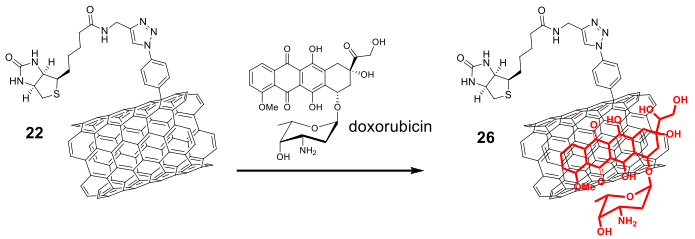

Compound 26 (DOX-loaded CNT): Nanotubes **22** (6 mg) were dissolved in a phosphate buffer solution 0.2 M at pH 7.4 (6 mL), the dispersion was sonicated for 5' and doxorubicin hydrochloride (4 mg, 0.007 mmol) was added. The mixture was stirred vigorously overnight at room temperature and in the dark. The reaction mixture was filtered on a Teflon filter (Whatmann, pore size 0.2 μm) washing six times with phosphate buffer to completely remove the unbound doxorubicin (constant content of doxorubicin in the washing water, measured by UV-visible analysis). The solid residue was dried under vacuum to obtain DOX-loaded CNT **26** as a black-brown powder (7.9 mg). DOX loading (evaluated by difference from filtration waters): 0.57 g DOX/g CNT. UV-Vis (nm, phosphate buffer pH 7.4): 233, 253, 481, 493.

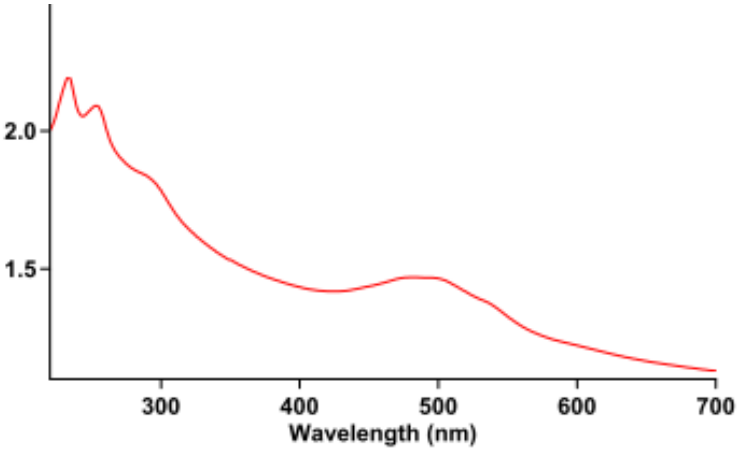

Figure 48. UV spectrum of compound **26**

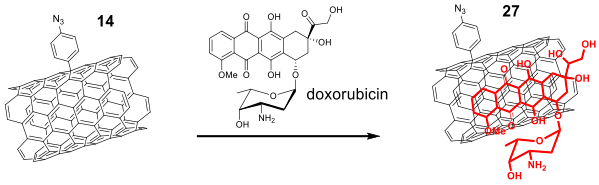

Compound 27 (DOX-loaded CNT): Nanotubes **14** (6 mg) were dissolved in a phosphate buffer solution 0.2 M at pH 7.4 (6 mL), the dispersion was sonicated for 5' and doxorubicin hydrochloride (4.2 mg, 0.007 mmol) was added. The mixture was stirred vigorously overnight at room temperature and in the dark. The reaction mixture was filtered on a Teflon filter (Whatmann, pore size 0.2 μm) washing six times with phosphate buffer to completely remove the unbound doxorubicin (constant content of doxorubicin in the washing water, measured by UV-visible analysis). The solid residue was dried under vacuum to obtain DOX-loaded CNT **27** as a black-brown powder (9.6 mg). DOX loading (evaluated by difference from filtration waters): 0.54 g DOX/g CNT. UV-Vis (nm, phosphate buffer pH 7.4): 233, 254, 472.

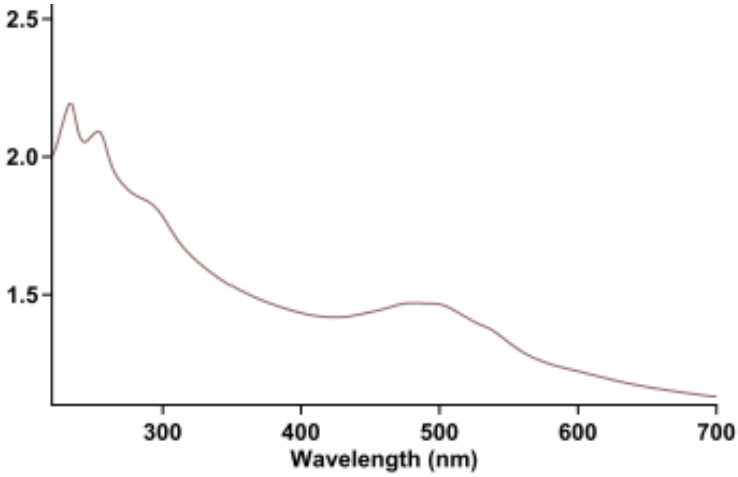

Figure 49. UV spectrum of compound **27.**

3.3 Biological assays

Cells cultures

Breast cancer cells (MCF-7), colon cancer cells (HT29) and prostate cancer cells (PC3) were routinely grown in 60 mm plates and maintained in monolayers to 80% confluence using DMEM supplemented with 10% fetal bovine serum, 1% penicillin–

streptomycin and 1% glutamine solutions, in a 5% CO_2 controlled humidified atmosphere at 37°C.

Flow Cytometric Analysis

MCF-7, PC3 and HT29 cancer cells were grown in 35mm dishes until 60% of confluence and treated with 10 μg/ml of fluorescent carbon nanotubes for 90 minutes at 37°C. Then, cells were detached by trypsinization and resuspended in DMEM medium. Cells were collected by centrifugation and washed with PBS before flow cytometric analysis using a FACSCanto flow cytometer (Becton-Dickinson).

Analysis of carbon nanotubes cells internalization with confocal microscopes

To evaluated the carbon nanotubes incorporation in MCF-7 cells, $0.5x10^6$ cells were plated on 35-mm dishes containing glass cover slips on the bottom and growth at 37°C under controlled atmosphere for 24 hours. Then, BODIPY decorated carbon nanotubes (10 μg/ml, final concentration) were added to cell cultures, and stored at 37°C for three hours. After this time, cells were extensively washed with PBS to remove the non-internalized nanotubes, and then cells were fixed in 3% paraformaldehyde for 30 min at room temperature before the analysis with the confocal fluorescence microscope. The analysis was made using a Leica TCS SP5 confocal scanning microscope (Leica Microsystems, Mannheim, Germany), equipped with an argon laser source and a Leica Plan Apo 639 oil immersion objective.

MTT test (toxicity tests)

Procedure

MCF-7 breast cancer cells were incubated for 24 hours in the presence of the test compounds. After this time, viability of cells was evaluated using MMT assay. Values obtained were normalized with respect to control experiments. Data reported represent the mean value S.E.M. (n = 3).

Experimental details

MCF-7 cells were grown in the presence of Dulbecco' s modified Eagle' s medium supplemented with 10% fetal bovine serum (FBS), 1% glutamine, and 1% penicillin-streptomycin, at 37 °C in controlled atmosphere with 5% CO_2. For the experiments, cells were seeded at a density of 80000 cells per well in P35 mm well plates; the day

after, compounds were added to growth medium and cells stored at 37 °C in 5% CO_2 for 24 h. After this time, the growth medium was removed and plates extensively washed with PBS. Then the media were replaced with medium containing 0.5 mg/mL of 3-(4,5-dimethylthiazol-2-yl)-2,5-diphenyltetrazolium bromide (MTT) and the cells were incubated for 1 h at 37 °C in 5% CO_2. Finally, the number of viable cells was quantified by the estimation of their dehydrogenase activity, which reduces MTT to water-insoluble formazan. Growth medium was removed and substituted with 1 ml of DMSO to dissolve the formazan produced. The quantification was carried out measuring the absorbance of samples at 570 nm.

3.4 UV and fluorescence spectra:

Compound **5** (DMF), UV and fluorescence spectra

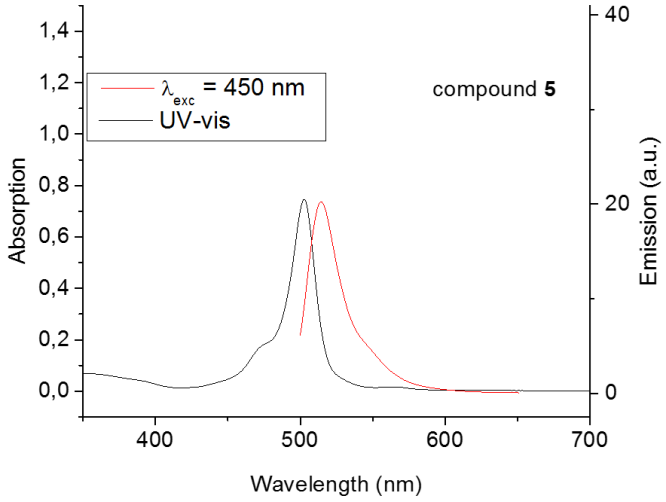

Compound **7b**: UV spectra

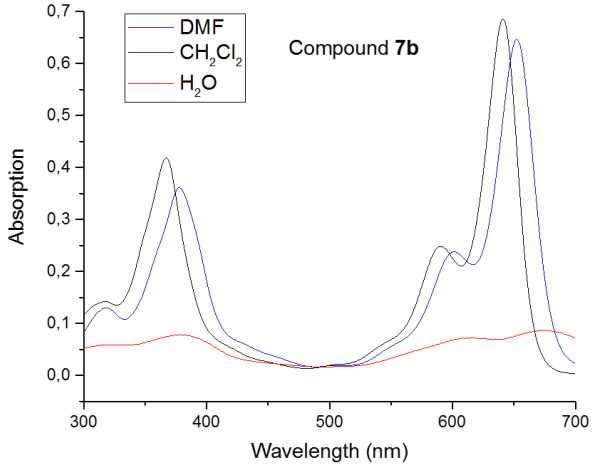

Compound **7b**: Fluorescence spectra

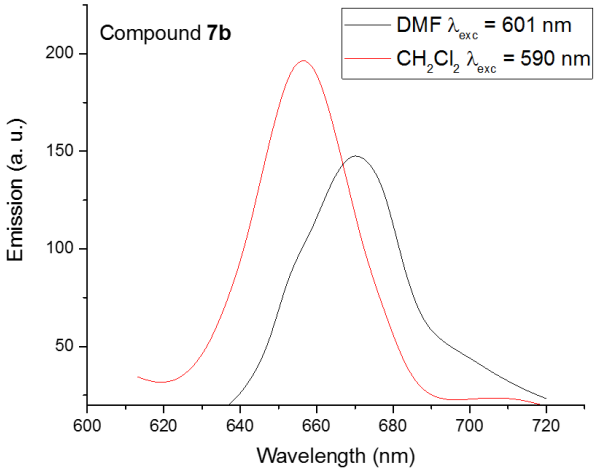

Compound **8b**: UV Spectra

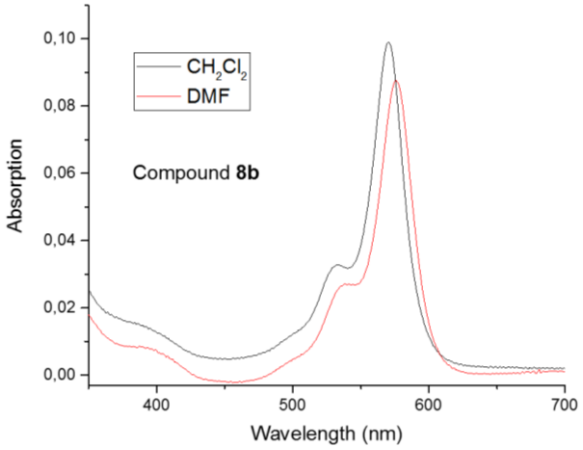

Compound **8b**: Fluorescence spectra

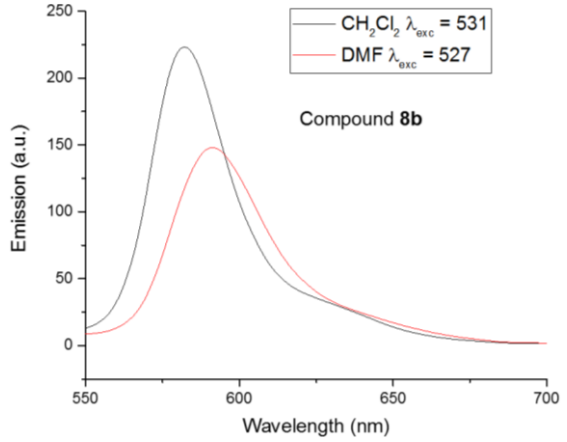

Compound **8c**: Uv spectra

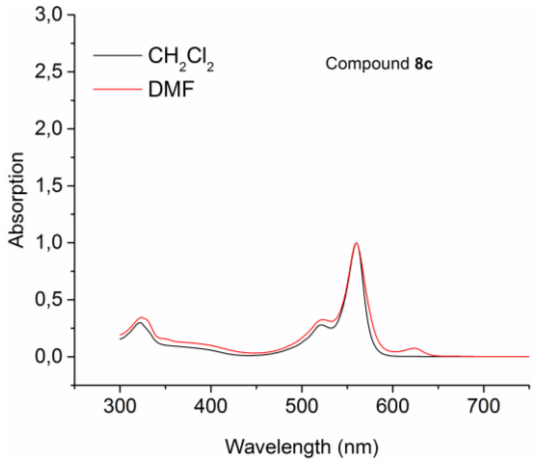

Compound **8c**: fluorescence spectra

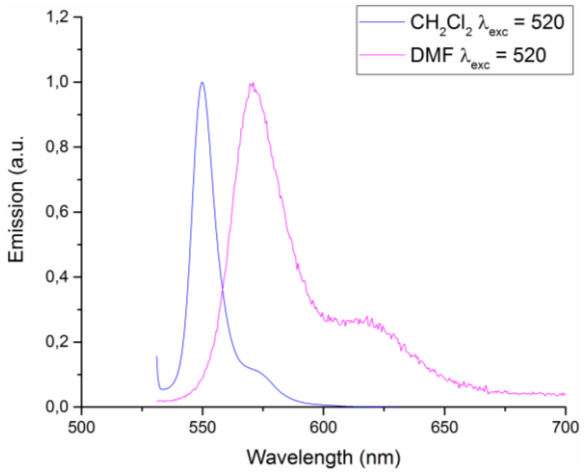

Compound **7d**: UV and fluorescence spectra

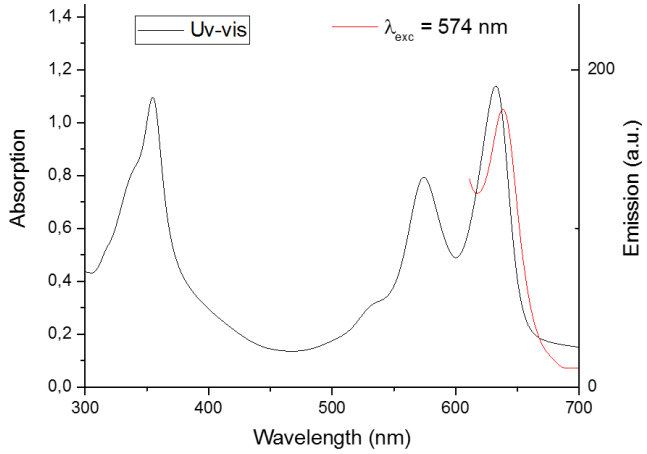

3.5 NMR spectra:

Compound **7b** ^{1}H NMR

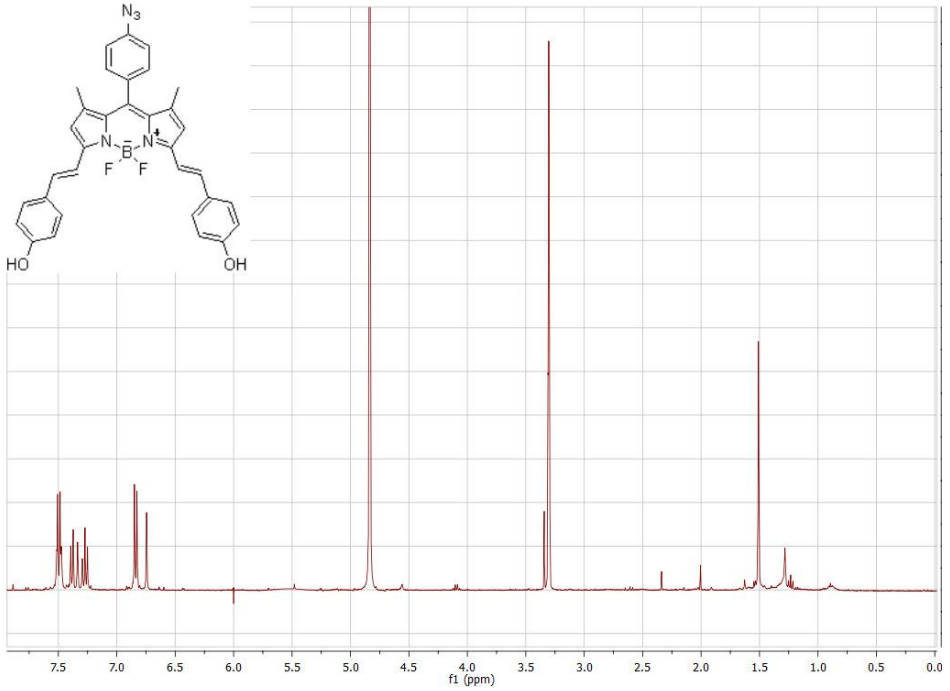

Compound **8b** ^{1}H NMR

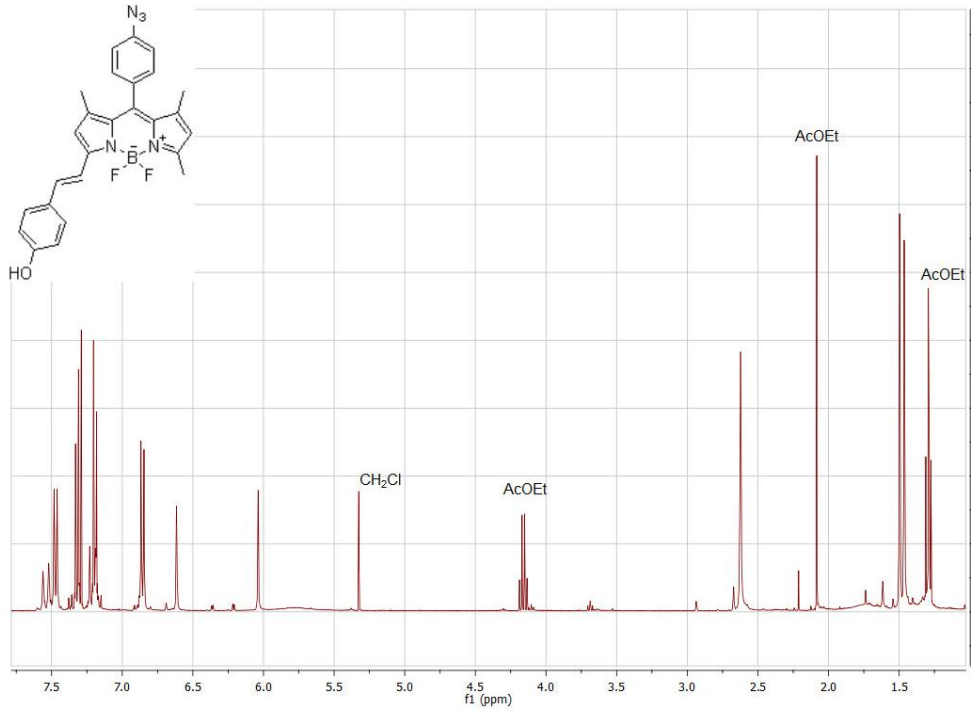

Compound **7c** ^{1}H NMR

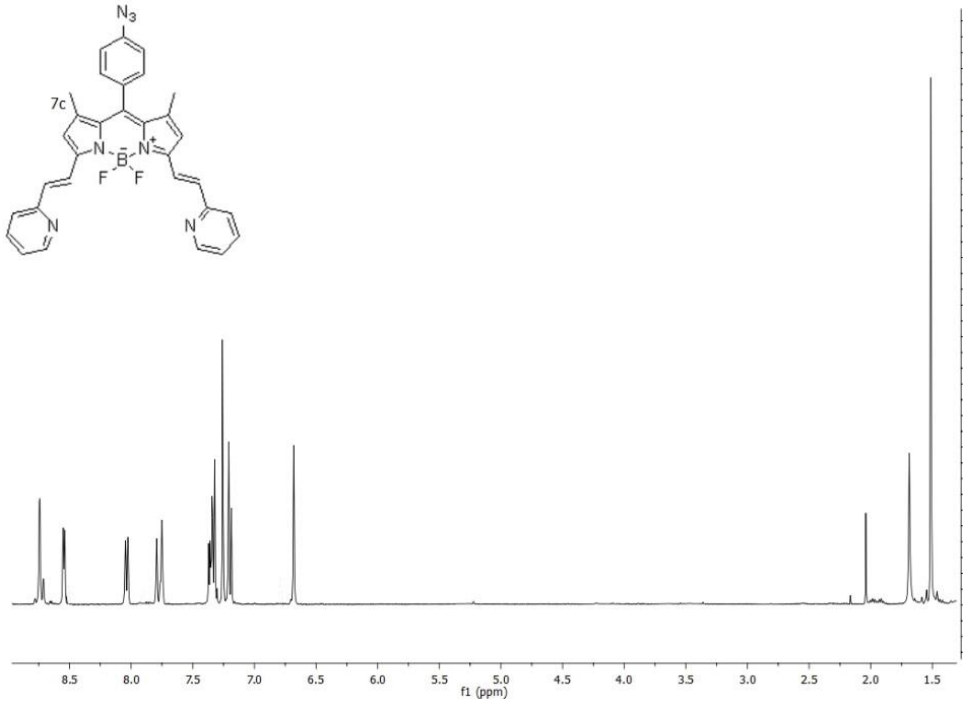

Compound **8C** ^{1}H NMR

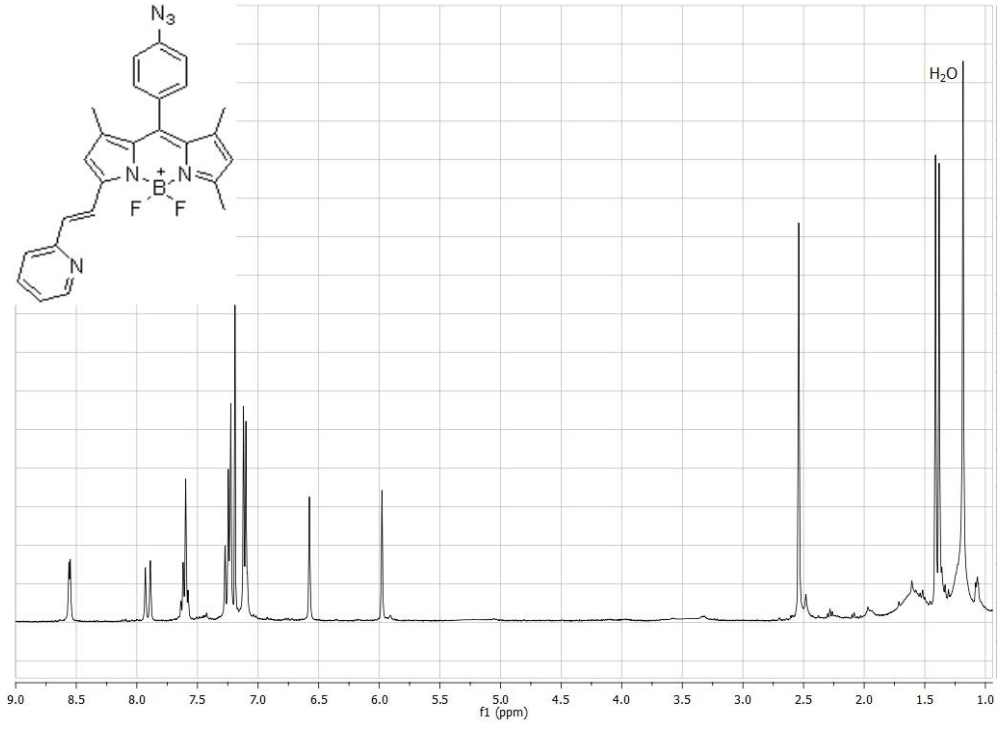

Compound **7d** ^{1}H NMR

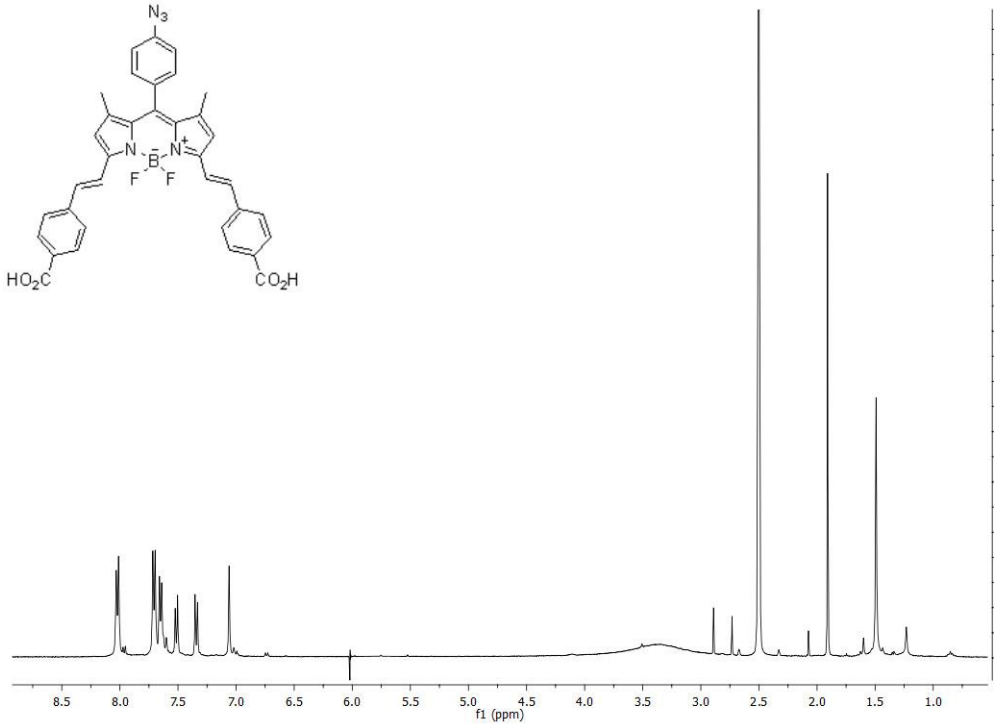

Compound **7b** ^{13}C NMR

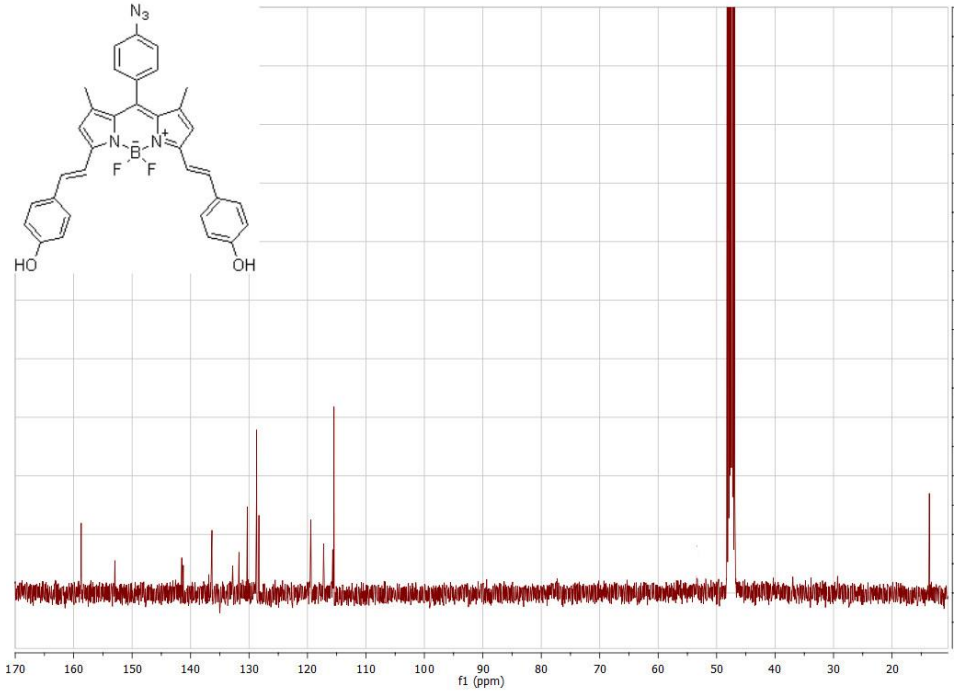

Compound **8b** ^{13}C NMR

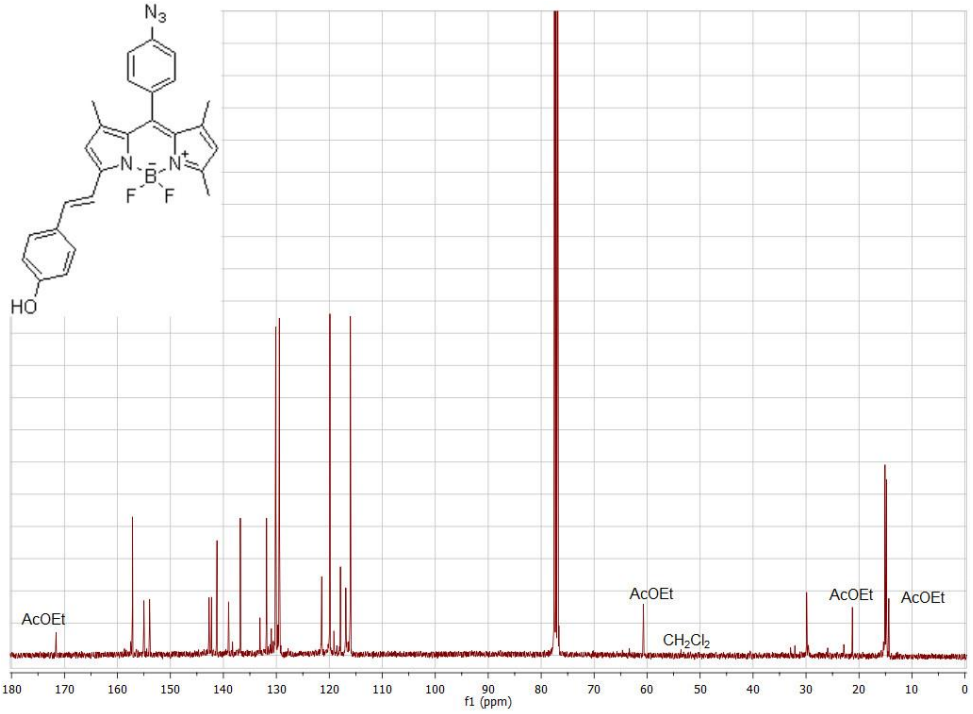

Compound **8C** ^{13}C NMR

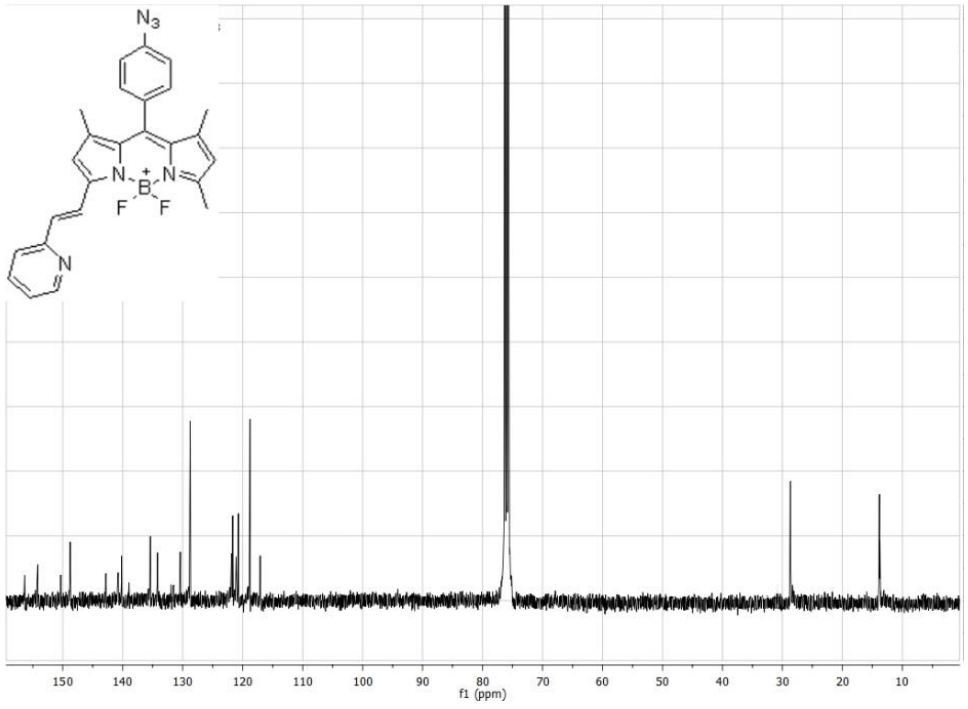

Compound **7d** ^{13}C NMR

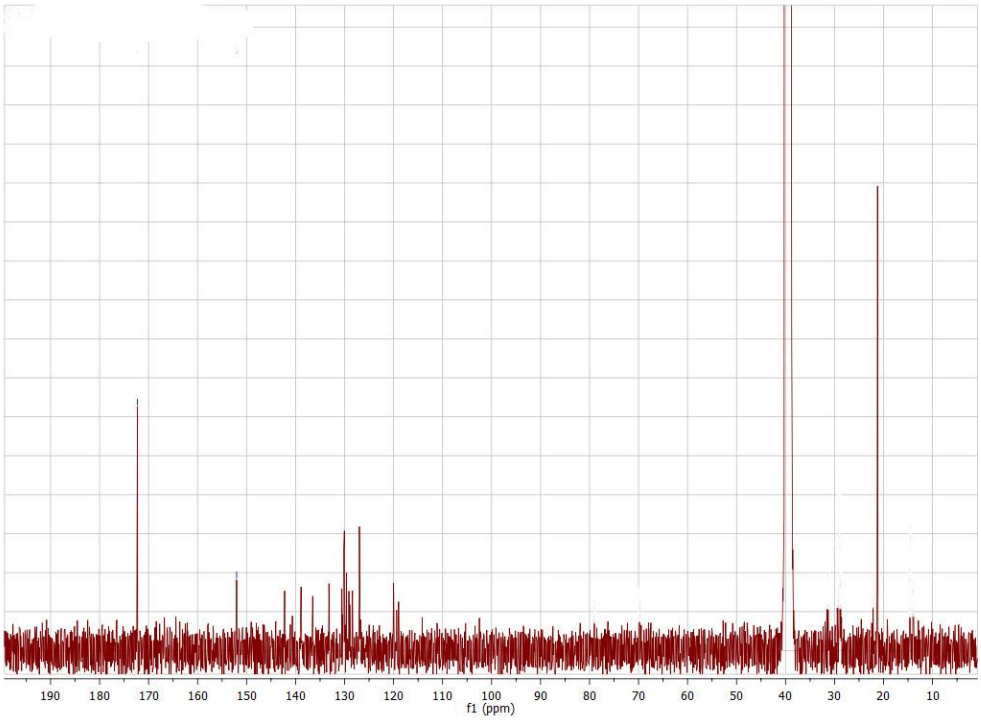

Appendix A

Combined experimental and theoretical study of efficient and ultrafast energy transfer in a molecular dyad[24]

It has been characterized the dynamics and the efficiency of electronic energy transfer (EET) in a newly synthesized molecular dyad, composed of a styryl-pyridinium donor and a BODIPY acceptor (Figure 50). The kinetics of the process has been studied with femtosecond transient absorption spectroscopy in different solvents. In all the analyzed media EET is quantitative and very fast, as we find that almost 70% of the overall excitation energy is transferred from the donor to the acceptor on a subpicosecond time scale. The experimental measurements have been supported by a theoretical analysis; the electronic couplings between the donor and acceptor moieties have been calculated at the (TD)DFT [Time-dependent density functional theory] level and complemented by a conformational analysis of the full dyad. The computed energy transfer times are in good agreement with the experimental values; this allowed us to verify the correctness of the Förster equation, demonstrating that, although EET in the examined system occurs on an ultrafast time scale, the approximations introduced in the case of the weak coupling regime remain valid.

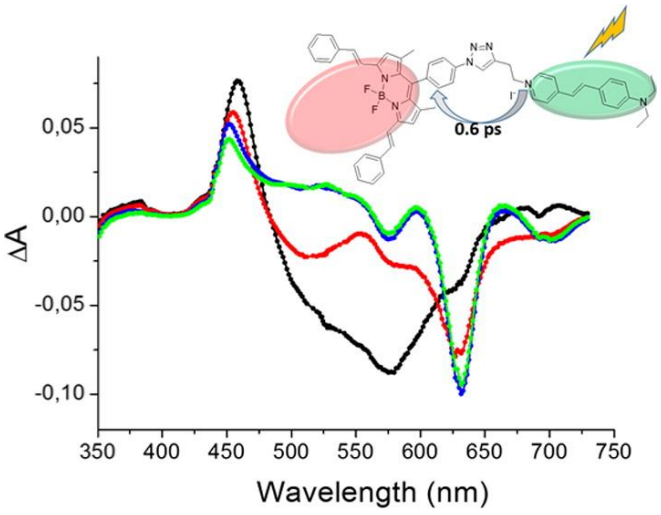

Figure 50. Evolution Associated Decay Spectra obtained from global analysis of the transient data of the bichromophore in chloroform

Synthetic procedure

The synthesis of the bichromophore was realized according to the following scheme:

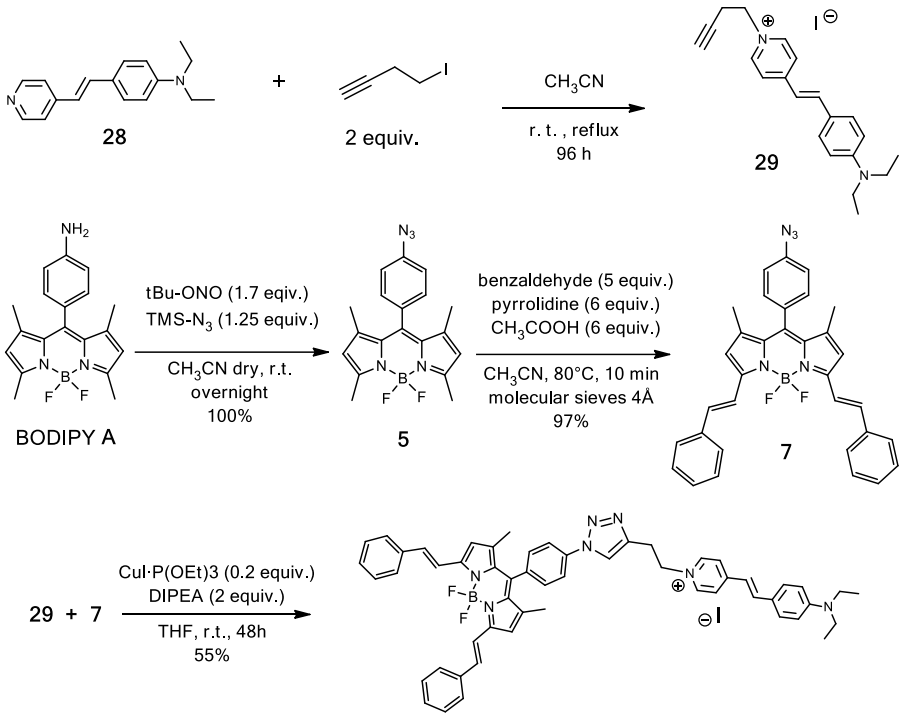

Synthesis of 1-But-3-ynyl-4-[2-(4-diethylamino-phenyl)-vinyl]-pyridinium iodide (**29**). 4-iodo-1-butyne (240 mg, 1.33 mmol) and 4-[2-[4-(diethylamino)phenyl]ethenyl]-pyridine **28** (168 mg, 0.67 mmol) were dissolved in anhydrous CH_3CN (12 ml). The mixture was refluxed under N_2 atmosphere. The reaction was monitored by TLC (CH_2Cl_2/MeOH 10:1, R_f = 0.38). After 96 h the solvent was evaporated and the reaction product was purified by flash chromatography, eluting first with CH_2Cl_2/MeOH 50:1 and then CH_2Cl_2/MeOH 25:1, to afford compound **29** (232 mg, 80% yield).

^{1}HNMR (300MHz, $CDCl_3$): δ = 8.85 (d, ^3J=6.9Hz, 2H), 7.82 (d, ^3J=6.9Hz, 2H), 7.63 (d, $^3J_{trans}$=15.9Hz, 1H), 7.53 (d, ^3J=9.0Hz, 2H), 6.85 (d, $^3J_{trans}$=15.9Hz, 1H), 6.64 (d, ^3J=9.0Hz, 2H), 4.79 (t, ^3J=6.0Hz, 2H), 3.41 (q, ^3J=7.2Hz, 4H), 2.95 (td, ^3J=6.0Hz, ^4J=2.7Hz, 2H), 2.12 (t, ^4J=2.7Hz, 1H), 1.19 (t, ^3J=7.2Hz, 6H) ppm; UV-Vis (CH_2Cl_2) λ_{max} = 533nm; Fluorescence (CH_2Cl_2) λ_{max} = 608 nm; MS (ESI): m/z (%) = 305.24 (100) $[M\text{-}I^-]^+$, 732.52 (14) $[M+(M\text{-}I^-)]^+$; Elemental analysis calcd for $C_{21}H_{25}IN_2$: N 6.48, C 58.34, H 5.83; found N = 6.08, C 57.97, H 5.89.

Synthesis of bi-chromophore. Compound **7** (126 mg, 0.23 mmol) and compound **29** (124 mg, 0.29 mmol, 1.25 equiv.) were dissolved in anhydrous THF (5 mL). Then *N,N*-diisopropylethylamine (81.1 µL, 60.2 mg, 0.46 mmol, 2 equiv.), and CuI·P(OEt)$_3$ (28 mg, 0.08 mmol, 0.3 equiv.) were added. The mixture was stirred at r.t. in N_2 atmosphere for 72h and it was monitored by TLC (CH_2Cl_2/MeOH 10:1). Then the solvent was evaporated and the crude was purified by flash chromatography on alumina (activity V, pH 7) eluting with CH_2Cl_2/MeOH 50:1 (R_f=0.22) to give the product as a dark powder (126 mg, 55% yield). ^{1}H NMR (400MHz, $CDCl_3$): δ = 9.03 (s, 1H), 9.01 (d, ^3J = 6.8 Hz, 2H), 8.04 (2H, ^3J = 8.4 Hz, 2H), 7.73 (d, $^3J_{trans}$ = 16.4 Hz, 2H), 7.68 (d, ^3J = 6.8 Hz, 2H), 7.65 (d, ^3J = 7.2 Hz, 4H), 7.54 (d, $^3J_{trans}$ = 15.6 Hz, 1H), 7.49 (pd, 4H), 7.40 (pt, 4H), 7.32 (m, 4H), 6.77 (d, $^3J_{trans}$ = 15.6 Hz, 1H), 6.67 (pt, 4H), 5.13 (t, ^3J = 7.0 Hz, 2H), 3.70 (t, ^3J = 7.0 Hz, 2H), 3.43 (q, ^3J = 7.1 Hz, 4H), 1.49 (s, 6H), 1.22 (t, ^3J = 7.1 Hz, 6H) ppm; ^{13}C NMR (100MHz, $CDCl_3$): δ = 154.6 (s), 153.0 (s), 150.5 (s), 143.6 (s), 143.2 (d), 142.7 (s), 142.0 (d), 137.4 (s), 137.1 (s), 136.6 (d), 136.5 (d), 133.2 (d), 131.2 (d), 130.2 (d), 129.0 (d), 128.8 (d), 127.6 (d), 122.8 (s), 122.1 (d), 121.4 (s), 120.9 (d), 119.2 (s), 118.1 (d), 115.4 (d), 111.6 (d), 58.4 (t), 44.7 (t), 27.7 (t), 15.1 (q), 12.6 (q) ppm; UV-Vis (CH_2Cl_2) λ_{max} = 350 nm, 533 nm, 574nm, 628nm; Fluorescence (CH_2Cl_2) λ_{max} = 643 nm; IR ($CDCl_3$) : ν = 3005 (w), 2974 (w), 2930 (w), 1710 (s), 1574 (s), 1541 (m), 1524 (s), 1508 (m), 1439 (m), 1411 (m), 1364 (s), 1325 (w), 1223 (m), 1164 (m), 1153 (m) cm^{-1}; MS (ESI): m/z (%) = 846.47 (100) $[M\text{-}I^-]^+$.

Appendix B

A Hetero-Bifunctional Spacer for the Smart Engineering of Carbon-Based Nanostructures[10]

It has been performed the synthesis of a linear hetero-functional crosslinker featuring a cleavable disulfide moiety for the covalent anchoring of a wide range of thiol end-capped (bio)molecules and, through a clickable terminal acetylene group, the CuAAC reaction at the surface of phenylazido-decorated carbon-based nanostructures. The bio-orthogonal character of the click reaction makes it highly desirable for conjugating CNTs and biomolecules.[50,51] The adopted methodology

generated multifunctional CNT platforms, in which disulfide bond cleavage, operating through sulfhydryl-containing molecules, occurred with the controlled release of a pyridine dye, the concentration of which was proportional to the extent of cleavage or conjugation by an incoming thiol end-capped molecule (Figure 51). As a result, the cleavage/functionalisation scheme provided a useful tool for the chemical linkage of a wide range of thiol-terminating probes to the carbon nanomaterial surface, and precise functionalization loading was simply assessed by UV/Vis measurements. Controlled CNT hetero-decoration through a one-step CuAAC reaction with an acetylene mixture composed of the bifunctional linker and an acetylene fluorescence dye (BODIPY derivative) was used to impart multifunctionality on the final carbon nanohybrid.

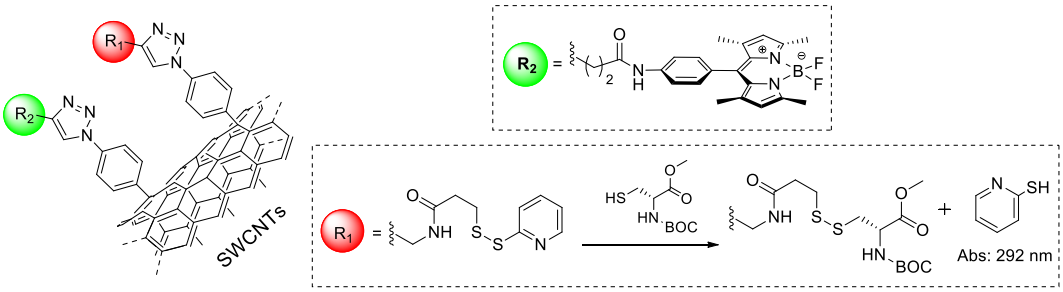

Figure 51. The single-walled CNTs doubly decorated and the release of pyridine dye upon exchange with the HS-terminating amino acid.

This approach generated optically traceable nanocarriers, the conjugation of which with sulfhydryl-containing (bio)molecules was allowed through simple ligand exchange at the disulfide bridge. Most importantly, each functionalization and post-derivatization step could be precisely followed by spectroscopic measurements (UV/Vis) of the reaction solutions by monitoring the release of a pyridine dye. A morphological study of the as-prepared hetero-decorated nanohybrids provided interesting insights into the ultimate distribution of the functional groups at the nanomaterial surface, as a consequence of the regiochemical attachment of radical species generated from aryldiazonium intermediates.

List of related published work

(During the three-year thesis period)

4. **Fedeli S**, Tuci G, Giambastiani G, Paoli P, Brandi A, Venturini L and Cicchi S.
   Azido substituted BODIPY dyes for the production of fluorescent carbon nanotubes.
   Chemistry - A European Journal - in press (online First published 24 August 2015*).*
3. Tuci G, Luconi L, Rossin A, Baldini F, Cicchi S, Tombelli S, Trono C, Giannetti A, Manet I, **Fedeli S**, Brandi A and Giambastiani G.
   A Hetero-Bifunctional Spacer for the Smart Engineering of Carbon-Based Nanostructures. **ChemPlusChem**, 2015, 80: 704-714.
2. Di Donato M, Iagatti A, Lapini A, Foggi P, Cicchi S, Lascialfari L, **Fedeli S**, Caprasecca, S, Mennucci B. Combined Experimental and Theoretical Study of Efficient and Ultrafast Energy Transfer in a Molecular Dyad.
   J Phys Chem C, 2014, 118: 23476-86.
1. Lascialfari L, **Fedeli S**, Cicchi S.
   Heterocyclic Chemistry: A Complete Toolbox for Nanostructured Carbon Materials.
   Progress in Heterocyclic Chemistry, Elsevier 2014, Volume 26, chapter 2, 29-54.

Bibliography

(1) Boens, N.; Leen, V.; Dehaen, W. Fluorescent Indicators Based on BODIPY. *Chem. Soc. Rev.* **2012**, *41*, 1130–1172.

(2) Ulrich, G.; Ziessel, R.; Harriman, A. The Chemistry of Fluorescent Bodipy Dyes: Versatility Unsurpassed. *Angew. Chem. Int. Ed.* **2008**, *47*, 1184–1201.

(3) Loudet, A.; Burgess, K. BODIPY Dyes and Their Derivatives: Syntheses and Spectroscopic Properties. *Chem. Rev. Wash. DC U. S.* **2007**, *107*, 4891–4932.

(4) Vendrell, M.; Zhai, D.; Er, J. C.; Chang, Y.-T. Combinatorial Strategies in Fluorescent Probe Development. *Chem. Rev. Wash. DC U. S.* **2012**, *112*, 4391–4420.

(5) Bessette, A.; Hanan, G. S. Design, Synthesis and Photophysical Studies of Dipyrromethene-Based Materials: Insights into Their Applications in Organic Photovoltaic Devices. *Chem. Soc. Rev.* **2014**, *43*, 3342–3405.

(6) Erbas, S.; Gorgulu, A.; Kocakusakogullari, M.; Akkaya, E. U. Non-Covalent Functionalized SWNTs as Delivery Agents for Novel Bodipy-Based Potential PDT Sensitizers. *Chem. Commun.* **2009**, 4956.

(7) Flavin, K.; Lawrence, K.; Bartelmess, J.; Tasior, M.; Navio, C.; Bittencourt, C.; O'Shea, D. F.; Guldi, D. M.; Giordani, S. Synthesis and Characterization of Boron Azadipyrromethene Single-Wall Carbon Nanotube Electron Donor-Acceptor Conjugates. *ACS Nano* **2011**, *5*, 1198–1206.

(8) Bartelmess, J.; Luca, E. D.; Signorelli, A.; Baldrighi, M.; Becce, M.; Brescia, R.; Nardone, V.; Parisini, E.; Echegoyen, L.; Pompa, P. P.; *et al.* Boron Dipyrromethene (BODIPY) Functionalized Carbon Nano-Onions for High Resolution Cellular Imaging. *Nanoscale* **2014**, *6*, 13761–13769.

(9) Tuci, G.; Vinattieri, C.; Luconi, L.; Ceppatelli, M.; Cicchi, S.; Brandi, A.; Filippi, J.; Melucci, M.; Giambastiani, G. "Click" on Tubes: A Versatile Approach towards Multimodal Functionalization of SWCNTs. *Chem. - Eur. J.* **2012**, *18*, 8454–8463.

(10) Tuci, G.; Luconi, L.; Rossin, A.; Baldini, F.; Cicchi, S.; Tombelli, S.; Trono, C.; Giannetti, A.; Manet, I.; Fedeli, S.; *et al.* A Hetero-Bifunctional Spacer for the Smart Engineering of Carbon-Based Nanostructures. *ChemPlusChem* **2015**, *80*, 704–714.

(11) Hein, J. E.; Fokin, V. V. Copper-Catalyzed Azide-Alkyne Cycloaddition (CuAAC) and beyond: New Reactivity of Copper(i) Acetylides. *Chem. Soc. Rev.* **2010**, *39*, 1302–1315.

(12) Ziessel, R.; Ulrich, G.; Harriman, A.; Alamiry, M. A. H.; Stewart, B.; Retailleau, P. Solid-State Gas Sensors Developed from Functional Difluoroboradiazaindacene Dyes. *Chem. - Eur. J.* **2009**, *15*, 1359–1369.

(13) Kolemen, S.; Bozdemir, O. A.; Cakmak, Y.; Barin, G.; Erten-Ela, S.; Marszalek, M.; Yum, J.-H.; Zakeeruddin, S. M.; Nazeeruddin, M. K.; Graetzel, M.; *et al.*

Optimization of Distyryl-Bodipy Chromophores for Efficient Panchromatic Sensitization in Dye Sensitized Solar Cells. *Chem. Sci.* **2011**, *2*, 949–954.

(14) Boens, N.; Qin, W.; Baruah, M.; De Borggraeve, W. M.; Filarowski, A.; Smisdom, N.; Ameloot, M.; Crovetto, L.; Talavera, E. M.; Alvarez-Pez, J. M. Rational Design, Synthesis, and Spectroscopic and Photophysical Properties of a Visible-Light-Excitable, Ratiometric, Fluorescent near-Neutral pH Indicator Based on BODIPY. *Chem. - Eur. J.* **2011**, *17*, 10924–10934, S10924/1–S10924/28.

(15) Kostereli, Z.; Ozdemir, T.; Buyukcakir, O.; Akkaya, E. U. Tetrastyryl-BODIPY-Based Dendritic Light Harvester and Estimation of Energy Transfer Efficiency. *Org. Lett.* **2012**, *14*, 3636–3639.

(16) Zhu, S.; Zhang, J.; Vegesna, G.; Tiwari, A.; Luo, F.-T.; Zeller, M.; Luck, R.; Li, H.; Green, S.; Liu, H. Controlled Knoevenagel Reactions of Methyl Groups of 1,3,5,7-Tetramethyl BODIPY Dyes for Unique BODIPY Dyes. *RSC Adv.* **2012**, *2*, 404–407.

(17) Palao, E.; Agarrabeitia, A. R.; Banuelos-Prieto, J.; Lopez, T. A.; Lopez-Arbeloa, I.; Armesto, D.; Ortiz, M. J. 8-Functionalization of Alkyl-Substituted-3,8-Dimethyl BODIPYs by Knoevenagel Condensation. *Org. Lett.* **2013**, *15*, 4454–4457.

(18) Lallana, E.; Sousa-Herves, A.; Fernandez-Trillo, F.; Riguera, R.; Fernandez-Megia, E. Click Chemistry for Drug Delivery Nanosystems. *Pharm. Res.* **2012**, *29*, 1–34.

(19) Hou, J.; Liu, X.; Shen, J.; Zhao, G.; Wang, P. G. The Impact of Click Chemistry in Medicinal Chemistry. *Expert Opin. Drug Discov.* **2012**, *7*, 489–501.

(20) Campidelli, S. Click Chemistry for Carbon Nanotubes Functionalization. *Curr. Org. Chem.* **2011**, *15*, 1151–1159.

(21) Yu, M.; Wong, J. K.-H.; Tang, C.; Turner, P.; Todd, M. H.; Rutledge, P. J. Efficient Deprotection of F-BODIPY Derivatives: Removal of BF(2) Using Brønsted Acids. *Beilstein J. Org. Chem.* **2015**, *11*, 37–41.

(22) Jameson, L. P.; Dzyuba, S. V. Expeditious, Mechanochemical Synthesis of BODIPY Dyes. *Beilstein J. Org. Chem.* **2013**, *9*, 786–790, No. 89.

(23) Yim, D.; Yoon, H.; Lee, C.-H.; Jang, W.-D. Light-Driven Au(III)-Promoted Cleavage of Triazole-Bearing Amine Derivatives and Its Application in the Detection of Ionic Gold. *Chem. Commun. Camb. U. K.* **2014**, *50*, 12352–12355.

(24) Di Donato, M.; Iagatti, A.; Lapini, A.; Foggi, P.; Cicchi, S.; Lascialfari, L.; Fedeli, S.; Caprasecca, S.; Mennucci, B. Combined Experimental and Theoretical Study of Efficient and Ultrafast Energy Transfer in a Molecular Dyad. *J. Phys. Chem. C* **2014**, *118*, 23476–23486.

(25) Uppal, T.; Bhupathiraju, N. V. S. D. K.; Vicente, M. G. H. Synthesis and Cellular Properties of Near-IR BODIPY-PEG and Carbohydrate Conjugates. *Tetrahedron* **2013**, *69*, 4687–4693.

(26) Lee, J.-S.; Kang, N.; Kim, Y. K.; Samanta, A.; Feng, S.; Kim, H. K.; Vendrell, M.; Park, J. H.; Chang, Y.-T. Synthesis of a BODIPY Library and Its Application to the Development of Live Cell Glucagon Imaging Probe. *J. Am. Chem. Soc.* **2009**, *131*, 10077–10082.

(27) Campidelli, S.; Ballesteros, B.; Filoramo, A.; DiÌ?az, D. D.; de la Torre, G.; Torres, T.; Rahman, G. M. A.; Ehli, C.; Kiessling, D.; Werner, F.; *et al.* Facile Decoration of Functionalized Single-Wall Carbon Nanotubes with Phthalocyanines via â€œClick Chemistryâ€? *J Am Chem Soc* **2008**, *130*, 11503–11509.

(28) Flavin, K.; Chaur, M. N.; Echegoyen, L.; Giordani, S. Functionalization of Multilayer Fullerenes (Carbon Nano-Onions) Using Diazonium Compounds and “Click” Chemistry. *Org. Lett.* **2010**, *12*, 840–843.

(29) Shaffer, M. S. P.; Fan, X.; Windle, A. H. Dispersion and Packing of Carbon Nanotubes. *Carbon* **1998**, *36*, 1603–1612.

(30) Kostarelos, K.; Lacerda, L.; Pastorin, G.; Wu, W.; WieckowskiSebastien; Luangsivilay, J.; Godefroy, S.; Pantarotto, D.; Briand, J.-P.; Muller, S.; *et al.* Cellular Uptake of Functionalized Carbon Nanotubes Is Independent of Functional Group and Cell Type. *Nat Nano* **2007**, *2*, 108–113.

(31) Chen, J.; Chen, S.; Zhao, X.; Kuznetsova, L. V.; Wong, S. S.; Ojima, I. Functionalized Single-Walled Carbon Nanotubes as Rationally Designed Vehicles for Tumor-Targeted Drug Delivery. *J Am Chem Soc* **2008**, *130*, 16778–16785.

(32) Patil, Y. B.; Toti, U. S.; Khdair, A.; Ma, L.; Panyam, J. Single-Step Surface Functionalization of Polymeric Nanoparticles for Targeted Drug Delivery. *Biomaterials* **2009**, *30*, 859–866.

(33) Lee, E. S.; Gao, Z.; Kim, D.; Park, K.; Kwon, I. C.; Bae, Y. H. Super pH-Sensitive Multifunctional Polymeric Micelle for Tumor pHe Specific TAT Exposure and Multidrug Resistance. *J. Controlled Release* **2008**, *129*, 228–236.

(34) Patil, Y. B.; Swaminathan, S. K.; Sadhukha, T.; Ma, L.; Panyam, J. The Use of Nanoparticle-Mediated Targeted Gene Silencing and Drug Delivery to Overcome Tumor Drug Resistance. *Biomaterials* **2010**, *31*, 358–365.

(35) Biju, V. Chemical Modifications and Bioconjugate Reactions of Nanomaterials for Sensing, Imaging, Drug Delivery and Therapy. *Chem Soc Rev* **2014**, *43*, 744–764.

(36) Liu, Z.; Cai, W.; He, L.; Nakayama, N.; Chen, K.; Sun, X.; Chen, X.; Dai, H. In Vivo Biodistribution and Highly Efficient Tumour Targeting of Carbon Nanotubes in Mice. *Nat. Nanotechnol.* **2007**, *2*.

(37) Mundra, R. V.; Wu, X.; Sauer, J.; Dordick, J. S.; Kane, R. S. Nanotubes in Biological Applications. *Curr. Opin. Biotechnol.* **2014**, *28*.

(38) Heister, E.; Lamprecht, C.; Neves, V.; Tîlmaciu, C.; Datas, L.; Flahaut, E.; Soula, B.; Hinterdorfer, P.; Coley, H. M.; Silva, S. R. P.; *et al.* Higher Dispersion Efficacy of Functionalized Carbon Nanotubes in Chemical and Biological Environments. *ACS Nano* **2010**, *4*, 2615–2626.

(39) Bianco, A.; Kostarelos, K.; Prato, M. Making Carbon Nanotubes Biocompatible and Biodegradable. *Chem Commun* **2011**, *47*, 10182–10188.

(40) Fabbro, C.; Ali-Boucetta, H.; Ros, T. D.; Kostarelos, K.; Bianco, A.; Prato, M. Targeting Carbon Nanotubes against Cancer. *Chem Commun* **2012**, *48*, 3911–3926.

(41) Bhirde, A. A.; Chikkaveeraiah, B. V.; Srivatsan, A.; Niu, G.; Jin, A. J.; Kapoor, A.; Wang, Z.; Patel, S.; Patel, V.; Gorbach, A. M.; *et al.* Targeted Therapeutic Nanotubes Influence the Viscoelasticity of Cancer Cells to Overcome Drug Resistance. *ACS Nano* **2014**, *8*, 4177–4189.

(42) Dyke, C. A.; Tour, J. M. Covalent Functionalization of Single-Walled Carbon Nanotubes for Materials Applications. *J. Phys. Chem. A* **2004**, *108*, 11151–11159.

(43) Beijnen, J. H.; van der Houwen, O. A. G. J.; Underberg, W. J. M. Aspects of the Degradation Kinetics of Doxorubicin in Aqueous Solution. *Int. J. Pharm.* **1986**, *32*, 123–131.

(44) Gerweck, L. E.; Seetharaman, K. Cellular pH Gradient in Tumor versus Normal Tissue: Potential Exploitation for the Treatment of Cancer. *Cancer Res.* **1996**, *56*, 1194–1198.

(45) Datir, S. R.; Das, M.; Singh, R. P.; Jain, S. Hyaluronate Tethered, "Smart" Multiwalled Carbon Nanotubes for Tumor-Targeted Delivery of Doxorubicin. *Bioconjug. Chem.* **2012**, *23*, 2201–2213.

(46) Fazio, M. A.; Lee, O. P.; Schuster, D. I. First Triazole-Linked Porphyrin−Fullerene Dyads. *Org. Lett.* **2008**, *10*, 4979–4982.

(47) Denton, T. T.; Zhang, X.; Cashman, J. R. 5-Substituted, 6-Substituted, and Unsubstituted 3-Heteroaromatic Pyridine Analogues of Nicotine as Selective Inhibitors of Cytochrome P-450 2A6. *J. Med. Chem.* **2005**, *48*, 224–239.

(48) Cordero, F. M.; Bonanno, P.; Chioccioli, M.; Gratteri, P.; Robina, I.; Moreno Vargas, A. J.; Brandi, A. Diversity-Oriented Syntheses of 7-Substituted Lentiginosines. *Tetrahedron* **2011**, *67*, 9555–9564.

(49) Langille, N. F.; Jamison, T. F. Trans-Hydroalumination-Alkylation of Propargylic Alcohols. *Synfacts* **2006**, *2006*, 1158–1158.

(50) Baskin, J. M.; Bertozzi, C. R. Bioorthogonal Click Chemistry: Covalent Labeling in Living Systems. *QSAR Comb. Sci.* **2007**, *26*, 1211–1219.

(51) Prescher, J. A.; Bertozzi, C. R. Chemistry in Living Systems. *Nat Chem Biol* **2005**, *1*, 13–21.

Farewells and Acknowledgments

ovvero, Commiati e Ringraziamenti…

«…Parsifal, Parsifal! Non ti fermare, e lascia sempre che sia, la voce unica dell'ideale, ad indicarti la via.»

Perché è con la canzone dell'ideale che mi è tornato in mente tutto ciò che mi aveva portato a Firenze, e come cominciai questo percorso.

Scrivendo questa tesi, quando sono arrivato verso la fine cominciai a riflettere che stavolta il capitolo dei ringraziamenti sarebbe stato il più faticoso. Sì… perché ormai il lavoro universitario aveva perso quel fascino iniziale, e l'idea romantica del dottorato aveva lasciato il posto ad una visione abbastanza scettica delle cose. L'unico obiettivo che mi era rimasto era di stampare la tesi quanto prima e dedicarmi all'unica cosa utile: la ricerca di una via lavorativa in grado di offrire prospettive, accademica o meno che fosse. L'idea dunque di appiccicare su questo quadro una sorta di abbraccio collettivo per salvare l'aspetto passionale delle cose, era qualcosa che davvero avrei fatto di malavoglia.

Così la pensavo, finché non mi è tornato in mente il Parsifal… E la canzone dell'Ideale, e da qui la ragione con cui ho cominciato questo lavoro. Avevo confidato nella Provvidenza, e cioè nella via che mia aveva portato fin lì, a Firenze, tre anni fa. Avevo scoperto come una traccia nella mia vita, una strada che si svela a poco a poco; con risvolti spesso impensati e talvolta faticosi, ma che alla fine era come un Affetto che non mi abbandonava, che ora chiamo Provvidenza. E guardando, ho trovato che non c'era un solo desiderio del cuore che non fosse un tappa di questa strada. È confidando in tutto ciò che scelsi questa grande opportunità di lavoro, con queste persone, ed in questo luogo. Il punto infatti non era tentare di pianificare il percorso, ma guardare a cosa mi aveva guidato fin lì.

In tre anni il lavoro è stato intenso, ma i risultati straordinari, è così che voglio ringraziare, salutare, e ricordare tutti i volti che sono e che sono stati parte viva di questo cammino di dottorato. Il primo pensiero va al mio mentore Stefano per la fiducia che ha riposto in me e per avermi sostenuto in questo lavoro, è superfluo dire che il merito di tutto è altrettanto suo. Per il rapporto straordinario e collaborativo che abbiamo saputo creare, che è fonte di consiglio e di confronto anche su molto oltre la chimica. Ringrazio molto Paolo per la grande collaborazione e l'apporto che ha fornito durante tutto questo lavoro, senza il quale davvero non sarebbe stato possibile neppure sperare di raggiungere i risultati ottenuti. Ringrazio di cuore anche Fabrizio per tutte le

occasioni di domande e di dibattito, dalla struttura alla reazione, e da questa al movimento reazionario! Desidero ringraziare in modo speciale Laura, la persona che Amo, perché da quando l'ho incontrata mi è a fianco ogni giorno, con i consigli e con l'amore che gratuitamente mi dona. Un grande grazie va anche a tutti i miei colleghi e compagni di lavoro, in modo particolare a Giacomo, per il suo essere partecipe e per la serenità del nostro lavorare insieme. Ringrazio qui anche Lorenzo (il Ventu per intenderci), sebbene di passaggio, ha saputo portare la giusta dose di spensieratezza e armonia, rendendo il lavoro più piacevole e le giornate più leggere. Il mio grazie va anche alle persone care che hanno saputo sostenermi al rientro da ogni giornata lavorativa, la mia famiglia: mia mamma Paola, Andrea, e Luca, per la spensieratezza che abbiamo insieme, per il sostegno, per gli incoraggiamenti accorti e per l'affetto incondizionato. Un altro ringraziamento ed un saluto di cuore a Daniele, ed a Matilde, la loro tenerezza verso di me ricorre sempre, e mi afferra, e ritorna ogni volta, e non mi lascia solo. Grazie anche a Lorenzo (e Valentina!), con cui i momenti insieme sono un'istante di conforto ed un respiro profondo di serenità. Grazie Riccardo, per i momenti di ritrovo che sai creare e perché stando insieme a te mi mostri ogni volta un'attenzione in più. Grazie anche Francesco (e Federica), seppure siete lontani, ogni volta che rammento i momenti passati insieme, ritrovo vive le esortazioni e le parole dei nostri incontri. Erica, Lilly, vi penso spesso, mi chiedo come state e come stanno i vostri cari, mi mancate, avrei voglia di rivedervi e di abbracciarvi presto.